Department of
Geological and Geophysical Sciences
Princeton University
Princeton, New Jersey

THE HIGH-TEMPERATURE CREEP OF DUNITE

by

Jerome F. Eaton

March 1, 1968

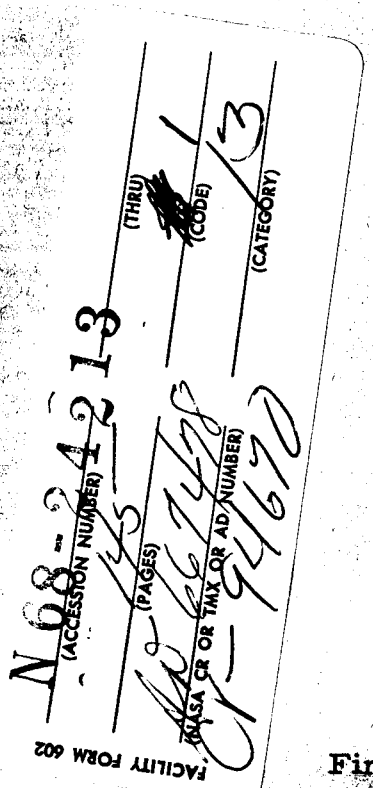

Final report prepared under contract
Nonr 1858-(44) to Princeton University by the
Office of Naval Research

A DISSERTATION

Presented to the
Faculty of Princeton University
in Candidacy for the
Degree of Doctor of Philosophy

Recommended for acceptance by the
Department of
Geological and Geophysical Sciences
March, 1968

Department of
Geological and Geophysical Sciences
Princeton University
Princeton, New Jersey

THE HIGH-TEMPERATURE CREEP OF DUNITE

By

Jerome F. Eaton

Final Report on Contract Nonr-1858(44) with the Office of Naval Research (W. M. Elsasser, Contract Supervisor).

TABLE OF CONTENTS

TABLE OF CONTENTS (Continued)

Page

LIST OF FIGURES

LIST OF FIGURES (Continued)

LIST OF TABLES

ACKNOWLEDGEMENTS

I am especially indebted to Professor Walter M. Elsasser for proposing the problem of my doctoral research and directing my efforts throughout the investigation. His standards of precise exposition severely tested my abilities in preparing the dissertation, for which I am now very grateful.

I am also indebted to Drs. W. J. Morgan and R. A. Phinney who gave very generously of their time to discuss various aspects of the investigation on innumerable occasions. Dr. E. Orowan of the Massachusetts Institute of Technology and Dr. H. H. Keith of the United States Naval Academy provided many invaluable suggestions pertaining to the design of the apparatus and the scope of the experiments.

I am also grateful to Mr. R. J. Lewis who assisted in developing some of the electronic circuitry, to Mr. T. C. Forseman who did such an excellent job of machining the mechanical components for the two units of apparatus, and to Mrs. Sue Vine who prepared the drawings for the dissertation.

I would would like to express my appreciation to the National Aeronautics and Space Administration and to the Department of Geological and Geophysical Sciences, Princeton University for the financial support awarded to me during my doctoral research. The experimental investigation was supported by the Office of Naval Research, Washington, D. C., under contract Nonr 1858(44).

And lastly, I shall always be grateful to my wife and to our parents for their understanding and encouragement throughout the years of my graduate study.

Chapter 1

INTRODUCTION

Preliminary Statement. -

The mechanical properties of rocks subjected to short-time deformational forces have long been the focal point of laboratory investigations. Primarily, these studies have been concerned with the effects of confining pressure, differential stress, and temperature, both individually and in combination, upon the position of the brittle-to-ductile transformation point in the stress-strain field. The ultimate strength and the total strain experienced by the specimen before rupture have also been studied. Such tests have been performed on a wide variety of rocks, and a comprehensive compilation of the published results has been provided by Handin (1966).

The influence of time on the measured deformational characteristics of rocks was ignored in many of the earlier experiments. However, it has become apparent as experimental techniques permitted increasingly sensitive observations that many physical properties of materials, heretofore determined in short-time experiments, exhibit a time dependence when subjected to longer intervals of testing. Among these, time-dependent strain or creep remains the most important time-dependent phenomenon that requires further study.

Creep is defined as the deformation occurring in a body over a period of time during which the body is subjected to a bounded, non-hydrostatic stress. This phenomenon is characterized in all materials by a three-stage strain-versus-time relation-

ship indicated schematically in Figure 1. Upon initial application of load and with the resulting stress near the yield stress of the material, a specimen undergoes a practically instantaneous, non-plastic deformation ϵ_0, the magnitude of which is dependent upon the stress level and corresponds primarily to the elastic properties of the material. Most previous investigations of the deformation of rocks have been concerned with the details of only this portion of the deformation record. However, if the applied stress is maintained constant at the value corresponding to ϵ_0 for a sufficiently long time, the distinguishing features of the time-dependent deformational process become apparent.

The first or primary stage of creep, shown in Figure 1, occurring in the time interval from t_0 to t_1, is indicated by a marked increase in the total strain, at a rate which decreases with time. The deformation occurs as the result of dislocation movement or slip induced by the applied stress and assisted by thermal stress fluctuations occurring within the material. The rapid decrease in the rate of deformation is brought about by the development of strain hardening which tends to impede the migration of defects (Orowan, 1947). At low temperatures and moderate stress levels, only this transient stage of creep is observable and the deformation ceases entirely when the resistance to creep brought about in the material by the effect of strain hardening is sufficient to prevent further slip from occurring. Consequently, the primary stage is sometimes referred to as "cold creep".

At higher stresses and temperatures, the transient creep stage is followed by a period of deformation during the interval in Figure 1 from t_1 to t_2 in which the strain rate remains constant

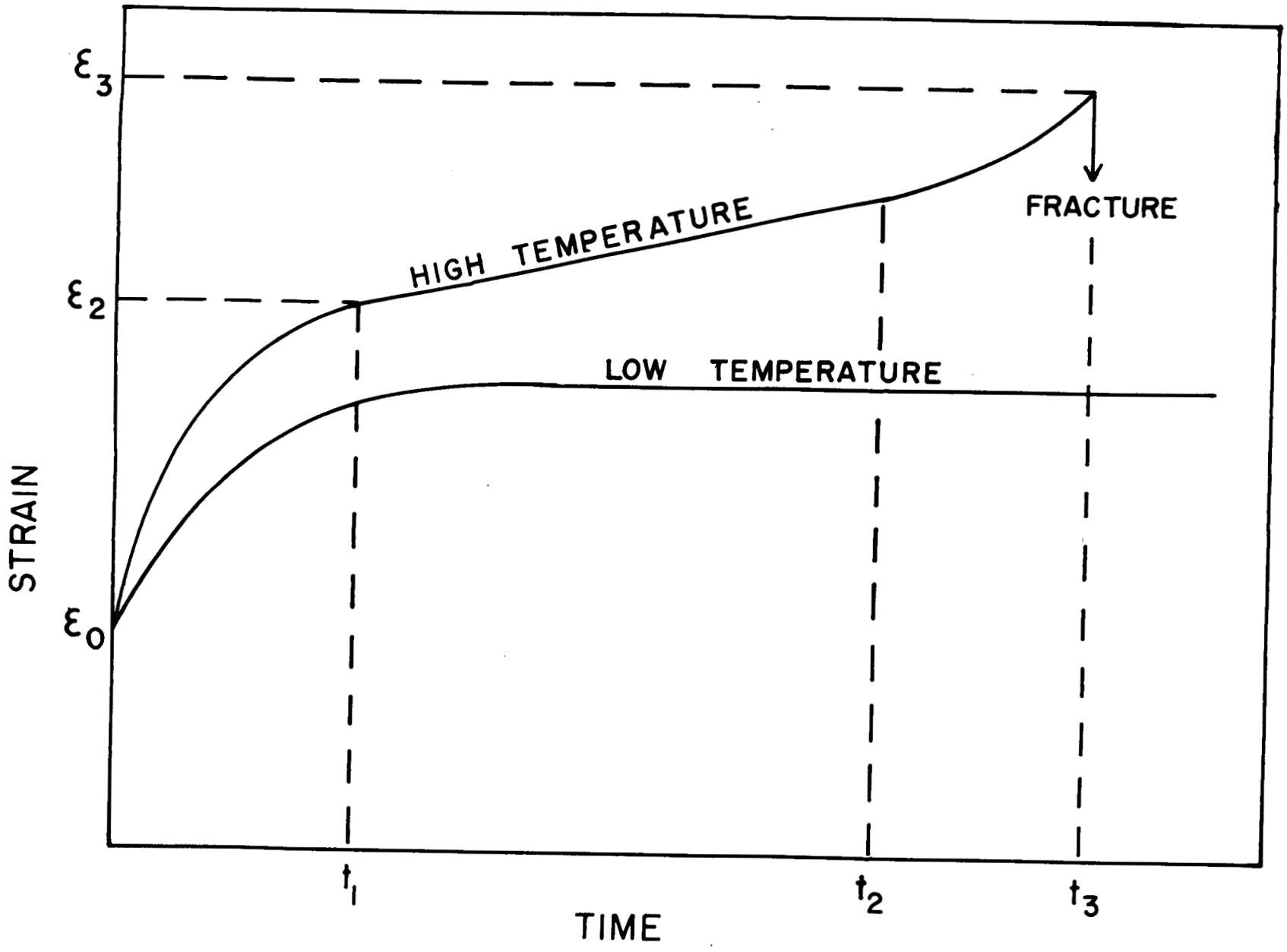

Figure 1. Typical creep curves exhibited by many solids as a function of temperature.

as the total strain of the specimen increases from ε_1 to ε_2. Due to the linear relationship between strain and time which characterizes this stage of the deformation, it is commonly referred to as steady-state or viscous creep. In ductile, polycrystalline materials, the dominant mechanism operating during steady-state creep is the diffusion of atoms at grain boundaries, or grain boundary sliding. Dislocation movement may be associated with the diffusion process as a second order effect. Steady-state creep is observed only at elevated temperatures approaching one-half of the absolute melting point of the material. Hence, this stage of creep is frequently called "hot-creep".

Steady-state creep is followed by a period of deformation shown in Figure 1 during the time interval from t_2 to t_3 in which the strain rate accelerates rapidly until deformation of the specimen is interrupted by fracture. In laboratory experiments, this stage of deformation is usually observed only during tensile loading and occurs infrequently in compressively stressed specimens. The deformation produced during this phase of deformation is termed tertiary creep. However, the processes involved with the appearance of the rapid increase in the rate of strain have not been studied very extensively and are not well understood.

The present state of our understanding of time-dependent strain as it occurs in most materials is derived primarily from detailed investigations of the phenomenon in metals. The quantitative time laws which have been found to accurately describe the deformation of all ductile, crystalline materials were first formulated by Andrade (1911, 1914) to describe his observations of the progressive elongation with time of fine metal filaments subjected

to a constant uniaxial stress. In contrast, however, to the great wealth of laboratory results obtained in short-time experiments on rocks and in both short- and long-time experiments with non-geologic materials, there is only a limited amount of data on the time-dependent deformational properties of rocks. Due to the direct relationship with tectonic processes occurring at depth within the Earth, it is now well recognized that the effect of temperature on the creep of rocks is the most geologically significant aspect of time-dependent deformational phenomena; yet, at the same time, with only a single previous quantitative investigation of the role of temperature in the creep of rocks reported in the literature, it is also the most neglected.

Objectives of the Investigation. -

The primary objective of the present work was to demonstrate in a quantitative manner the effects of temperature and applied stress upon the deformation with time of silicate rocks subjected to uniaxial compressive loading. The considerable expenditure of time required for creep tests necessitated some limitation of the scope of the experimental phase of the study. Rather than performing only cursory observations on a wide variety of silicate rock types, a systematic examination was carried out of the creep of dunite rock from Jackson County, North Carolina. In particular, the investigation was oriented toward a comprehensive determination of the steady-state creep rates in dunite at temperatures over the range 500° - 1000°C, and differential stresses up to 400 bars at atmospheric pressure, leading to a quantitative assessment of the functional relationship between the observed strain rates and the experimental parameters.

Chapter 2

PREVIOUS RESEARCH

The initial quantitative demonstrations of the time-dependent character of deformations occurring in crystalline solids under an applied differential stress were performed by Phillips (1905) and Andrade (1911) using metal wires loaded in tension. Since then, extensive investigation of the time-dependent straining of metals has supplied much of the data upon which our present understanding of creep is based. In addition, quantitative observations of the creep of concrete (Watstein, 1953; and others), ice (Glen, 1952, 1955, 1958; Griggs and Coles, 1954; Jelinek and Brill, 1956; and others), and various ceramic oxides (Wachtman and Maxwell, 1954; Stavrolakis and Norton, 1950; and others), have been made. By comparison, few observations of time-dependent deformation occurring in rocks at high temperatures have been reported in the literature, and our knowledge of this phenomena is therefore very meager.

Michaelson (1917, 1920) performed torsional experiments at constant torque on thin, cylindrical rods of marble, limestone, shale, slate, and talc at room temperature and atmospheric pressure. Griggs (1936) studied the compressive creep in one specimen of Solenhofen limestone at room temperature and under a confining pressure of 10 kilobars. Various constant differential stresses were applied for periods from 1 to 12 hours during which the longitudinal strain was recorded. Transient and steady-state creep were observed at differential stresses of 3200, 4300, and 5400 bars, while all three stages of creep were observed at 6600

bars before rupture occurred in the specimen. In subsequent studies, Griggs (1939, 1940) investigated the effect of confining pressure and the presence of hydrous pore fluids on the compressive creep of marble, limestone, and gypsum. He also studied the behavior of Solenhofen limestone under very long-term loading at room temperature and atmospheric pressure. After 1100 days under an axial compressive stress of 1400 bars, the specimen exhibited only transient creep. However, all three stages of creep were achieved in Solenhofen limestone at room temperature under a confining pressure of 10 kilobars and a differential stress of 5500 bars after a period of only three hours. It was observed that failure in geological materials occurred under differential stresses well below the yield points measured in short-time tests if applied for sufficiently long time durations. Griggs described the observed strain-time behavior of the materials tested as elasticoviscous and found that the results could be well represented by the empirical time law, due to Andrade (1911, 1914):

$$\epsilon = a + b \cdot \log t + c \cdot t \quad , \qquad (1)$$

where ϵ is longitudinal strain, t is time, and a, b, and c are "constants" which, in general, depend upon the material and the differential stress, confining pressure, and temperature of the test. The first term represents the elastic deformation of the specimen, the second describes the transient creep stage, and the third describes the behavior during primary creep or pseudoviscous flow. Griggs, Turner, Borg, and Soska (1951, 1953) conducted creep tests on Yule marble at temperatures up to 300°C. Unfortunately, quantitative observation of the primary creep stage of the deformation was obscured by deviations from

conditions of constant differential stress. However, analysis of thin sections made from the deformed specimens disclosed that significant changes in the prime flow mechanism had occurred as the temperature was increased. In the range from room temperature to 150°C, twin and translation gliding had prevailed, while at 300°C, intergranular motion or recrystallization became the dominant deformational mechanism. Nisihara (1952) studied the effects of direction of loading relative to the planes of bedding and the presence of water on the transient creep behavior of shale and sandy-shale. Lomnitz (1956) deformed slender, cylindrical bars of granodiorite and gabbro in torsion at room temperature and atmospheric pressure. Hardy (1959) employed uniaxial compression apparatus to study the creep of a single specimen of weakly cohesive iron ore and several specimens of sandstone at room temperature. Viscoelastic behavior was observed in each run. Creep data were compiled by Robertson (1960) from an extensive series of experiments in which specimens of Solenhofen limestone, marble, and calcite were compressed under differential stresses up to 4000 bars and confining pressures ranging from 3000 to 8000 bars at room temperature. Only the transient stage of creep was observed, but substantial variations of the differential stress and confining pressure during the tests vitiated the observations made of the deformations experienced by the specimens and precluded any quantitative conclusions. Iida, Wada, Aida, and Shichi (1960) conducted bending experiments on basalt, rhyolite, serpentine, andesite, and some granitic rocks under normal temperature and confining pressure conditions. Only small strains were achieved, and transient creep was the only

phase of time-dependent deformation observed. LeComte (1960) performed a comprehensive study of the creep of rock salt using triaxial compression apparatus. Temperatures up to 300°C, confining pressures to 1000 bars, and stress differences up to 138 bars were applied to artificial polycrystalline specimens. Grain size was maintained at a reasonably uniform level for most of the test runs. However, the effect of increased grain size on the observed creep rates was determined in two runs where the grain size of the specimens was deliberately coarsened prior to the tests. Significant increases in the creep rate were noted as temperature and differential stress were increased. However, only negligible reduction of the rate of deformation was observed with an increase in the confining pressure. The observed creep behavior was found to agree well with the equation, due to Andrade (1911):

$$\epsilon = a + b \cdot t^{n} \quad , \qquad (2)$$

where, as before, ϵ is strain, t is time, and a, b, and n ($0<n<1$) are material parameters which, in general, depend also on the stress level, confining pressure, and temperature. The fractional power dependence of the deformation on time represented by the second term of equation (2) has been termed the β-creep stage by Andrade. Heard (1963) performed a series of constant strain-rate experiments on Yule marble. Deformation was observed as a function of the imposed strain rate over the range from 0.4 second^{-1} to $3.3 \cdot 10^{-8}$ second^{-1} at temperatures up to 500°C., and confining pressures up to 5000 bars. Misra and Murrell (1965) deformed anhydrite, dolomite, sandstone, marble, microgranodiorite, and peridotite under constant compressive stress and

sandstone under constant torsional stress at atmospheric pressure and temperatures up to 750°C. Transient and β-creep of nearly perfect Andradian form (i.e., with $\epsilon \approx t^n$, and $n \cong 0.3$), were observed in this single previous investigation of the effect of high temperatures on the creep of rocks. The creep theory of Mott (1953) was invoked in calculating a steady-state rate of creep for peridotite based on the experimentally determined rate of β-creep.

Several generalizations can be derived from these earlier investigations of the time-dependent behavior of rocks: (1) the rate of creep is altered by the presence of aqueous solutions in the pore spaces of the specimen (Griggs, 1940); (2) the rate of creep exhibits only a weak dependence on changes in confining pressure, and is reduced only slightly by a thousand-fold increase in isotropic confinement (Robertson, 1960; LeComte, 1960); (3) transient and steady-state creep proceed at a markedly higher rate as temperature and stress difference are increased (LeComte, 1960; Heard, 1963); and (4) increased grain size results in a retardation of the rate of creep (LeComte, 1960).

Recapitulating, it is apparent that, at best, the present level of understanding of time-dependent strain in geologic materials is only qualitative. The primary parameters which affect the creep of rocks have been evaluated in a relatively general way for only a few types of rocks. In particular, the details of the steady-state creep behavior of rocks as a function of temperature have been largely neglected. Rheological processes in the mantle have been subject to conjecture and theory, but a clarification based on experimental evidence of the time-dependent

properties of appropriate polycrystalline aggregates under suitable environmnental conditions is necessary to understand the mechanisms of deformation.

Chapter 3

APPARATUS

Preliminary Remarks.-

In the course of determining the scope of the experiments to be performed, it became apparent that the testing machines available from commercial sources would not adequately provide the desired ranges of the experimental parameters. Hence, it became necessary to prepare the design for and construct a suitable test apparatus. In a preliminary analysis, the requirements for and the interrelated operational effects of temperature, stress, confining pressure, total strain, and strain rate were evaluated on the basis of the proposed experimental objectives. From this study, the primary guidelines for the final mechanical design were established as follows:

(1) Test Mode.- The primary consideration in formulating the design of an apparatus with which to impose mechanical deformation is the selection of a suitable test mode. Time-dependent deformation is observed in laboratory experiments in which either the stress applied to the test specimen or the imposed strain-rate is maintained at a constant value. Constant stress or creep tests have the disadvantage that an individual experiment tends generally to be of long duration compared to constant strain-rate tests where the time required to obtain any given value of specimen deformation can be predetermined. Either mode is amenable to compressional, tensile, or torsional loading techniques. However, several factors were discovered which weighed heavily against utilizing the constant strain-rate test mode:

(i) In mechanical deformation tests where the strain rate is taken as the independent experimental parameter, stress is the dependent observational variable. The absolute magnitudes of the strain-rate which are of interest in rock deformation experiments are relatively small, of the order of 10^{-4} sec.$^{-1}$ and slower. To produce a deformation in which the strain-rate is induced by mechanical means and also held at a small, constant value, the apparatus must employ a loading device which incorporates a mechanical transmission stage. Consequently, an inherent characteristic of the constant strain-rate apparatus operated at geologically interesting deformation rates is a "stick and slip" motion imparted by the loading mechanism due to friction and back-lash between the components. The immediately observable effect produced by the stick-slip action of the apparatus is an oscillatory perturbation of the stress applied to the specimen with an associated amplitude which depends upon the strain rate and the period of the stick-slip cycle. The resulting uncertainties produced in the observations of stress can introduce significant obstacles to accurate determinations of the functional relationship between the experimental parameters.

(ii) Dillon (1963, 1966) has indicated that in experiments in which the test specimen is subjected to an applied stress for long periods of time, as is the case in creep testing, the observed strain may develop not as the smooth function of the applied stress commonly observed in short-time experiments, but in a step-wise continuous fashion. Observation of such fine structure characteristics in the stress-strain relationship has led to differentiation between

the various possible mechanisms operating during deformation. However, observation of such deformational modes is obviated in experiments carried out by imposing a constant rate of strain, since an incremental, dynamic response exhibited by the specimen during the deformation would be indistinguishable from the stick-slip characteristics of the loading mechanism.

(iii) Direct observation of the transient and tertiary stages of creep is necessarily forfeited when the deformation of the specimen is mechanically induced at a constant rate.

On the basis of these considerations, it is evident that the constant strain-rate mode carries with it rather formidable experimental limitations and the choice of a test mode was made in favor of constant stress.

In practice, creep tests with a truly constant stress are extremely difficult to implement due to the continual change of the cross-sectional area of the test specimen during the course of the deformation. However, if only small strains are produced by the deformation process, the condition of constant stress can be closely approximated if the load applied to the specimen is kept constant. Since it was anticipated that only small strains would be encountered in the experiments, it was decided that the testing could be performed satisfactorily under conditions of constant load and with only small deviations from conditions of constant stress.

The test mode requirements of the apparatus were completed by selecting the compressional method of loading to take advantage of the strength characteristics of polycrystalline mater-

ials which exhibit a greater resistance to brittle fracture under compression than in either extension or torsion.

(2) Confining Pressure. - In the past, many laboratory investigations of the deformational properties of geological materials have been carried out with the specimen confined by a hydrostatic fluid pressure superposed on the primary uniaxial deforming stress. A confining pressure is employed in rock deformation work primarily to simulate the isotropic overburden pressures which exist at depth within the Earth. Also, since unconfined rocks at temperatures well below half the absolute melting temperature exhibit extreme brittleness, the use of a confining pressure in previous investigations of the deformational phenomena occurring in rocks has effectively raised the fracture stress of the material thereby permitting the deformations to proceed to measurable amounts before the occurrence of failure. Most of the previous creep results for rocks have been obtained for confined specimens. However, the only observed effect of a confining pressure on the time-dependent deformation of many rocks is a negligible decrease of the creep rate (Robertson, 1960; LeComte, 1965). It is apparent then that the use of a confining pressure in creep testing tends to lengthen the already considerable time necessary to complete an individual experiment and to reduce the observable deformation.

The use of a fluid confining pressure also necessitates the incorporation into the apparatus of pressure seals at the points where the loading pistons enter the test chamber. In addition to the primary function of preventing leakage of the confining pressure fluid, the seals must also permit friction-free motion of the loading pistons; otherwise, a stick-slip action is imparted to the

loading mechanism which is then transmitted to the specimen. The seals that have been used previously are of two general types: (1) a low-friction, controlled leak packing that requires a servo-compensated pumping system to maintain the pressure level of the confining medium; and (2) a high-friction seal, which has a tendency to produce non-uniform applications of load to the specimen. Both types of seals have performed satisfactorily in short-time duration experiments. For tests carried out over long intervals of time, however, the low-friction seal is undesirable since it necessitates addition of an operating system which must be kept stable for the duration of the experiment; while the high-friction seal is unsatisfactory due to the stick-slip action imparted to the loading mechanism which becomes indistinguishable from incrementally dynamic responses of the specimen under stress. Due to these undesirable consequences implied by the utilization of a confining pressure during long-term experiments, the complexities involved in implementing a workable pressure system, and the almost total lack of quantitative experimental data concerning the effect of temperature on the creep of rocks, either confined or unconfined, it was decided that meaningful and significant results could be obtained from a study of high temperature creep performed at normal atmospheric pressure. Professor E. Orowan (personal communication) has indicated that, based on his experience, the creep properties of a compact, non-porous material should show only a very weak dependence on isotropic pressure; hence, omission of the confining pressure would not make the present experiments an unrealistic simulation of the lower crust and top layers of the mantle!

General Description. -

A test apparatus capable of long term deformation experiments at temperatures up to 1000°C, and applied compressional loads up to 12000 pounds was designed. (Tension tests may also be performed with the apparatus but require some modification of the upper ram assembly.) All creep experiments reported here were carried out in two identical units of the apparatus. Figure 2 shows an isometric representation of the apparatus, and Figure 3 provides the details of the assembly. The design of the apparatus is the result of a comprehensive stress analysis based on optimization techniques and critical load criteria. Each load-bearing member of the apparatus is dimensioned so that, at maximum specimen loading, the induced stress does not exceed one-quarter of the yield stress. Scaled drawings of all mechanical components of the apparatus are provided in Appendix I.

The apparatus consists of three separate but integrated operating systems: (1) a loading system for the application, maintenance, and recording of a constant uniaxial load on the specimen; (2) a strain measurement system for the determination and recording of the deformation experienced by the specimen; and (3) a system for the application, recording, and control of the temperature of the specimen.

The three subsystems are constructed around a test stand fabricated of mild steel. The test stand consists of two plates separated by four supporting bars. The bottom end of each of the support members (Det. 2) is built into the base plate (Det. 1) and secured by a flange and lock-nut assembly. (The detail numbers included in the text correspond to the assembly designations shown in Figure 3.) The top ends of the support members pass

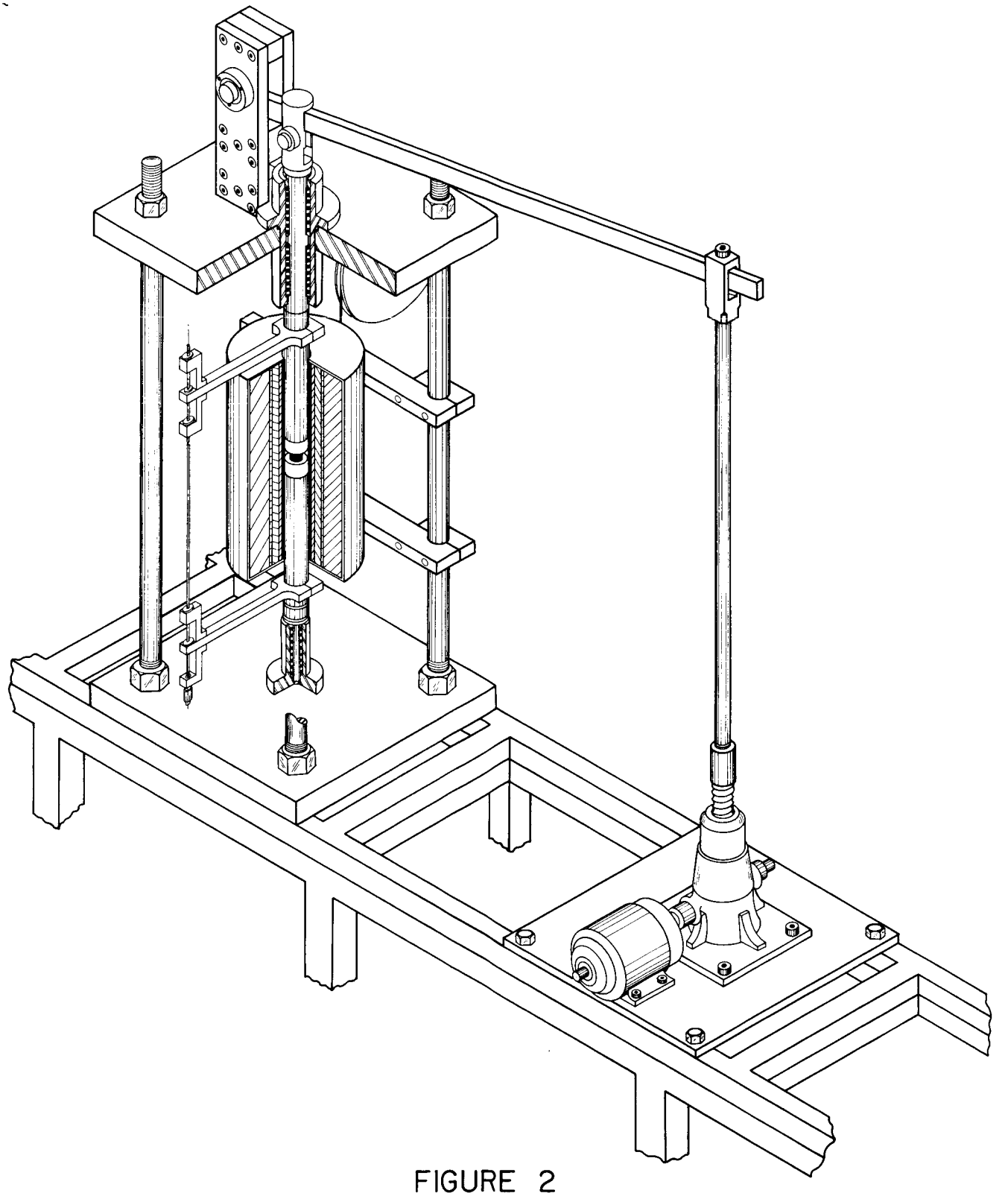

FIGURE 2

ISOMETRIC VIEW OF ASSEMBLY

Scale: $\frac{1}{4}$" = 1"

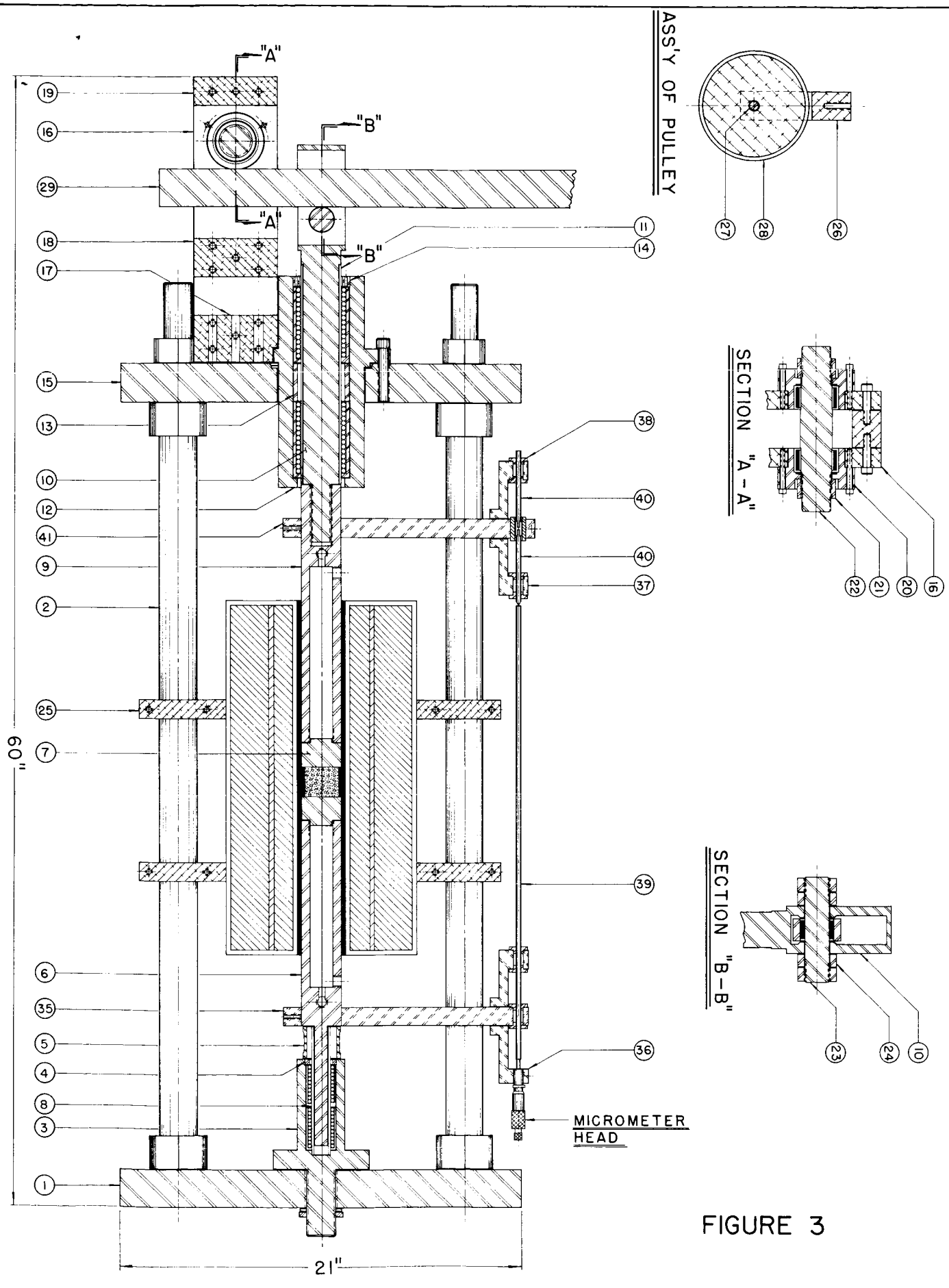

FIGURE 3

SECTION THRU ASSEMBLY

Scale: $\frac{1}{2}" = 1"$

through bored holes located at the corners of the top plate (Det. 15). The top plate rests on the four flange-type retaining surfaces provided by this construction and is secured by a double lock-nut assembly at each corner; this arrangement also serves to maintain the top plate in the parallel alignment with the bottom plate required for proper functioning of the loading mechanism.

The horizontal surfaces of the base and top plates were planed flat and parallel to within 0.001 inches per foot to facilitate leveling of the apparatus after final assembly and to secure proper allignment of the support members. After machining of these surfaces had been completed, the plates were clamped firmly together, and the mounting holes for the support bars and the locating holes for the upper and lower bearing housings (Dets. 12, 3) were bored simultaneously in both plates in order to ensure concentric allignment of the loading pistons and to minimize non-axial motions in the load column.

Detailed Description of the Operating Systems. -

Loading System. - It is essential for accurate interpretation of the data obtained in laboratory deformation experiments to have a very precise knowledge of the stresses imposed by the test apparatus on the specimen. In the particular case of uniaxial compression experiments, it is imperative that the loading mechanism be free of any shearing forces which might be applied to the specimen. In the design of the present apparatus, considerable effort was directed toward achieving a purely axial loading column devoid of any external lateral forces. The importance of this point cannot be overemphasized, for if shear forces are inadvertantly superposed on the uniaxial load the results are untenable.

Compressional loading of the specimen is obtained with the apparatus by means of a simple single-staged lever arm (Det. 29) with a fixed ratio of 12:1. One end of the lever arm is acted upon by a worm-gear driven jack-screw actuator of the ball-nut type (Duff-Norton Company). The actuator mechanism is mounted on a thick plate (Det. 43) fixed to the end of the test structure and is driven by a fractional horsepower DC gear motor (see Figure 2). Primary loading of the lever arm up to 1000 pounds is obtainable with the actuator-motor combination. Alternately, the linkage rod (Det. 32) connecting the jack to the lever arm may be replaced with a weight pan assembly and loading of the specimen can be effected with dead weights. Because of the extreme simplicity of this method of loading, it is particularly attractive if a continuous range of the applied stress is not required and was employed in many of the experiments reported here.

The primary load applied to the lever arm is amplified by the effective ratio, and the resulting force appears at the loading bar (Det. 21; see also Section A-A of Figure 3), which acts as a fulcrum for the lever arm. The loading bar is fabricated of drill rod material and is mounted in an aluminum bearing block assembly (Dets. 16-20) rigidly fixed to the top plate of the test stand. Thrust bearings are used to support the ends of the loading bar and buffer the buckling forces encountered when loading the specimen. Roller bearings mounted in the block assembly permit friction-free rotational motion of the load bar which effectively removes from the loading system any non-axial forces resulting from the metal-to-metal contact between the lever arm and loading bar.

The vertical axis of the loading column is located between the load bar assembly and the end of the lever arm acted upon by the jack screw. The mechanical advantage of the system is determined by the ratio of the distances separating these three points of loading on the lever arm. The lever arm passes through a milled slot in the upper ram (Dets. 9, 10; see also Section B-B of Figure 3). A threaded shaft (Det. 23) is held in this slot with clamping washers and hex nuts (Dets. 22, 24); and yoke-mounted on the shaft is a cam-type roller bearing upon which the lever arm bears to exert the force applied to the specimen. The loading bar assembly and the yoke-mounted load bearing employed in the design represent a modified adaptation of the familiar knife-edge fulcrum configuration utilized in conventional mechanical deformation devices of this type; the present design offers the advantage that, because both of the loading points acting on the lever arm are provided with the capability for frictionless rotational motion, any lateral forces developed in the lever arm-to-actuator linkage (Dets. 30-34) do not become sources of non-axial force in the loading column.

Located on the top surface of the upper plate of the test stand is a bell-shaped housing (Det. 12), containing a pair of precision recirculating ball-bearing type bushings. The housing is mounted in a counter-bored opening in the plate, the dimensions of which were carefully machined to a sliding fit with the stepped flange at the base of the housing to ensure precise allignment of the vertical axis of the load pistons. The ball bushings are separated by a mild-steel spacer (Det. 13) and held in the housing by means of a threaded retaining ring (Det. 14). A hardened sleeve (Det. 11) was pressed onto the portion of the upper ram normally

positioned within the housing to provide a suitable surface for the ball bearings. The entire assembly serves as a passage for the upper ram through the top plate. The ball-bearing bushings permit friction-free linear motion of the upper ram (Dets. 9, 10) along the axis of the loading column but prohibit lateral deflections from occurring.

A similar construction was employed in the design of the lower ram assembly. A bell-shaped housing (Det. 3) is mounted on the top surface of the base plate of the test stand. The threaded shaft extending from the base of the housing passes through the bored hole in the center of the plate; the housing is fixed in place by a flat washer and locking-nut assembly threaded onto the end of the shaft and tightened against the lower surface of the base plate. Some clearance is available between the threaded stud and the surface of the opening to allow manual correction of any misalignment of the rams. The lower housing also contains a pair of ball-bearing bushings held in position by a threaded retaining ring (Det. 4). As before, a hardened bushing shaft was pressed onto the portion of the lower piston that is inside the bearing housing during normal operation so as to prevent wearing of the ram (Det. 6).

Very stringent tolerances must be held on the clearances between the effective inside diameter of the ball bushings and the outside diameter of the rams, so as to insure friction-free operation of the loading system. Water cooling of the load rams is required to prevent the conduction of heat into the upper and lower bearing housings which, if it occurs, will produce sufficient thermal expansion to cause binding of the ball-bearing bushings.

The water cooling is also required to maintain the strength and dimensional stability of the pistons during the high-temperature tests. A commercially available water refrigeration unit (Filtrine Corporation), proved adequate for this purpose. The cooling system recirculates distilled water through a closed loop (see Figure 4), and consists of the following: (1) a refrigeration-compressor unit capable of maintaining a differential of five degrees between the supply and return sides of the system; (2) a pump to drive the coolant through the system; and (3) valve controls and flow gauges to adjust the rate of flow for varying heat inputs of the temperature system.

The portions of the rams which remain within the high-temperature zone during a test are bored out and threaded to accept a closure plug (Det. 7). At the base of each water chamber, a hole was drilled to accept a length of thin-walled stainless steel tubing. The aperture of the tubing is joined by an opening bored from the outside surface of each piston and threaded to accept standard pipe fittings. A similarly threaded hole is located at the base of each water chamber. These two holes serve as the intake and outlet, respectively, of the water chambers. Water passing into the rams flows through the tubing and is emitted at the opposite end of the chamber near the base of the closure plug. The flow is forced to continue along the water jacket between the outside surface of the tubing and the inner walls of the chamber before passing out through the threaded opening at the base. Since all coolant entering the water jacket traverses the entire heated length of the ram, the design provides high efficiency.

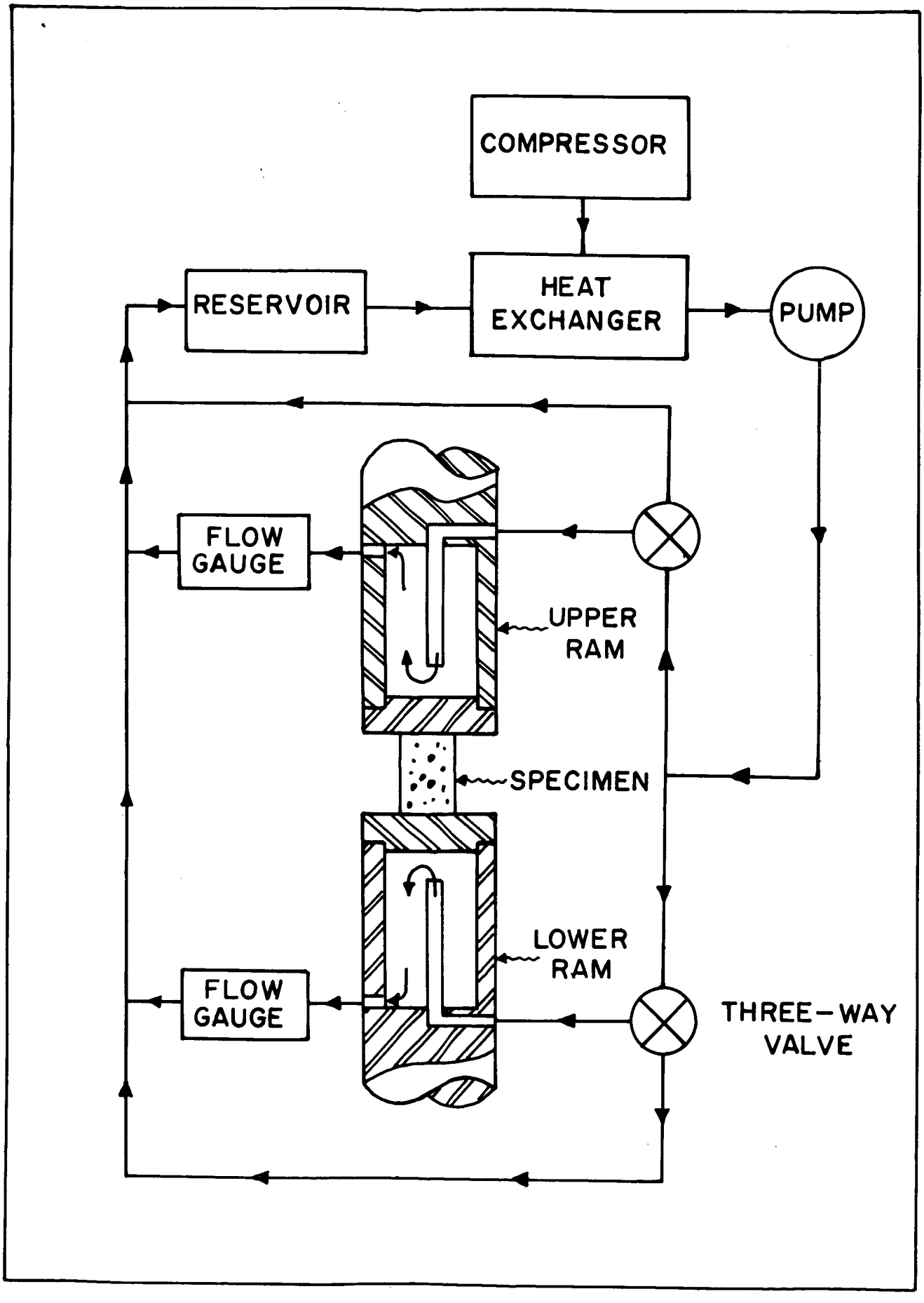

Figure 4. Schematic diagram of the water cooling system. The loading rams are not drawn to scale.

A dual Wheatstone bridge-type load cell (Det. 5) was designed to serve both as the sensing element of the load measuring circuitry and as an integral member of the loading column. The cell is of tubular design with bell-sectioned flanges at each end which provide uniform distribution of the applied load. It is positioned between the flat surfaces at the base of the lower ram and the top of the lower housing assembly, respectively. The cell consists of a hollow, cylindrical carrier machined of high strength aluminum upon which are mounted the two Wheatstone bridge circuits. The internal diameter of the carrier was governed by the support area at the top of the lower housing assembly; the outside diameter was then adjusted to provide a cross-sectional area corresponding to an axial strain of 0.1% at maximum loading. Temperature-compensated SR-4 type strain gages were bonded to the outer surface of the carrier and form the active arms of the bridge circuits. Gage lengths of the adjacent arms of each bridge are oriented mutually orthogonal, with one element of each adjacent pair parallel and the other perpendicular to the axis of the carrier. By employing four temperature-compensated, active arms in the bridge circuit, the output signal in response to an imposed load is maximized, and optimum suppression of the error signals induced by transient thermal strains is obtained. Silicon-regulated DC power supplies operating in the constant voltage mode were used to energize the bridge circuits.

The output signal from one bridge of the load cell forms the input to one channel of a two-channel strip-chart recorder (Texas Instruments, Inc.), providing both a permanent record and a means of visually monitoring the loading applied to the specimen.

The second bridge circuit of the load cell functions as the sensing element of a potentiometric servo network which maintains control of the constant load applied to the specimen (Figure 5). The output signal from the bridge circuit is compared with the signal from a constant voltage source; and the DC difference signal is converted to an AC signal by the photo-chopper stage which uses the 60 cps line voltage as a reference. The alternating difference signal produced by the photo-chopper is then amplified, passed through an impedance matching network, and applied to the SCR switching stage which controls the power input to the DC motor driving the jack-screw actuator. The network is initially balanced for a given specimen load by means of a ten-turn potentiometer. Any subsequent deviation from the desired level of loading results in a non-zero difference signal and activation of the motor-actuator assembly by the SCR switching circuit until balance is restored. It was determined that the network is capable of detecting and correcting deviations from balance which correspond to approximately 0.1% of the minimum stress reported. The extreme sensitivity of the servo network and the high efficiency of the motor-actuator assembly resulted in a very stable, accurate constant loading system.

Strain Measurement System. - The most critical measurement in a study of the time-dependent characteristics of deformation is, of course, the determination of the relative change in initial length of the specimen. The measurement of very small changes in length is most conveniently accomplished by means of an electro-mechanical transducer. For the present experiments, a linear variable differential transformer, or LVDT for short, was employed. The LVDT provides a voltage output directly propor-

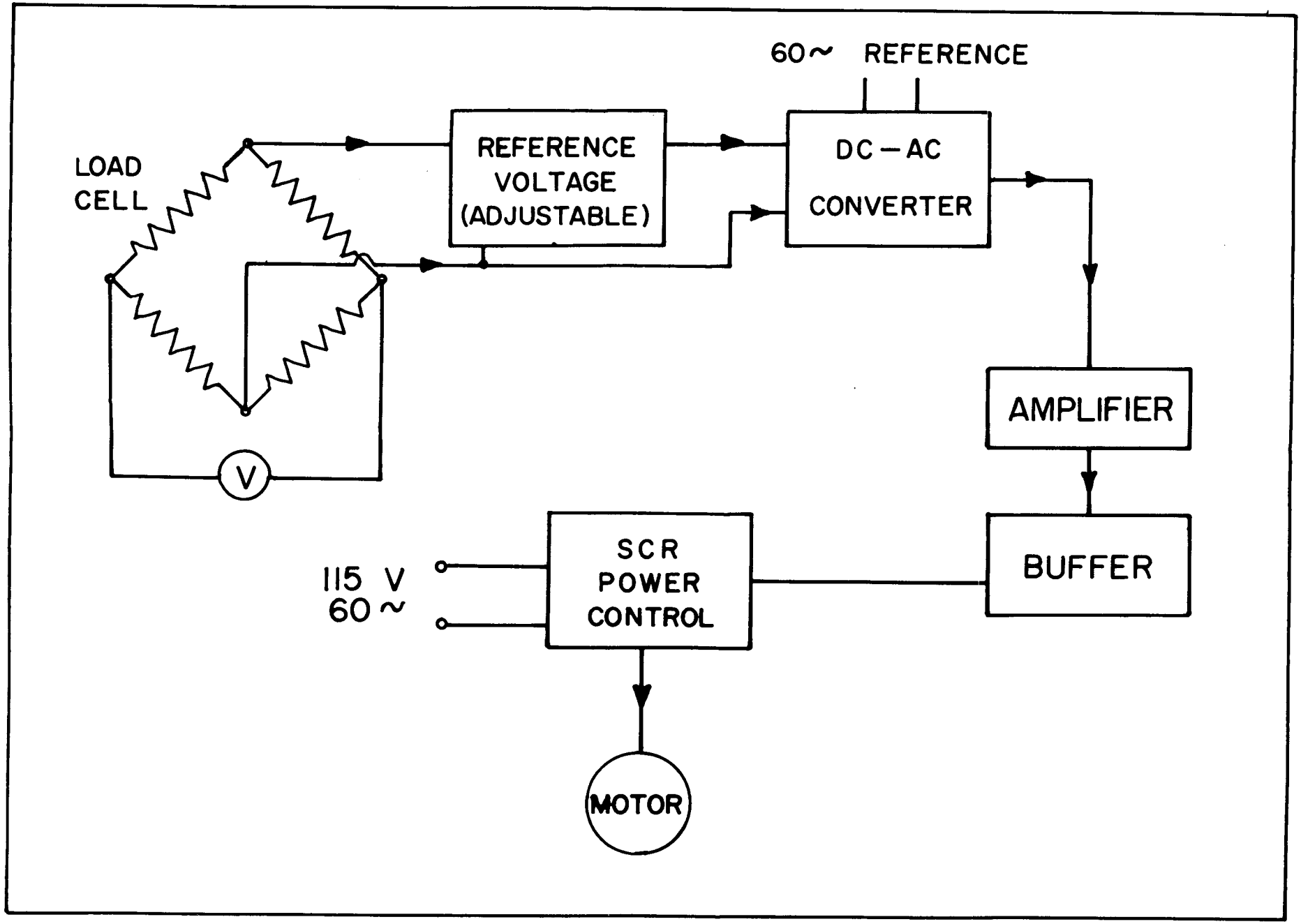

Figure 5. Block diagram of the potentiometric servo network used to control the constant loads applied to the specimens.

tional to the displacement of a movable magnetic core. This type of transducer element was selected for the following reasons: (1) the high linearity of the output signal with respect to core displacement provides simplification of the calibration routine and enhances the accuracy of the data; (2) the sensitivity of the output is extremely high; (3) the transducer configuration was easily integrated into the design of the apparatus; and (4) high immunity of the output signal from stray noise pickup due to shielding techniques employed in the construction. The LVDT consists of an electrostatically and magnetically shielded coil form assembly upon which are wound three separate, equally-spaced, inductive windings and a separate rod-shaped magnetic core which is positioned axially inside the coil form assembly. Energizing the center or primary winding with alternating current induces a voltage in each of the outer coils which act as the secondary windings of the transformer. Normally, the secondary windings are connected in series opposition, so that the two induced voltages are exactly opposite in phase. The output signal of the transformer is then the difference of the separate secondary voltages. For one position of the central magnetic core, the net output voltage will be minimum, thereby providing the null or balance position. Any displacement of the core from the null point relative to the coil form will induce an increase in the voltage of the secondary winding toward which the core is displaced and a corresponding decrease in the voltage in the other secondary winding. The resulting output signal of the transducer induced in this fashion varies linearly with the displacement of the core with respect to the coil form.

The method by which the LVDT is integrated into the

apparatus and employed as a strain transducer is shown in Figure 3. Support arms (Dets. 35, 41) are fabricated of an epoxy-glass phenolic (NEMA grade G-7) which exhibits superior high-temperature dimensional stability; these arms are mounted to the upper and lower rams at points just above and below water cooling tubes respectively. The LDVT is located in a bored hole at the extreme end of the upper arm (Det. 41) and held in position by a screw which compresses the split end of the arm. In order to maintain the high linearity characteristics of the output signal of the LVDT, it is imperative that the moveable core be exactly concentric with the bore of the coil form. To accomplish this, threaded rods (Det. 40) were inserted into each end of the core; the core rods extend vertically in each direction through miniature ball bushings mounted in each of two L-shaped blocks (Det. 37) attached to the upper and lower surfaces of the support arm. The bearings are held in position by means of retaining rings (Det. 38) secured to the L-blocks with small, non-magnetic screws. Proper positioning of the moveable core is obtained by alligning the axis of each bearing mounting assembly with the axis of the coil form. In addition to providing the correct orientation, the ball bushings also afford friction-free travel of the core rod through the bore of the coil form.

The support arm (Det. 35) mounted to the lower load ram is fitted with a similar assembly of L-blocks (Det. 36, 37), retaining rings (Det. 38), and miniature precision ball bushings. In this case, the ball bushings maintained proper allignment of a stainless steel push rod (Det. 40) which supports the core rod assembly and provides mechanical linkage between the load rams. A precision micrometer head is mounted in the lower L-block to

provide a means of precisely positioning the moveable core of the LVDT at the null point and to facilitate calibration.

With the strain transducer assembly mounted on the loading rams, the effective gage length of the system is composed of the specimen length and the portions of the loading rams situated between the points of mounting of the phenolic support arms. Hence, in addition to changes in the length of the specimen as it deforms, the output of the strain transducer is subject to error components resulting from thermal expansions and contractions of the assembly and from mechanical deformation of the portions of the load rams between the support arms. In practice, however, the load rams under the maximum design stress of the apparatus are approaching only one-fourth of the yield stress, and the water cooling provides adequate protection against the possibility of plastic deformation. After a total of twenty-seven separate experiments involving temperatures from 500° to 1000°C., no permanent deformation of the rams was detected. Also, since all reported tests were performed under conditions of constant temperature, the deleterious effects of thermal expansion and contraction on the transducer output were minimal. Hence, the output signal of the LVDT reflects only the change in length of the specimen.

The primary coil of the LVDT is excited with a 3 kc signal. The induced secondary potential is fed into a shielded signal conditioning circuit which demodulates the AC signal to DC, thus providing a signal suitable for display and recording of the deformation on the second channel of the strip-chart recorder. Analysis of the experimental data was greatly facilitated by the simultaneous recording of stress (load) and strain on the same

chart, obtainable with the electronic circuit configurations described.

Temperature System. - Two separate resistive heating elements were employed to attain the range of temperatures required for the creep experiments. In the original design of the apparatus, provisions for accommodating only a single heat source in the form of a commercial, tubular muffle furnace were included. This furnace is assembled on a pair of mounting blocks (Det. 25) attached to two of the support bars (Det. 2) that separate the plates of the test stand. Vertical positioning of the furnace is accomplished by sliding the mounting block assembly along the support rods. This operation is facilitated by a pulley system (Dets. 26-28) mounted on the underside of the top plate; this allows a counterweight to be connected with a steel cable to the furnace mounting blocks.

Located along the length of the furnace are five equally spaced thermocouple wells oriented normal to the axis of the muffle; these provide access for sensing elements employed to measure the temperature of the specimen and monitor the temperature gradient along the rams.

In several preliminary test runs carried out to check the operation of the apparatus, it was evident that the heat losses resulting from the combined effects of the water cooling of the rams, convection and radiation of heat from the outer jacket of the furnace, and conduction along the rams were such as to prevent the temperature of the specimen from exceeding 650°C. In addition, the temperature gradient over the length of the specimen position was found to be of the order of 15°C. To counteract these deleter-

ious effects, a small, tubular heating element was designed which fits around the specimen and rests on top of the lower ram platen (Det. 44). Dramatic improvement of the temperature gradient over the specimen position was noted after installation of the heating element (see Chapter 4), and temperatures in excess of 1000°C are obtainable.

Chromel-alumel thermocouples were employed as sensing elements and compensated lead wires were used throughout the temperature system. Specimen temperatures are obtained directly from one thermocouple junction which passes through openings in the insulated jackets of both furnaces and contacts the specimen at the midpoint. The output signals of the thermocouples are indicated and recorded with a 24-channel recorder compensated for chromel-alumel junctions.

The specimen could be brought up to test temperature in either of two ways: (1) manually, by adjustment of the setpoint of a time-proportioning temperature controller; or (2) automatically, with a commercial, cam-type program controller operating with a current-proportioning function amplifier and a silicon-controlled power regulator. Upon reaching the test temperature in either mode, control is switched over to the time-proportioning controller which then maintains a constant temperature within ±1 °C. (The temperature recorder and controllers employed here were obtained from the Barber-Colman Company.)

Chapter 4

CALIBRATION

Temperature System. -

Chromel-alumel thermocouples encased in thin-walled stainless steel protection tubes were employed as sensing elements throughout the temperature system. The recorder and controllers used in the creep experiments to monitor and control temperatures were of the potentiometric type with calibrations based on the standard tables of electromotive force established by the National Bureau of Standards. Consequently, if the emf of a thermocouple used as the sensing element for one of these devices deviated from the standard value for a given temperature, the temperature actually measured would be in error by an amount proportional to the deviation. In order to eliminate this source of error in the temperature measurements, it was necessary to normalize the output of each thermocouple junction used in the experiments to the values specified in the NBS standard tables.

In order to establish reference points for the calibration procedure, five freezing-point standards were obtained from the National Bureau of Standards with values of the freezing points which nicely spanned the temperature range from 200° to 1000°C (see Table 1). These standard materials were used to calibrate a laboratory standard thermocouple; in turn, the junction was used to calibrate the working junctions used for experimental measurement.

TABLE 1

THERMOCOUPLE CALIBRATION POINTS

Freezing Point Standard	Freezing Point (C°)
Tin	231.88
Lead	327.417
Zinc	419.50
Aluminum	660.00
Copper	1083.30

To establish our laboratory standard thermocouple, each of the standard materials was melted in a crucible with a thin-walled protection tube and a cover (Figure 6). To prevent contamination of the standard materials, each crucible assembly was fabricated entirely of high purity graphite which also provided a reducing atmosphere for the metals while near their freezing points. In addition, a thin layer of powdered graphite was sprinkled on the exposed surface of the metals in the crucible. The precautions taken to prevent contamination and oxidation of the standard metals were necessary to ensure that the freezing points were not altered during the several temperature cycles to which each of the samples was exposed during the calibration. With a thermocouple junction inserted in the protection tube, each of the standard metals was heated to a temperature roughly 20°C above the freezing point and then allowed to cool slowly down through the calibration point while the emf of the thermocouple junction was observed with a Leeds & Northrup, Type K-3 potentiometer. The reference junction of the thermocouple was main-

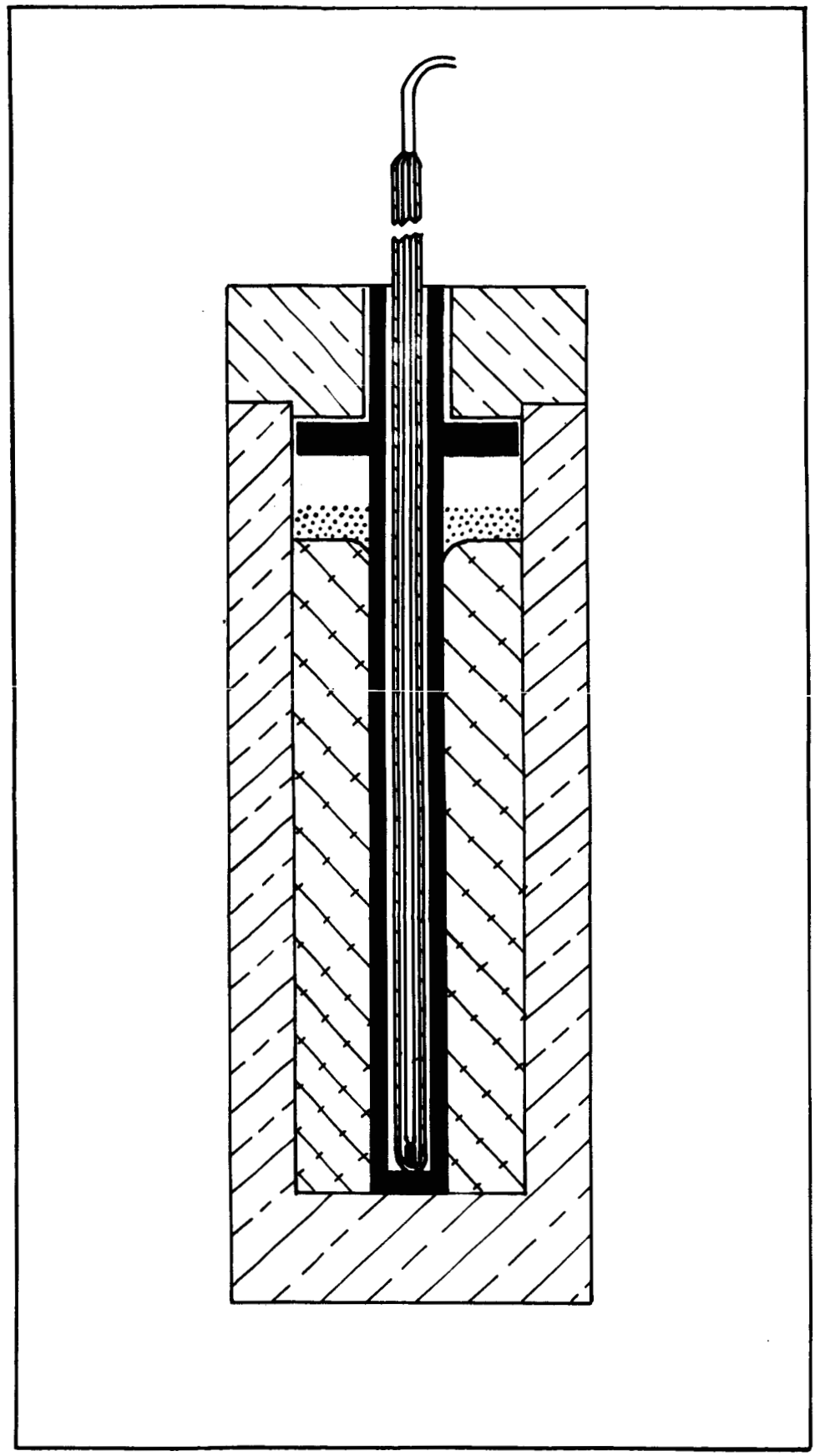

Figure 6. Graphite crucible and protection tube assembly used to protect the standard freezing point metals and the thermocouple during calibration.

tained at 0°C, during the calibration in an electronic ice-point bath accurate to ±0.025°C. The deviation between the observed and the standard value of the emf at each of the freezing point temperatures provided the data for a difference curve, which established the laboratory standard thermocouple. The junctions of our working thermocouples used in the creep tests and the laboratory standard were then simultaneously exposed to a succession of constant temperatures from 400° to 1000°C. while the emf of each junction was recorded. The differences in emf between each of the working junctions and the standard junction at each fixed temperature were then normalized by comparison with the difference curve previously established for the standard; and the calibration was completed by plotting a separate difference curve for each of the working junctions.

The experimental uncertainty associated with each emf difference value due to the combination of instrumental and observational errors is ±2 microvolts. In the temperature range from 500° to 1000°C, this error corresponds to a maximum uncertainty of ±0.05°C in the temperature indicated by the working junctions used in the creep tests, a negligible amount. Hence, the total uncertainty associated with the absolute temperature measurements is attributable solely to inaccuracies in the recorder and controllers which are of the order of ±0.25%.

The temperature associated with each of the creep experiments reported here was determined by the emf of the thermocouple junction located at the midpoint of the test specimen. In order that the measurements accurately reflect the temperature of the entire sample, it was necessary to verify the absence of an appreciable temperature gradient over the length of the specimen

while it was in the loading column. A preliminary test run was performed in which the temperature of a dunite specimen was determined at three points along the length. The maximum temperature difference observed between the center and ends of the sample was 1.5° at 500°C, 2.5° at 800°C, and 4.5° at 1000°C. Based on these observations, the total error in the absolute temperature measurements reported here is placed at ±6° over the range from 500° to 1000°C.

Strain Measurement System. -

As previously described, the strain measurement system consists of a transducer (LVDT) with an output signal which varies linearly in response to changes in length of the specimen, an electronic signal-conditioning network which provides the AC excitation and the demodulated output for the transducer, and a strip chart recorder for observation of the DC output signal of the transducer (see Chapter 3).

A common technique for calibrating a strain measurement system with this general configuration is to balance the AC voltage level energizing the primary coil of the transducer against the effective output response of the secondary coils. In this manner, the scale of the recording device indicates directly in absolute units of strain. An obvious advantage of this method is that the data is obtained in final form and requires no further reduction. However, since the scaling of the recording device involves an implicit dependence on the initial length of the sample, the calibration procedure must be repeated for each experiment if the initial lengths are not the same. Because the required adjustments are tedious and time consuming, this technique is practical only if the

test specimens are all of the same length initially.

The following approach to the calibration procedure was taken. When the initial lengths of the test specimens are not all identical but can be accurately determined, as is the case here, the measurement of the changes in length need not depend upon an absolute scale reference, but can be obtained on the basis of the relative differences between the initial and final values. In this situation, the variable actually measured is the change in length, and the strain is determined by a simple computation involving the known initial length. This approach is particularly suited to the strain apparatus employed here, since the only requirement is a determination of the sensitivity of the output signal of the transducer to an unit change in specimen length. By eliminating separate adjustments of the interrelated electrical parameters of the transducer for each test run, the technique provides a significant simplification without a sacrifice in accuracy.

For the calibration, the apparatus is assembled in the normal operational configuration, and the demodulated output signal of the transducer is displayed on the strip-chart recorder. By manually advancing the spindle of the micrometer head mounted in the lower support arm of the transducer assembly (Figure 3), a relative displacement of the ferrite core with respect to the transducer coils is produced which simulates a specimen deformation. The sensitivity of the strain measurement system was thus established at 3.0 millivolts per 0.001 inches of deformation with an experimental uncertainty estimated at $\pm 0.5\%$. A minor adjustment of the effective AC voltage energizing the primary winding of the transducer was required to place the sensitivity at this convenient value. With the sensitivity of the transducer

established at 3.0 millivolts per mil and a specimen length of one inch, the system is capable of resolving strains of the order of 10^{-6}.

Since the transducer assembly is mounted close to the outer jacket of the larger furnace, the ambient temperature of the transducer varied during the experiments from 15° to 25°C, above room temperature. The dependence of the sensitivity upon operating temperature was evaluated by repeating the calibration procedure with the specimen position stabilized at each of several typical test temperatures. Within the experimental error, no deviation of the sensitivity from the value determined at room temperature was detected at specimen temperatures of 500°, 750°, and 950°C.

The total experimental error associated with the strain measurements reported here includes contributions from the sensitivity calibration, the micrometer measurements of the initial specimen lengths, and reading errors in interpolation of the strip chart records; the overall uncertainty is estimated at ±2%.

Loading System. -

The loading system was calibrated by determination of the emf-force transfer characteristic of the load cell built into the loading column of the apparatus. For this purpose, a Baldwin-Lima-Hamilton Type C3P1 precision load cell was used with a known transfer characteristic accurate to ±0.1%. The calibration was carried out in the test apparatus; by removing the lower ram assembly and bearing housing, the standard load cell could be accommodated on the lower plate of the test stand. The cell to be calibrated was then positioned between the load button of the

standard cell and the upper ram. This assembly was loaded by activating the motor-actuator at the end of the lever arm. Both transducers were energized with remote-sensing, constant voltage sources. The output signals were simultaneously displayed on the dual-channel strip chart recorder, as the load applied to the assembly was varied over the linear range of the standard load cell.

A separate determination was made of the effective stress applied to the specimen by each of the cast iron plates used in several of the experimental runs to load the specimen in the dead-weight mode. With the BLH load cell resting on the base plate and accurately centered on the axis of the loading column of the apparatus, the change in output response resulting from the addition of each of the weights to the lever arm was recorded. As a check of the reproducibility of the calibration and to demonstrate the validity of the transfer characteristic established for the working load cell, the same procedure was repeated with the standard cell replaced with the working transducer. Within the experimental errors involved, the two determinations thus obtained for the stress produced by each of the weights were found to be in excellent agreement.

An overall uncertainty of ±1% is attributed to the applied stress values reported here.

Chapter 5

EXPERIMENTAL RESULTS

Introductory Remarks. -

By means of the two identical units of the uniaxial compression apparatus previously described, a total of twenty-two creep experiments have been carried out on unjacketed, cylindrical specimens of dunite from the Webster-Addie ultramafic ring in Jackson County, North Carolina. All of the experiments were performed at atmospheric confining pressure at temperatures ranging between 500° and 1000°C, and axial stresses up to 408 bars. The creep tests were carried out for durations ranging from 270 minutes to 61 hours. In order to obtain consistent results, a standard test procedure was adopted and systematically followed throughout.

Specimens. -

Dunite, or olivine rock, was selected as a specimen material primarily because of its close approximation to the composition generally considered to predominate in the top layers of the mantle. The Webster-Addie dunite was chosen because of its relatively competent, fracture-free mechanical structure. Since the petrologic aspects of the Webster-Addie intrusive complex have been previously described in considerable detail (Miller, 1953), only a brief summary of the pertinent characteristics of the dunite material used in the experiments will be presented here.

The dunite consists of transparent, colorless, angular-shaped grains of olivine imbedded in a serpentinized matrix. The olivine grains are well crushed and granulated; the grain fragments range in size from about 0.05 to 0.90 mm, with the average about 0.30 mm. The magnesium-iron ratio of the olivine is remarkably consistent throughout the complex; it varies over a very narrow range and, on the average, corresponds to approximately ninety-three percent Mg_2SiO_4. Compositionally, the dunite consists of approximately eighty-five percent olivine; the remaining fifteen percent is composed mostly of serpentine (antigorite) with very sparsely scattered grains of enstatite and chromite. The enstatite grains are also well crushed and fragmented. According to Miller (1953), the serpentinization of the olivine occurred during a post-intrusive stage of alteration; and at least two stages of post-emplacement deformation are responsible for the granulation and crushing of the olivine and enstatite apparent in thin-sections. The olivine grains are randomly oriented; apparently, any initial preferred orientation the grains may have exhibited after intrusion was eliminated during the several subsequent deformational episodes. The serpentinized material which surrounds the individual olivine grains is uniformly fine grained, with an average grain size of about 0.05 mm. Overall, the dunite is quite uniform in texture and composition, mechanically isotropic, and free of macroscopic structural defects.

The twenty-two specimens were diamond-core drilled from two large blocks of the Webster-Addie dunite. Due to the random orientation of the grain elements, it was unnecessary to

consider the relative orientation of the specimens cored from the two separate blocks. However, the specimens obtained from each block were identically oriented. Cylinders cored from the blocks were first cut to appropriate length, and the ends were then lapped flat and parallel to within ±0.0001 inches to ensure full contact with the loading surfaces of the rams. The specimens were approximately 0.725 inches in diameter and from 1.000 to 1.090 inches in length.

Experimental Procedure. -

The standard experimental procedure adopted in the creep tests was as follows:

With the prepared specimen and small furnace inserted between the load rams, the outer furnace was positioned so that the specimen was at the mid-point of the heating element. In this position, the central thermocouple well of the large furnace was precisely alligned with a small opening in the wall of the inner furnace, thus permitting direct contact of a thermocouple junction with the surface of the specimen. After water cooling of the rams was initiated, the temperature indicated by the thermocouple in direct contact with the specimen was raised at the rate of 100°C. per hour until the pre-determined test temperature was attained. Thereupon the specimen was heat-soaked at constant temperature for a period of twelve hours to permit the system to reach thermal equilibrium. At the completion of the thermal equilibration loading of the specimen was carried out and observation of the deformation began. And at the termination of a run, the specimen was unloaded and allowed to cool at about the same rate as before, 100°C. per hour.

During the heating and soaking procedure, the only load applied to the specimen was the negligible tare weight exerted by the upper ram. Also, since the rates of heating and cooling of all specimens were slow, it is unlikely that the instantaneous temperature difference between the center and surface of the specimens exceeded 1°C. Therefore, it is reasonable to assume that no significant internal stresses were developed in the specimens prior to loading.

In addition to the time involved with the actual test which varied from 270 minutes to 61 hours, each experiment required from 40 to 50 hours for preparation of the specimen, assembly of the apparatus, and the heating and cooling of the specimen. Reduction of the data required about 10 hours for each experiment.

Discussion of the Results. -

Each of the twenty-two creep experiments was carried out at a single, constant temperature. In eighteen tests, the axial stress was also maintained at the same level throughout, and in four experiments the stress was varied in discrete increments during the course of the runs. The deformation records of the twenty-two creep tests are shown in Figures 7 to 10, and the pertinent experimental data and conditions of deformation are summarized in Table II. Each test run was identified by either a "W" or a "WA" designation, indicating from which of the two dunite blocks that particular specimen was obtained. The curves plotted in Figures 7 to 10 represent exact reproductions of the original data recorded on the strip-charts, but with the time scale considerably foreshortened. Fluctuations in room

TABLE II
SUMMARY OF EXPERIMENTAL CREEP DATA

Run Number	Temp. (°C.)	Axial Stress (bars)	Max. Strain (%)	Steady-State Creep Rate (10^{-7} sec^{-1})	Duration of Run (mins.)
W-1	900	408	1.255	0.942	1680
W-2	800	408	0.585	0.183	1320
W-3	600	408	0.339	~0.0	1440
W-4	700	408	0.543	0.104	1440
W-5	500	408	0.261	~0.0	3660
W-6	1000	408	1.752	4.039	270
W-7	900	226	0.549	0.239	1300
WA-1	950	408	0.697	1.656	360
WA-2	950	408	1.195	1.952	480
WA-4	850	288	1.329	0.833	465
WA-6	600	408	0.311	~0.0	1400
WA-7	850	408	0.441	0.679	480
WA-8	850	408	0.367	0.341	420
WA-9	900	288	0.558	0.372	513
WA-11	850	226	0.281	0.273	490
WA-23	950	288	0.521	0.659	489
WA-25	800	226	0.270	0.301	491
WA-27	800	226	0.342	0.326	628

TABLE II (con't.)

Run Number	Temp. (°C.)	Axial Stress (bars)	Max. Strain (%)	Steady-State Creep Rate (10^{-7} sec^{-1})	Duration of Run (mins.)
WA-27	800	288	0.342	0.715	628
WA-27	800	226	0.342	0.321	628
WA-30	850	408	0.612	0.886	552
WA-44	800	226	0.469	0.199	1410
WA-44	800	288	0.469	0.285	1410
WA-44	800	408	0.469	0.345	1410
WA-45	850	226	0.391	0.350	615
WA-45	850	288	0.391	0.661	615
WA-45	850	226	0.391	0.352	615
WA-47	950	288	0.562	0.740	690
WA-47	950	226	0.562	0.441	690
WA-47	950	408	0.562	1.402	690
WA-47	950	226	0.562	0.462	690

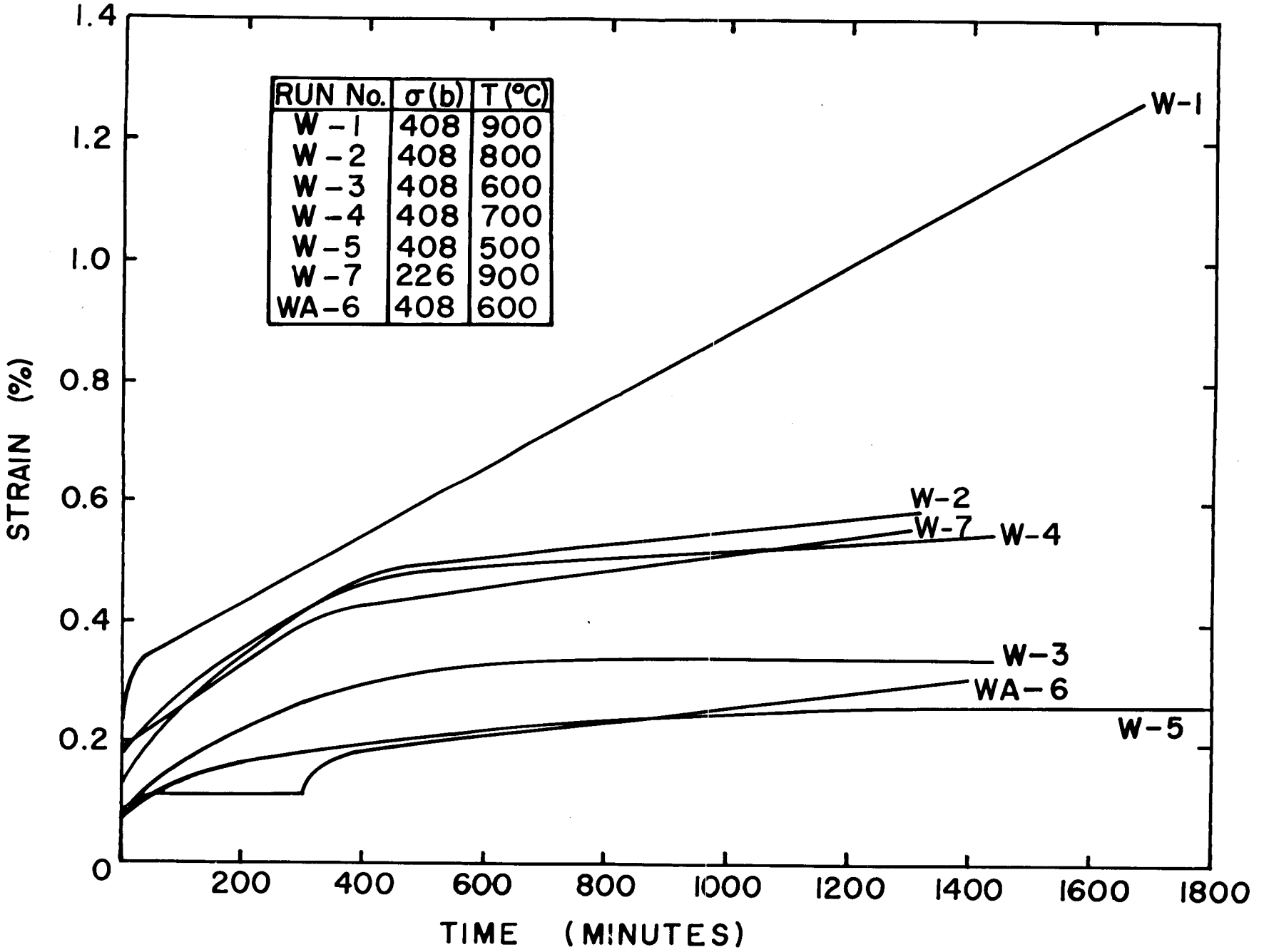

Figure 7. Creep curves for experiments of longest duration showing the effects of temperature.

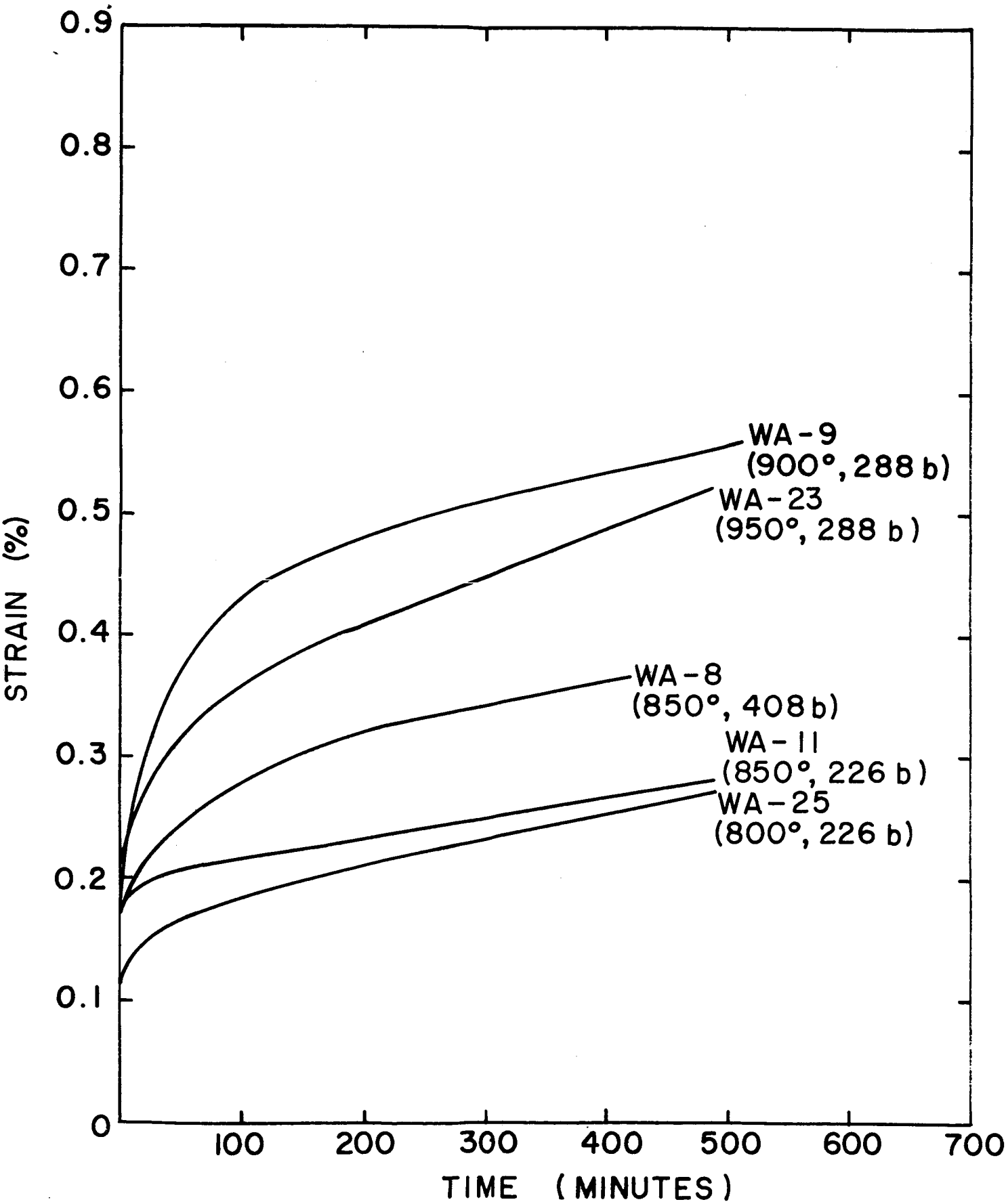

Figure 8. Effect of high temperature and low to intermediate axial stress on the creep of dunite.

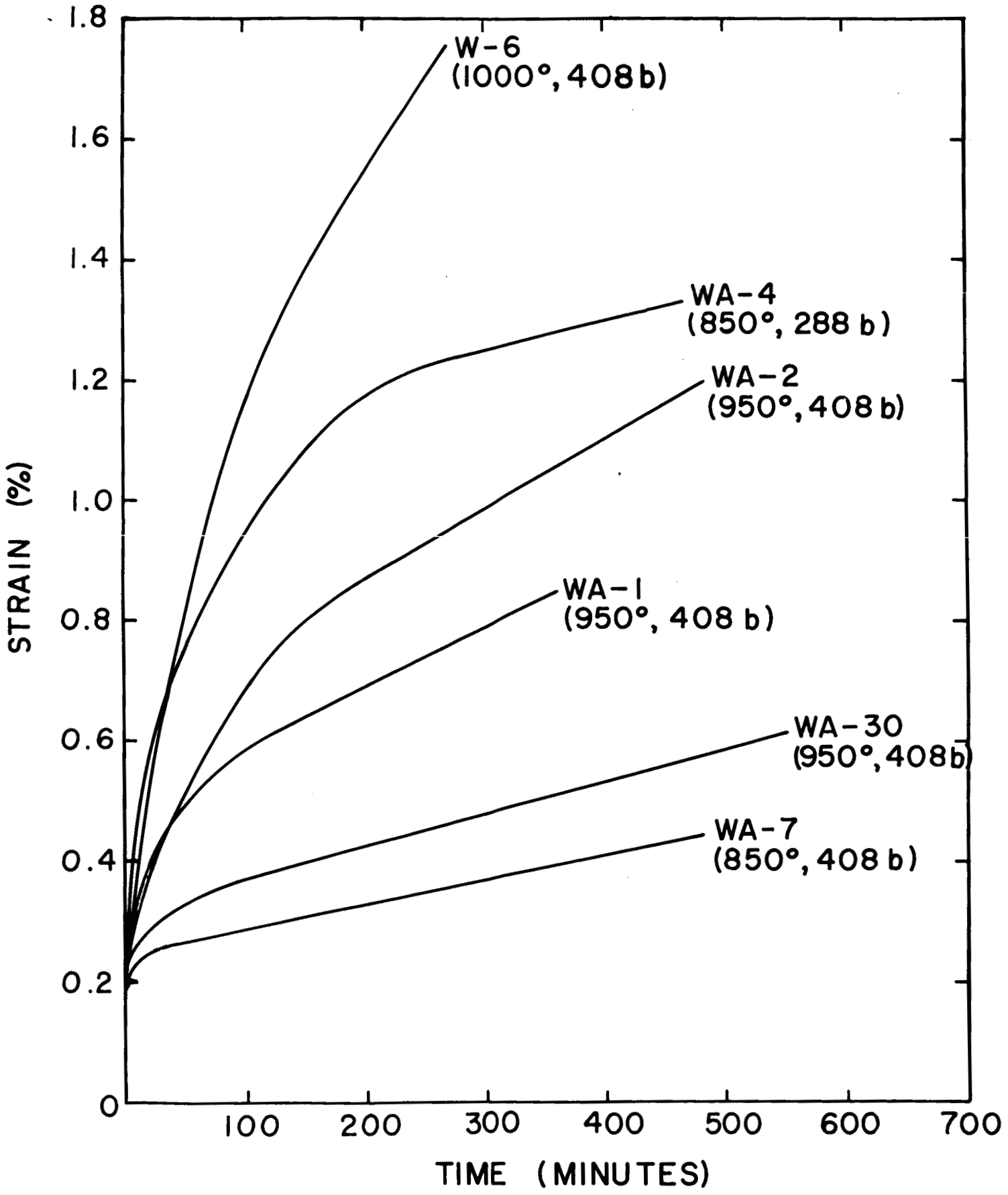

Figure 9. Effect of high temperature and intermediate to high axial stress on the creep of dunite.

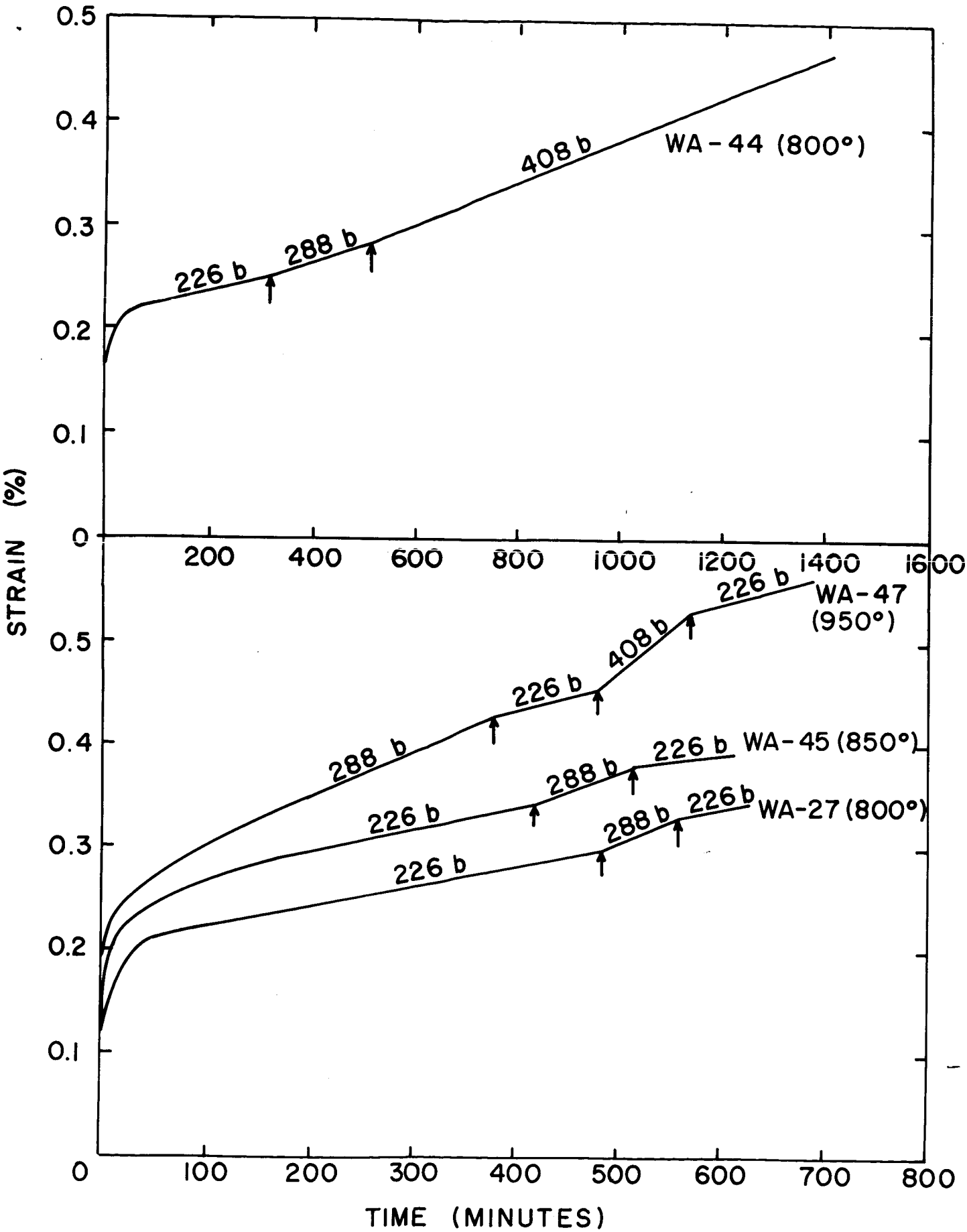

Figure 10. Effect of incremental loading at constant temperature on the creep of dunite.

temperature during the experiments caused thermal contraction and expansion of the push rod (Det. 39) in the strain transducer assembly, which produced small, short-period excursions from the mean, instantaneous strain in the original records. Since these thermal perturbations never exceeded about 2% of the instantaneous value of strain, the fine-structured details of the deformation records were lost in the scale reduction and lie within the line width of the curves shown in the figures.

The creep curves exhibited by the dunite specimens are generally similar to those obtained by previous investigators for most other materials and consist of several components: (a) an instantaneous, mostly elastic deformation represented by the non-zero strains indicated at zero time, which may also contain components due to non-elastic effects, such as the closing of voids; (b) a period of deformation in which the total strain increases with time but at a decreasing rate, or transient creep; and (c) a deformation which proceeds uniformly with time, or steady-state creep. Tertiary, or accelerated-rate creep did not occur in the experiments.

Figure 7 shows the creep curves obtained in the experiments of longest duration. Six of the seven runs shown were carried out under a stress of 408 bars at temperatures ranging from 500° to 900°C., thus providing an indication of the effect of temperature. At 500°C. (W-5), and in one of the two runs at 600°C. (W-3), only the transient stage of creep was observed, with the deformation either ceasing completely or continuing at an imperceptible strain rate after a time, as is characteristic of the "cold creep" stage. Run WA-6 was also performed at 600°C. and at a stress difference of 408 bars, but the test pro-

duced the only singular results of the investigation. The data obtained in run WA-6 are discussed separately later and are excluded for the present. Transient creep was also observed at temperatures from 700° to 900°C., at 408 bars; in this temperature range, however, the deformation also continued into the "hot creep", or steady-state creep regime, as indicated by the linear increase of the total deformation with time following the transient creep stage (runs W-1, W-2, W-4). Run W-7 was carried out at the same temperature (900°C) as run W-1, but at roughly one half the stress difference, and is included in Figure 7 to indicate the general effect on the steady-state creep behavior of increasing axial stress at constant temperature.

It was apparent from these initial results that the steady-state creep behavior of dunite could be expected to occur at perceptible rates of deformation only at temperatures above 700°C. Hence, the remainder of the investigation was devoted to determination of the details of the steady-state creep deformations exhibited at temperatures from 800° to 1000°C. Figures 8 and 9 show the results of eleven creep tests carried out at temperatures in this range, and at axial stress differences ranging from 226 to 408 bars. Both transient and steady-state creep were observed in each experiment. Only one test, run W-6, was performed at 1000°C; the experiment was terminated prematurely when the Nichrome heating element of the internal furnace burned out, but a steady-state deformation rate was established prior to the failure.

Figure 10 shows the results obtained in the four experiments in which several different stresses were applied to the specimen during the course of the tests. In these runs, the stress was incremented only after a rate of steady-state creep had been

established at the initial stress level; thus, several steady-state creep rates were obtained for each of the specimens deformed in this manner.

(1) Total Strain. -

As anticipated, only small total strains were produced by the conditions of deformation imposed in the experiments. As shown in Figures 7 to 10 and in Table II, the largest deformation observed was the 1.75% strain experienced by specimen W-6, deformed at 1000°C, and a stress difference of 408 bars. Only four specimens were deformed by more than 1%, and most of the deformations proceeded to only about 0.5% strain. Assuming a Poisson's ratio of 0.3 for dunite, the deviation from constant stress conditions occurring during a total deformation of 1% amounts to only 0.3%. Thus, to a very good approximation, the constant loads applied to the specimens resulted in deformations at constant stress.

In general, the total strain experienced by the specimens exhibited good consistency. Increases of either temperature or stress difference produced systematic increases of the total deformation. However, there are some noticeable deviations from this general pattern. The creep curves shown in Figures 8 and 9 have been combined and replotted in Figure 11 to illustrate the discrepancies in the total deformation obtained in the experiments. For example, specimen WA-4 was deformed at a temperature of 850°C., and a stress difference of 288 bars; yet, the total strain observed during the run was exceeded only by that experienced by the single specimen (W-6) deformed at 1000°C., and 408 bars stress difference. Similarly, the total strain

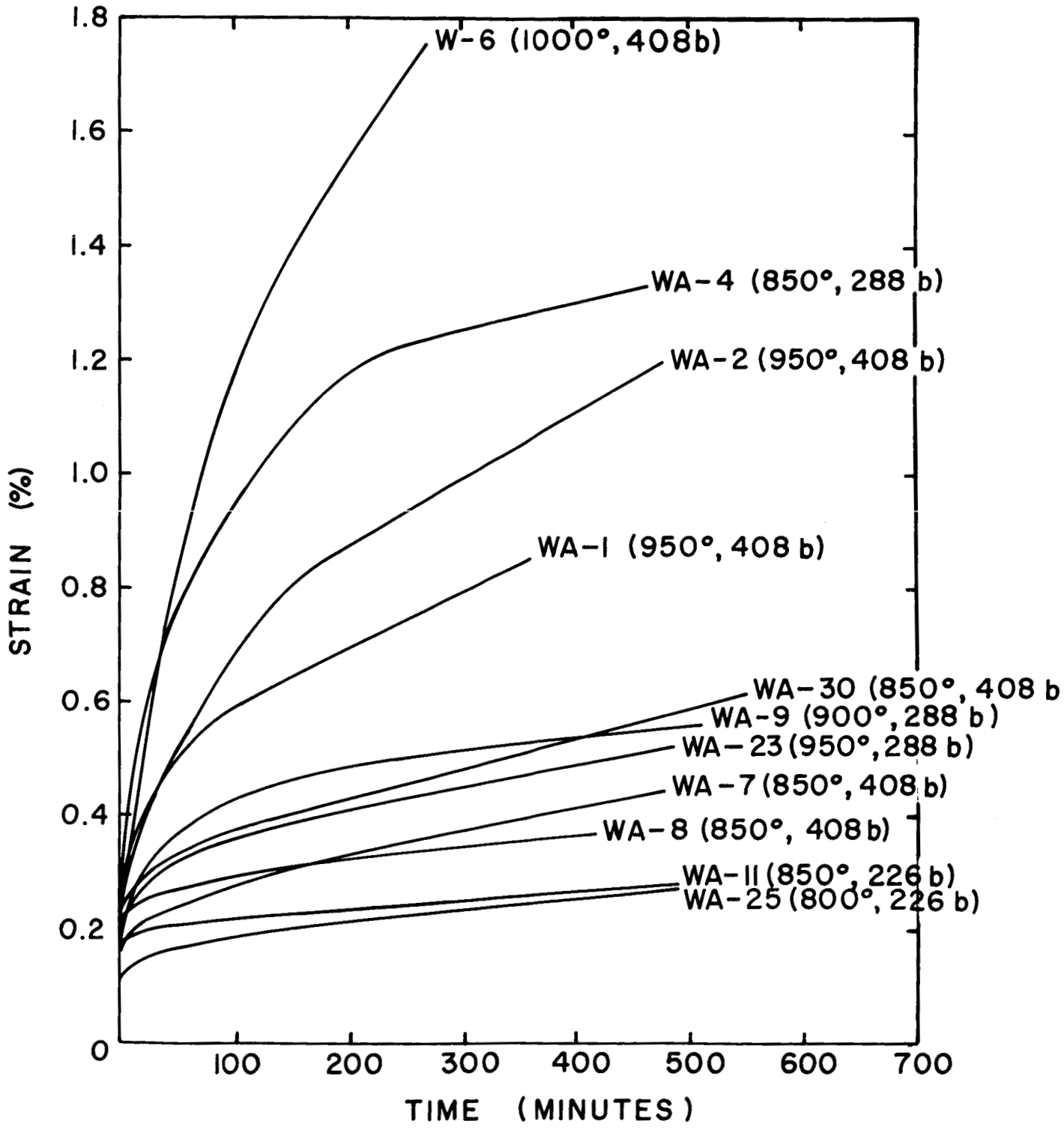

Figure 11. Reproducibility of creep curves.

experienced by specimen WA-23 deformed at a temperature of 950°C., and a stress difference of 288 bars was less than that of three specimens (WA-4, WA-9, WA-30), deformed at either lower stress difference or lower temperature.

(2) Reproducibility of the Data.-

Because creep experiments consume a great deal of time, it was not possible to repeat all of the tests reported here. However, to gain some knowledge of the reproducibility of the results, two sets of experimental conditions at which steady-state creep deformation was observed were each repeated three times. The experimental conditions and the results obtained in these six tests are summarized in Table III, and the creep curves are shown in Figure 12.

Shown in Figure 12(a) are the creep curves obtained for the three specimens (WA-25, WA-27, WA-44), deformed at a temperature of 800°C., and under a differential stress of 226 bars. It should be noted that specimens WA-27 and WA-44 were also deformed at several other values of applied stress; however, the creep curves for these specimens shown in Figure 12(a) include only the deformation record for 226 bars. The differences in total strain experienced by the three specimens are very small; after five hours of deformation at 226 bars, the maximum difference recorded was less than 0.03% strain. The steady-state creep rates observed in the runs ranged from $0.199 \cdot 10^{-7}$ sec.$^{-1}$ to $0.324 \cdot 10^{-7}$ sec.$^{-1}$, with an arithmetic mean of $0.274 \cdot 10^{-7}$ sec.$^{-1}$. The creep rates obtained for specimens WA-25 and WA-27 are in excellent agreement and differ by less than 8%. The creep rate recorded for specimen WA-44 differed from the values obtained for specimens WA-25 and WA-27 and

TABLE III
REPRODUCIBILITY OF DATA

Run Number	Temp. (°C.)	Axial Stress (bars)	Strain after 5 Hours (%)	Steady-State Creep Rate (10^{-7} sec^{-1})
WA-25	800	226	0.235	0.301
WA-27	800	226	0.259	0.324
WA-44	800	226	0.250	0.199
WA-7	850	408	0.370	0.679
WA-8	850	408	0.342	0.341
WA-30	850	408	0.478	0.886

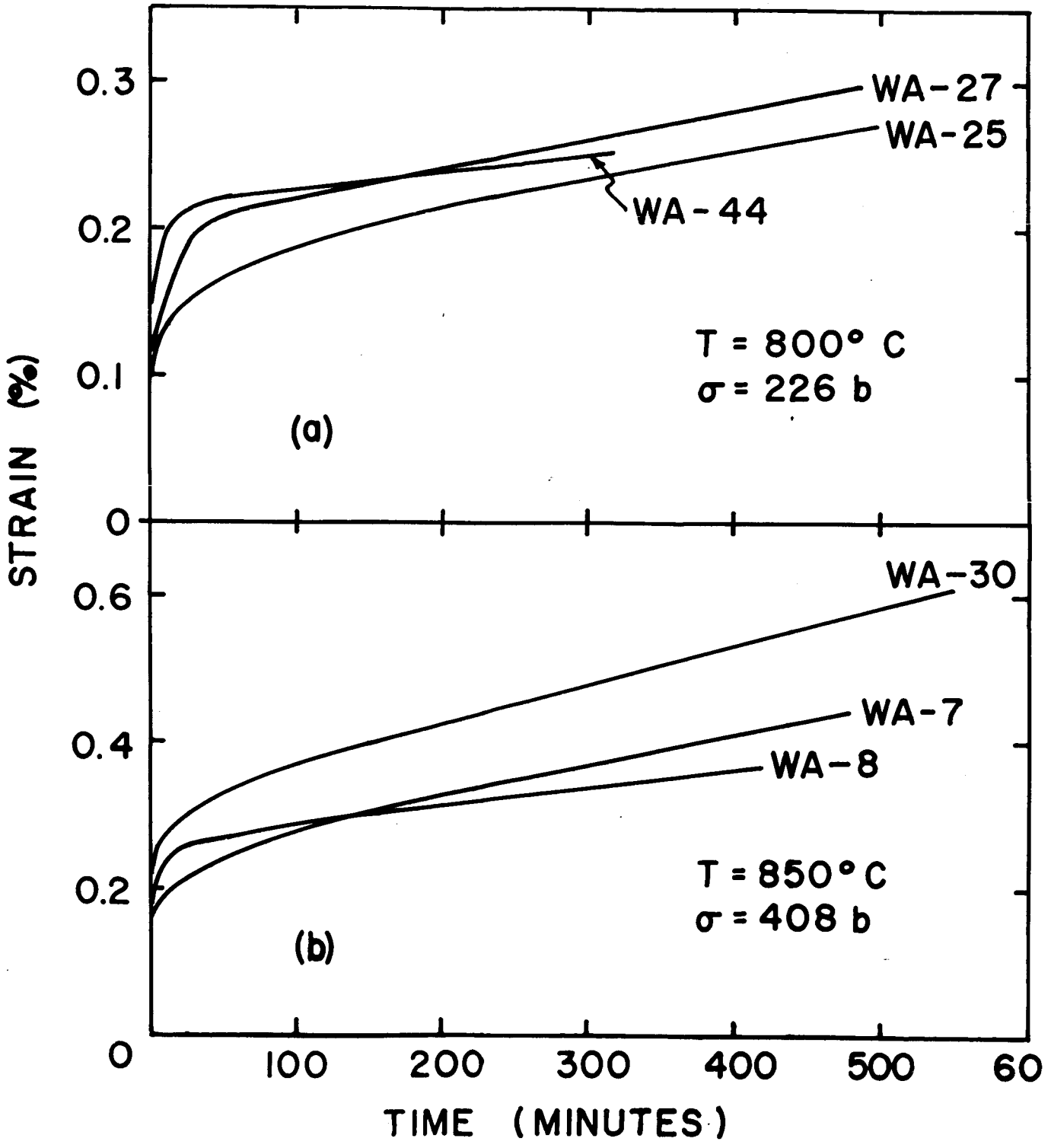

Figure 12. Reproducibility of creep curves.

(3) Effect of Stress on Steady-State Creep.-

The creep curves for the seventeen experiments performed at temperatures from 800° to 950°C., in which steady-state creep was observed are plotted separately according to temperature in Figures 13 to 16. In general, the results show that an increase in axial stress at constant temperature gives rise to an increase in both the rate of steady-state deformation and the total strain experienced by the specimen during all stages of the deformation; this effect is most clearly indicated by the creep curves for the four specimens (WA-27, WA-44, WA-45, WA-47), on which the differential stress was incremented during the steady-state phase of the deformation.

Figure 17 shows the experimentally observed steady-state creep rates plotted as a function of axial stress difference with temperature as a parameter. The curves shown in Figure 17 represent the best fit to the data points obtained for each test temperature in the range from 800° to 950°C., and indicate the magnitude of the dependence of steady-state creep rate upon axial stress. An increase in axial stress from 226 bars to 408 bars increases the steady-state creep rate by a factor of 1.5 at a temperature of 800°C; at 950°C., the same change in axial stress difference increases the rate of viscous creep by a factor of 4.0.

The non-linearity of the curves shown in Figure 17 illustrates the extremely non-Newtonian behavior of the specimens in steady-state creep. The non-Newtonian viscosity exhibited by crystalline materials in the region of viscous creep has been established experimentally, first by Andrade, and leads to the

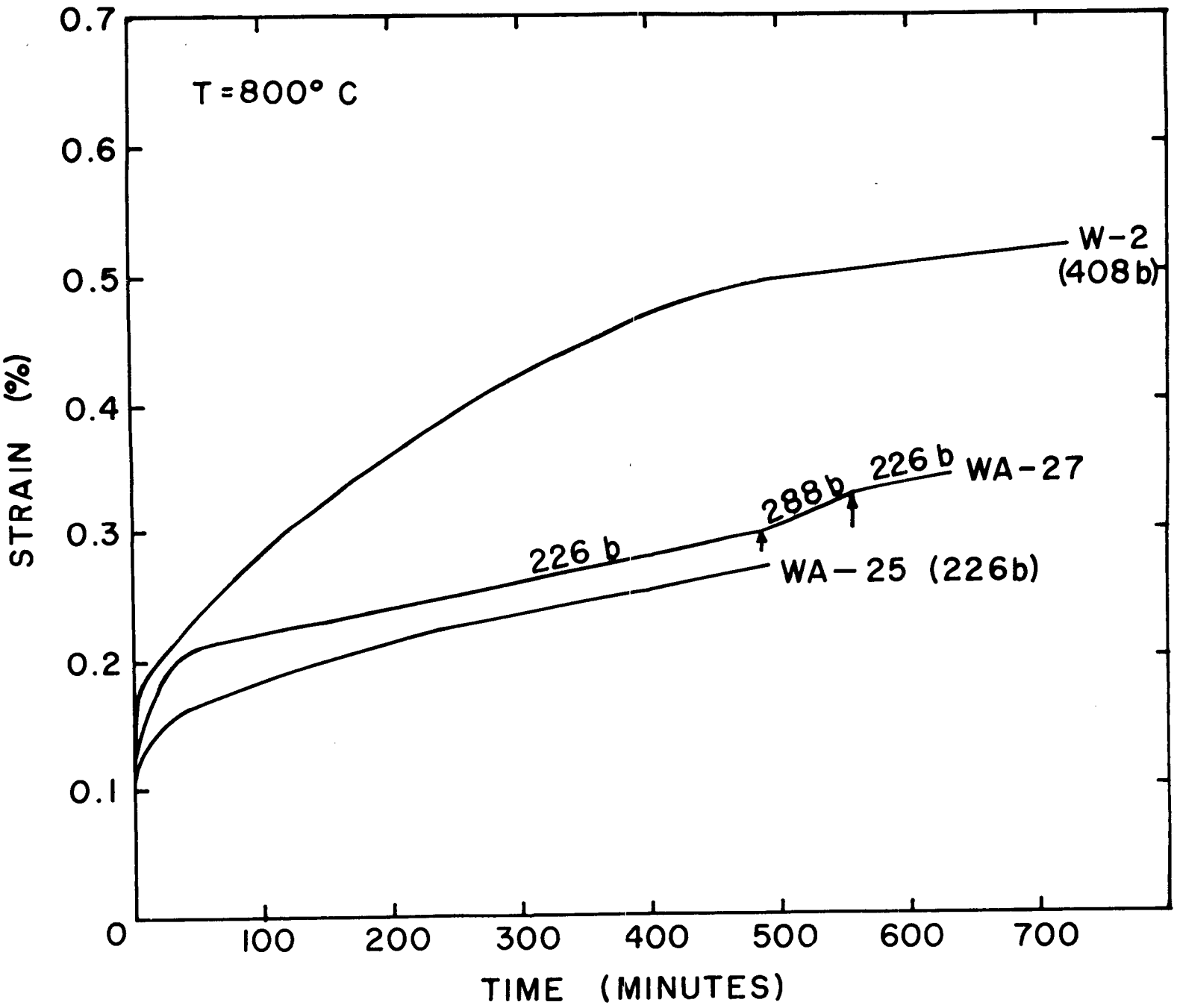

Figure 13. Effect of axial stress at 800°C.

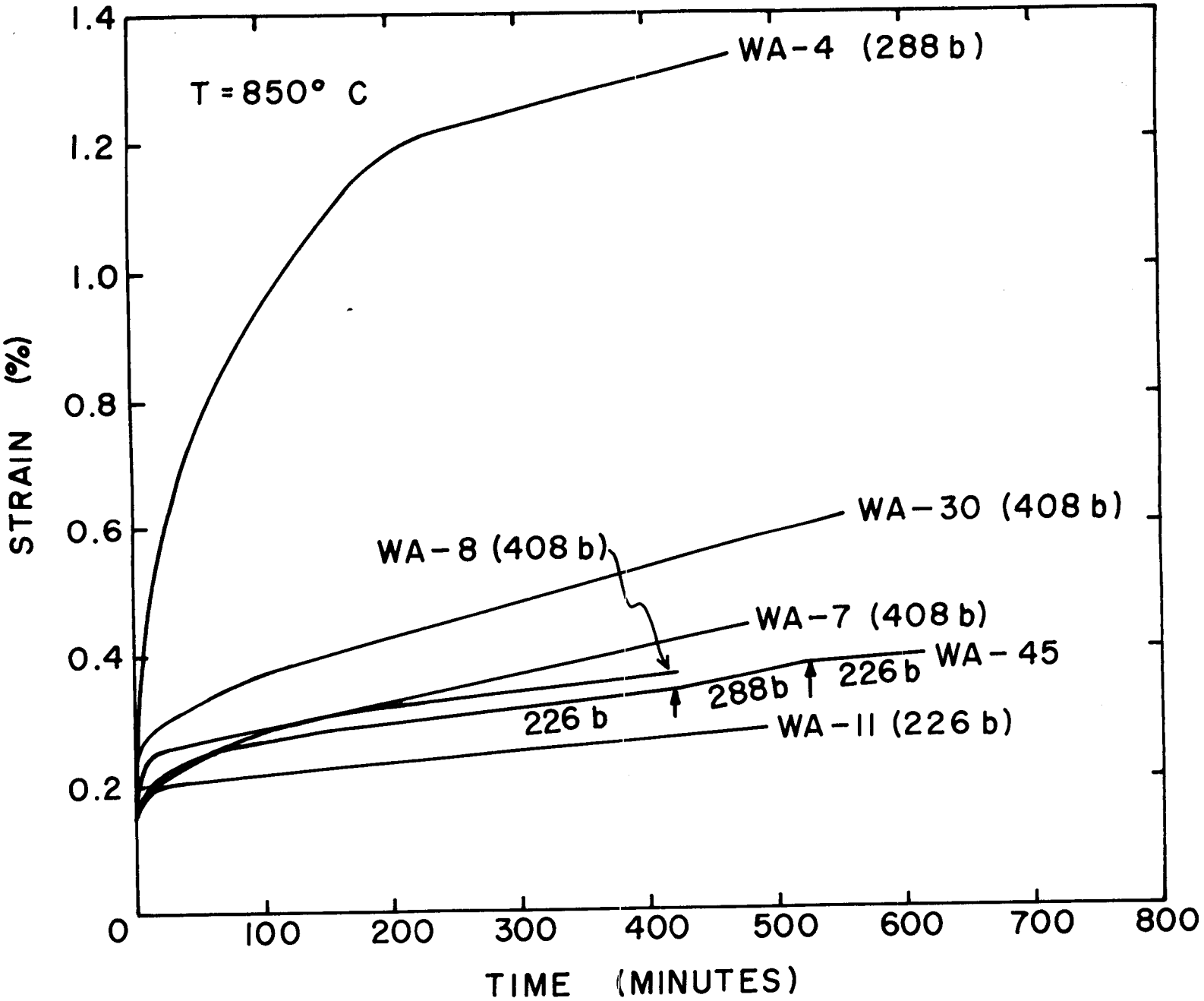

Figure 14. Effect of axial stress at 850°C.

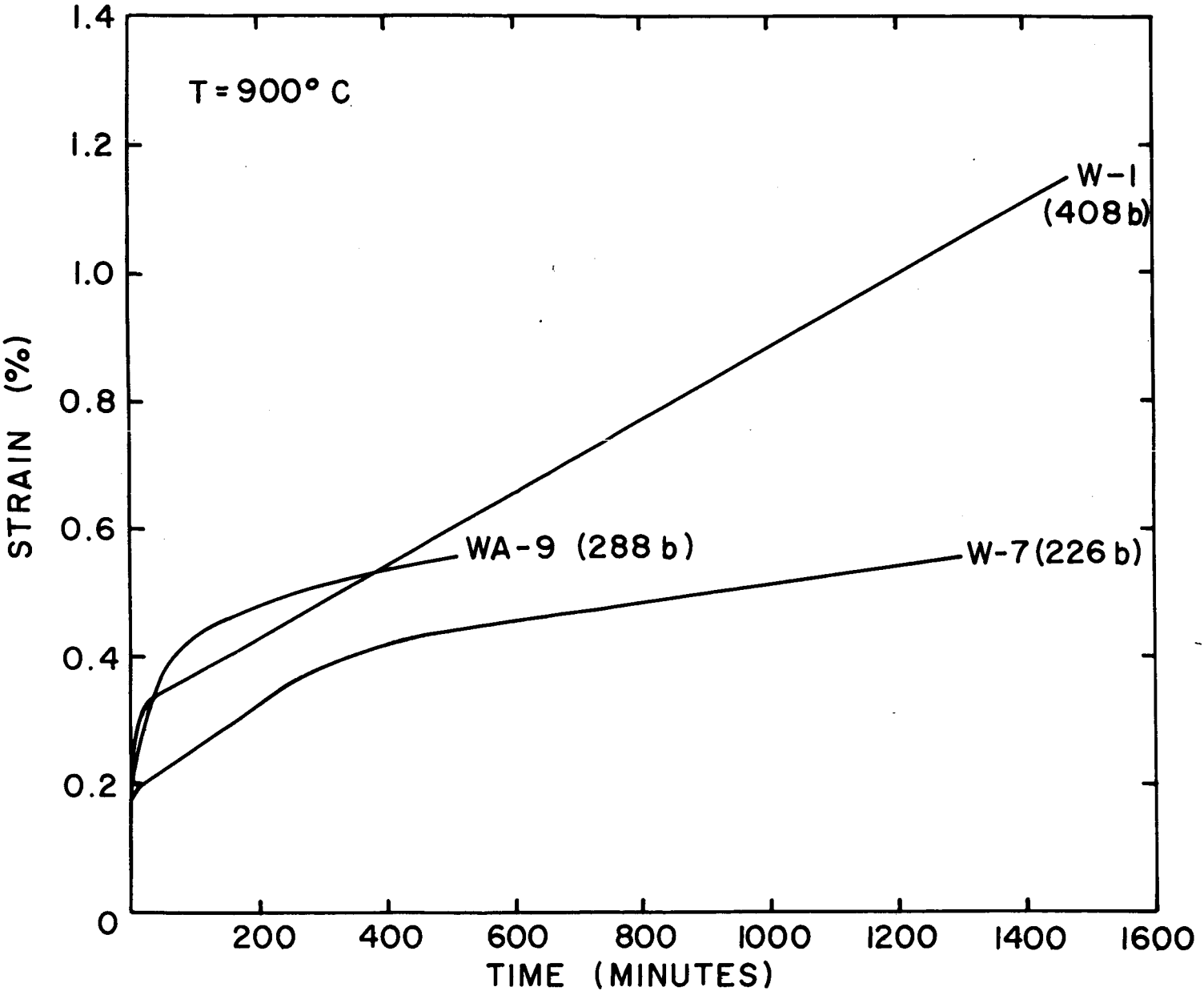

Figure 15. Effect of axial stress at 900°C.

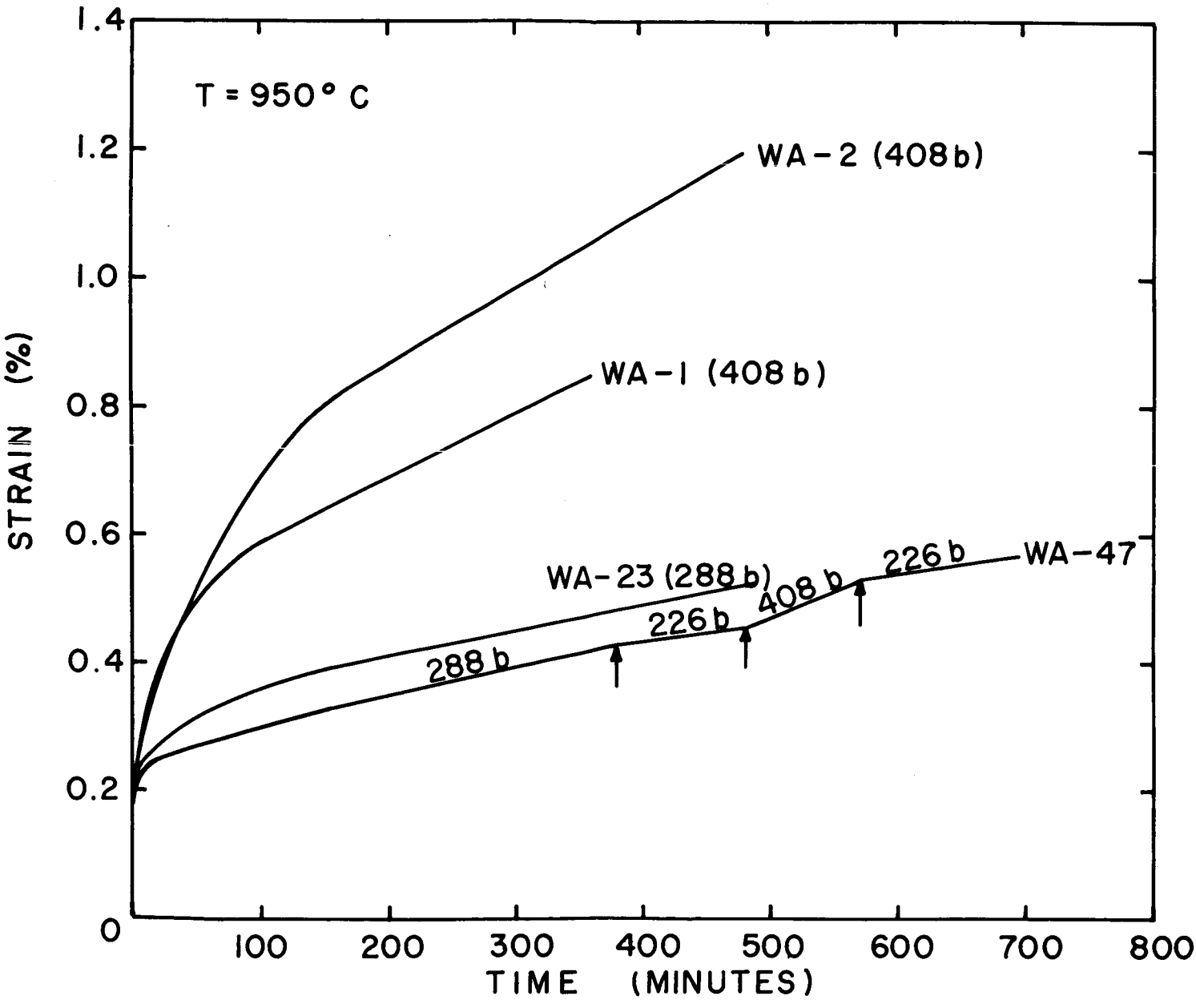

Figure 16. Effect of axial stress at 950°C.

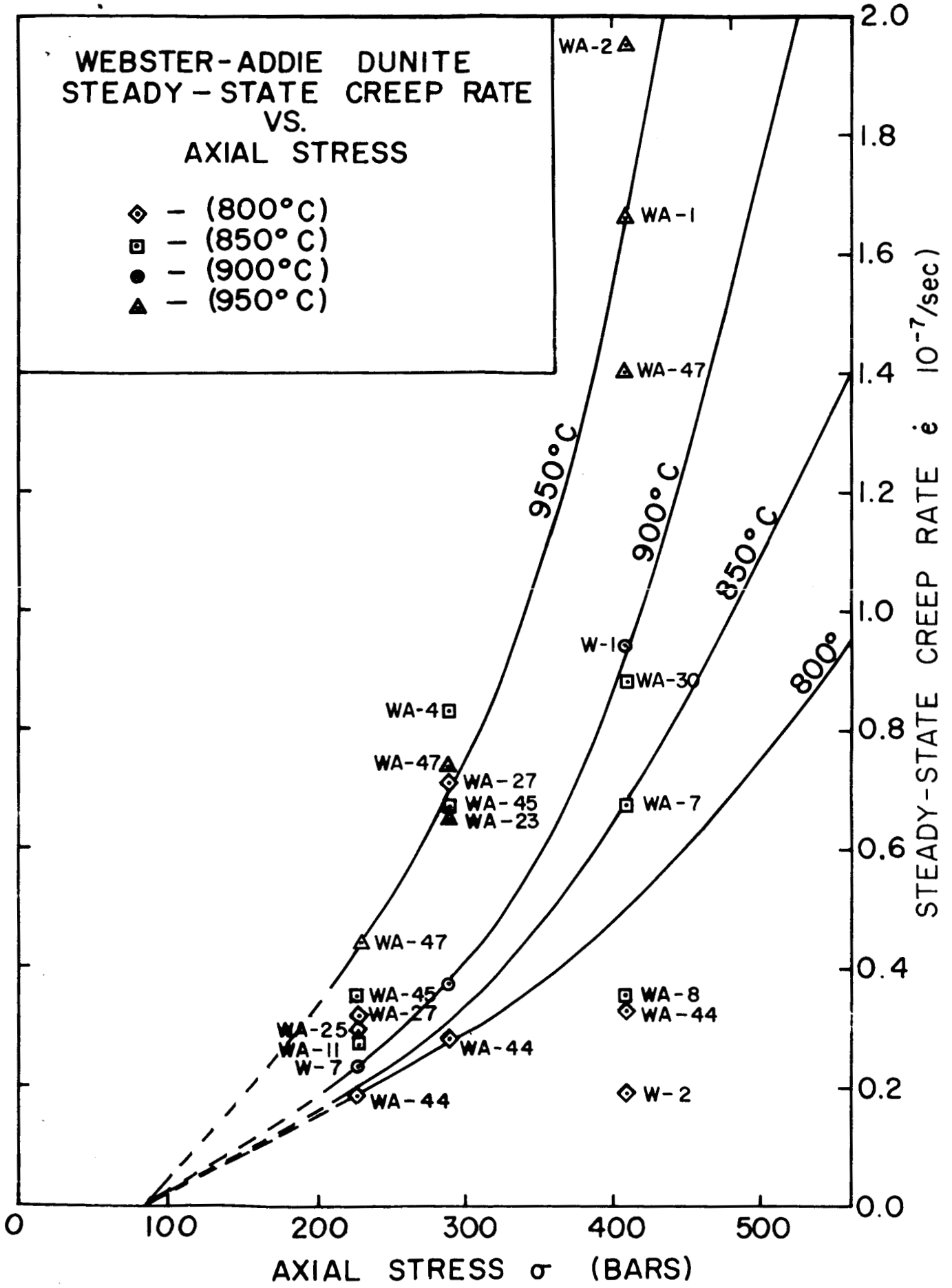

Figure 17. Variation of the steady-state creep rate with axial stress at constant temperature.

concept of a "creep strength", or a stress below which steady-state creep proceeds at a slow or imperceptible rate. The extrapolations of the curves shown in Figure 17 to zero creep rate indicated by the dashed-line segments represent continuations of the minimum slope obtained in the curves fitted to the data points and are, therefore, only approximate. However, the extrapolations do provide an order of magnitude estimate of the Andradian creep strength of dunite in the region of "hot creep" behavior of about 80 bars.

(4) Effect of Temperature on Steady-State Creep. -

In Figure 18, the steady-state creep rates observed in the experiments are plotted as a function of temperature with the applied stress difference as a parameter. The curves represent the best fit to the data obtained at 226, 288, and 408 bars. The results show a systematic increase in the rate of steady-state creep with temperature. The data obtained at stress differences of 226 and 408 bars show excellent consistency; at a stress of 288 bars, the data points exhibit some scatter, but the overall pattern is apparent. As shown by the curves in Figure 18, temperature is the dominant parameter affecting steady-state creep; a small increase in temperature produces a marked increase in the rate of steady-state creep at all stress differences employed in the experiments. The results indicate that for an increase in temperature from 700° to 950°C., the rate of deformation is increased by a factor of 5 at 226 bars stress difference, by a factor of 9 at 288 bars, and by a factor of 17 at 408 bars. The magnitude of the temperature dependence thus obtained for 408 bars is also consistent with the results obtained in the single

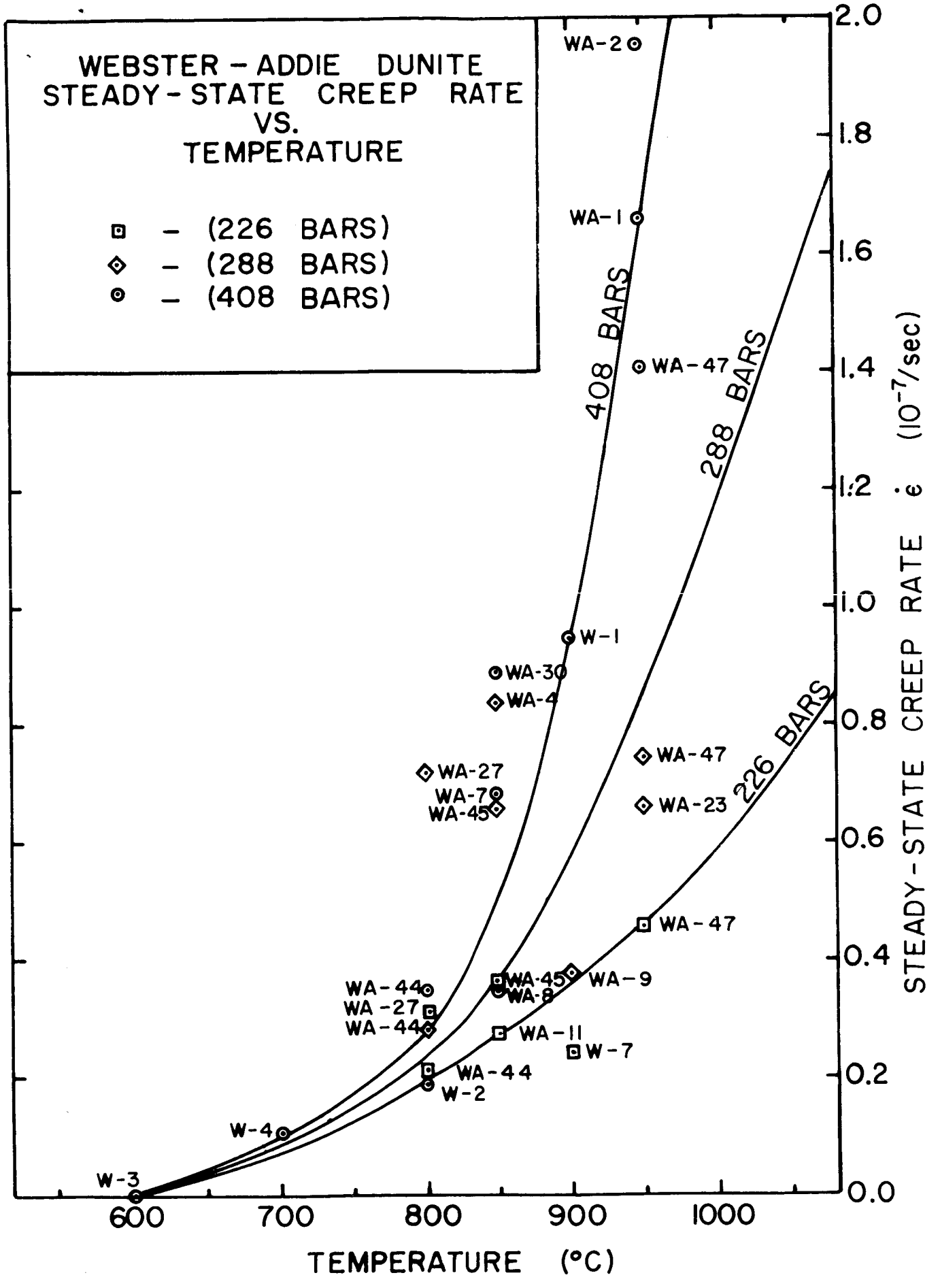

Figure 18. Variation of the steady-state creep rate with temperature at constant axial stress.

experiment carried out at a temperature of 1000°C., in which a steady-state rate of creep of $4.039 \cdot 10^{-7}$ sec.$^{-1}$ was obtained. The results indicate that compared to the effects of temperature, there is a relatively small dependence of the rate of steady-state strain on axial stress; this demonstrates that temperature, and not stress difference, is the primary rate-limiting parameter affecting viscous creep.

(5) X-Ray Analysis of the Deformed Specimens. -

To ascertain whether the specimens had experienced any changes in mineralogy as a result of the conditions of temperature and axial stress difference imposed in the experiments, powder samples of the test specimens as well as the original, undeformed material were subjected to x-ray diffraction analysis (Cu-$K\alpha_1$). The results of the analysis are the following:

(i) Two samples of the undeformed dunite rock were analyzed, representing each of the two blocks of material from which the test specimens were obtained. The x-ray patterns were essentially identical and indicated the presence of the olivine, serpentine, and sparsely scattered grains of enstatite apparent in thin-section. Due to the very small amount of enstatite in the original dunite, only the three peaks of greatest intensity were represented in the x-ray pattern.

(ii) The x-ray patterns obtained for the samples deformed at 500°C. (W-5), and 600°C. (W-3), were found to be practically identical to those of the undeformed material. Bowen and Tuttle (1949) have reported that magnesian serpentine cannot exist at tempera-

tures above 500°C., but undergoes dehydration at this temperature. Presumably, the rate of reaction is sufficiently slow to account for the presence of antigorite in specimen W-3, deformed at 600°C. It is unlikely that the measured temperature of the specimen is in error by more than a few degrees, an amount insufficient to explain the presence of the serpentine.

(iii) The x-ray patterns obtained for the specimens deformed at temperatures from 700° to 1000°C. are all very similar with respect to structure and peak intensity. The peaks corresponding to serpentine are uniformly absent, and the intensities of the olivine and enstatite peaks show systematic increases with temperature, relative to the corresponding peaks represented in the pattern of the undeformed material. These results indicate that the serpentine (antigorite) originally present in the specimens has been dehydrated and transformed to olivine and enstatite, following the reaction:

$$Mg_6Si_4O_{10}(OH)_8 \qquad 2Mg_2SiO_4 + 2MgSiO_3 + 4H_2O\,.$$

Bowen and Tuttle (1949) have shown that the dehydration process is independent of pressure and depends only on temperature. Therefore, it is reasonable to assume that the transformation to olivine and enstatite of the serpentine was completed in the specimens deformed at temperatures of 700°C., and above, prior to the time of initial loading. It also follows that the

volume changes accompanying the dehydration occurred before the specimens were loaded, and, therefore, do not appear in the creep records as a pseudo-deformation. Consequently, the steady-state creep data obtained in the investigation refer to specimens composed only of olivine and enstatite.

(iv) Referring again to Figure 6, the only anomalous behavior observed in the investigation occurred during the deformation of specimen WA-6. Specimen WA-6 was deformed under the same conditions of temperature (600°C.), and stress difference (408 bars), as specimen W-3, which exhibited only transient creep behavior, with the deformation terminating completely after about fifteen hours of loading at constant stress. However, the results obtained for specimen WA-6 were quite different. After an initial, rapidly developed transient creep stage had terminated in an extended period during which no measurable deformation was observed, specimen WA-6 suddenly experienced a second, distinct deformational episode; the characteristics of both transient and steady-state creep were exhibited during this second period of deformation. The reasons for this unusual behavior were not immediately apparent; later, the x-ray analyses of the deformed specimens provided the basis for some reasonable hypotheses to account for the observed deformations.

As previously mentioned, x-ray analysis of specimen W-3 showed that the original mineralogy of

the dunite had been preserved. However, the x-ray pattern obtained for specimen WA-6 revealed that the serpentine had been dehydrated to form olivine and enstatite. It is hypothesized, on the basis of these results, that the dehydration of the serpentine did not take place in specimen WA-6 before the time of loading, but occurred during the deformation process. In particular, it is postulated that during the test the conversion of serpentine to form olivine and enstatite was initiated at the point in time corresponding to the beginning of the second period of apparent deformation. During the dehydration process, the change in volume resulting from the loss of water vapor would account for the sudden increase in the total strain and the gradual decay of the deformation with time shown in the creep curve in Figure 6. With these assumptions, the results of the two tests (W-3, WA-6), performed at a temperature of 600°C., and an axial stress of 408 bars are brought into agreement and indicate only the occurrence of transient creep.

(6) Thin-Section Analysis of Specimens. -

Thin-section slides were made from the original, undeformed dunite and several of the deformed specimens. Since the total strains produced by the time-dependent deformations are small, it was anticipated that microscopic examination of the test specimens would provide little, if any, information pertaining to the mechanisms involved in the deformations; indeed, this was the case.

The original olivine grains showed no change after deformation. In the thin-section slides of the undeformed material, it was observed that the scattered enstatite grains are well fractured but that the fragments of an individual grain are identically oriented, as indicated by the simultaneous extinction observed under crossed Nichol prisms; while in the thin-section slides of several of the deformed specimens, it was noted that the fragments of some enstatite grains had experienced a relative rotation, as indicated by an undulatory extinction pattern. The included angles of extinction observed for the rotated grain elements ranged from 2° to 4°. Other than the apparent rotation of grain fragments, the enstatite grains exhibited no affects of the deformation. Because of the small number of enstatite grains in each thin-section slide, it is difficult to assess quantitatively the significance of the relative rotations observed; however, the results suggest that the creep deformation observed in the experiments occurred largely by straining of the matrix material initially surrounding the olivine grains.

Chapter 6

ANALYSIS OF EXPERIMENTAL RESULTS

In the previous chapter, the experimentally observed effects of temperature and axial stress on the time-dependent deformational behavior of dunite have been discussed. The results indicate that increases in either temperature or axial stress give rise to increases in the total deformation and the rate of creep but that temperature is the dominant parameter for steady-state creep. There now remains the task of formulating a functional relationship between axial stress, temperature, and the rate of steady-state deformation which describes the experimental observations.

As previously mentioned, all viscous creep is caused by some diffusion process. In crystalline materials, viscous deformation can occur only in the presence of defects in the crystalline structure. In polycrystalline aggregates, the most important deviations from perfect crystalline order are dislocations, point defects, and the boundaries between grains, and the creep behavior of the aggregate is determined largely by the interaction of these defects.

At low temperatures, the self-diffusion of vacancies and interstitial atoms is negligible, and the grain boundaries are essentially rigid; but dislocations can readily migrate in response to an applied stress until blocked by other immobile defects. Consequently, viscous deformation is imperceptible, since time-dependent deformation caused only by the motion of dislocations is transient creep which decelerates rapidly at constant stress

due to the effects of strain hardening. At higher temperatures, the grain boundaries and point defects in a material are more mobile than dislocations. The transient stage of creep occurs, but the deformation is dominated by the viscous behavior associated with thermally-activated diffusion. However, diffusion is a many-faceted phenomenon and does not provide a unique specification of the atomic mechanism involved in the deformation; indeed, more than one atomic process may be operating simultaneously to produce the overall steady-state creep behavior observed in the laboratory.

In grain boundary creep, viscous deformation is initiated by sliding between adjacent grains due to thermal softening of the boundaries and slip induced by the migration of dislocations, both of which establish local concentrations of internal stress in the material. This initial plastic behavior is quickly impeded by the intersection of irregular shaped grains and strain hardening, and the deformation can continue only if thermally-activated diffusion of point defects is sufficient to relieve the internal stresses induced by dislocation slip and thermal softening. Viscous creep occurs at a perceptible rate by the migration of atoms along grain boundaries from regions where slip and grain boundary sliding have caused compression to nearby areas in tension.

In recovery creep, or annealing-recrystallization creep, the effective yield stress of the material is reduced by thermal softening, and steady-state creep occurs under conditions of constant stress at a rate corresponding to the rate at which strain hardening is lost through diffusion. Mott (1951) has suggested that the primary process causing thermal softening is dislocation

climb induced by the diffusion of point defects around edge dislocations.

Grain bulk diffusion creep, or Herring-Nabarro creep, is very similar to grain boundary creep but is usually observed only at temperatures approaching the melting point of the material. Here, the deformation is caused by the rearrangement of atoms at the grain boundaries resulting from the diffusion of vacancies and interstitials through the bulk of the grains. The driving forces of the diffusion process are derived only from externally applied stresses, as distinct from grain boundary creep where the deformation is induced by internal stress.

From the preceding paragraphs, it is apparent that viscous creep on the atomic scale is a highly complex phenomenon. However, there is a common denominator in all mechanisms which produce viscous behavior in polycrystalline materials; namely, thermally-activated diffusion. Since steady-state creep was observed in the experiments, it is reasonable to assume that the deformations were caused largely by diffusion effects, and the results were analyzed on this assumption.

Previous investigators of viscous creep have established a number of empirical relationships to describe the effect of temperature and stress difference on the rate of strain. The stress dependence of the rate of steady-state creep in many materials follows the expression, due to Prandtl (1928):

$$\dot{\epsilon} = \dot{\epsilon}_0 \sinh\left(\frac{\sigma}{\sigma_0}\right) \quad , \qquad (1)$$

where $\dot{\epsilon}$ is the steady-state creep rate, σ is the stress applied to the specimen, and ϵ_0 and σ_0 are constants. Equation (1) has

been used to describe the viscous behavior at high temperatures of metals (Nadai, 1938; Nadai and McVetty, 1943), magnesium oxide (Wygant, 1951), and alabaster (Griggs, 1940). Dorn (1957) performed an extensive analysis of the high temperature creep data obtained for metals. The results showed that for most metals the activation energy for creep is equal to the energy required to promote self-diffusion at temperatures greater than 0.45 of the absolute melting temperature, and that the temperature dependence for viscous creep fits an equation of the form:

$$\dot{\epsilon} = \exp\left(-\frac{\Delta H}{RT}\right) \quad , \qquad (2)$$

where $\dot{\epsilon}$ is the steady-state creep rate, ΔH is the activation energy for creep, R is the universal gas constant, and T is the absolute temperature. The good agreement found for the previous creep data with equations (1) and (2) suggests that the stress and temperature dependence of the observed steady-state creep of dunite may follow a relationship obtained by combining the two results in the form:

$$\dot{\epsilon} = \dot{\epsilon}_0 \sinh\left(\frac{\sigma}{\sigma_0}\right) \exp\left(-\frac{\Delta H}{RT}\right) \quad . \qquad (3)$$

In addition to the development by empirical methods, equation (3) has also been deduced from theoretical considerations; it is the so-called Ree-Eyring equation, derived by applying the theory of rate processes to a theoretical model based on the mechanism of thermally-activated self-diffusion describing steady-state creep at high temperatures where the activation energy for creep is equivalent to the energy of self-diffusion (Ree, Ree, and Eyring, 1960). The atomic mechanism causing the deformation effectively describes grain boundary creep. According to the model, steady-state creep occurs as the result of slip due to

the migration of dislocations toward grain boundaries along planes of slip and the diffusion of point defects in response to the internal stresses induced by the slip. Since the activation energies for creep and self-diffusion are equal at high temperature, the viscous deformation is rate-limited by the rate of thermal diffusion. The Ree-Eyring equation has been employed to describe the high-temperature creep behavior of aluminum, aluminum-based alloys, and nickel (Ree et. al., 1960), and Heard (1963) has fitted constant strain-rate data for Yule marble to the formula.

To determine to what extent diffusion dominated the creep behavior of dunite, the steady-state creep rates observed in the experiments were fitted to equation (3). To facilitate the analysis several simplifications were introduced. If we assume that $(\frac{\sigma}{\sigma_0}) \gg 1$, the hyperbolic sine term can be approximated by an exponential, thus reducing equation (3) to the form:

$$\dot{\epsilon} = \frac{\dot{\epsilon}_0}{2} \exp\left(\frac{\sigma}{\sigma_0}\right) \exp\left(-\frac{\Delta H}{RT}\right) , \qquad (4)$$

or

$$\dot{\epsilon} = \frac{\dot{\epsilon}_0}{2} \exp\left(\frac{\sigma}{\sigma_0} - \frac{\Delta H}{RT}\right) . \qquad (5)$$

From equation (5), it follows that:

$$\ln \dot{\epsilon} = \ln\left(\frac{\dot{\epsilon}_0}{2}\right) + \frac{\sigma}{\sigma_0} - \frac{\Delta H}{RT} . \qquad (6)$$

At constant stress, we obtain from equation (6):

$$\frac{d(\ln \dot{\epsilon})}{d\left(\frac{1}{T}\right)} = -\frac{\Delta H}{R} . \qquad (7)$$

The maximum axial stress applied to the specimens in the present experiments was 408 bars; hence, this is the stress value which best satisfies the basic assumption that $\frac{\sigma}{\sigma_0} >> 1$. Thus, to obtain a value for ΔH, the activation energy for creep, from equation (7), the natural logarithms of the steady-state creep rates observed at a stress of 408 bars were computed and plotted as a function of the inverse absolute temperature as shown in Figure 19. The line shown in Figure 19 represents a first-order fit to the data points determined by the method of least squares. The slope of the line determined by the least squares computation is $17.65 \cdot 10^3 K° second^{-1}$, yielding a value for the activation energy for creep of 35.1 kcal per mole.

At constant temperature, we obtain from equation (6):

$$\frac{d(\ln \dot{\epsilon})}{d\sigma} = \frac{1}{\sigma_0} \quad . \qquad (8)$$

To compute a value for the constant σ_0 from equation (8), the natural logarithms of the steady-state creep rates observed at temperatures of 900° and 950°C. were calculated and plotted as a function of axial stress difference as shown in Figure 20. The curves shown in Figure 20 were also obtained from a first order least squares fit to the data points. The computed slopes of the lines were found to be in excellent agreement: 7.72 $kb.^{-1}$ $second^{-1}$ at 900°C., and 7.64 $kb.^{-1}$ $second^{-1}$ at 950°C. The two values were averaged and σ_0 was computed to be 130 bars.

By substituting the values of ΔH, σ_0, and the arithmetic mean value of the steady-state rate of creep observed at a temperature of 950°C., and a stress difference of 408 bars into equation (6), the third constant, $\dot{\epsilon}_0$, was determined to be

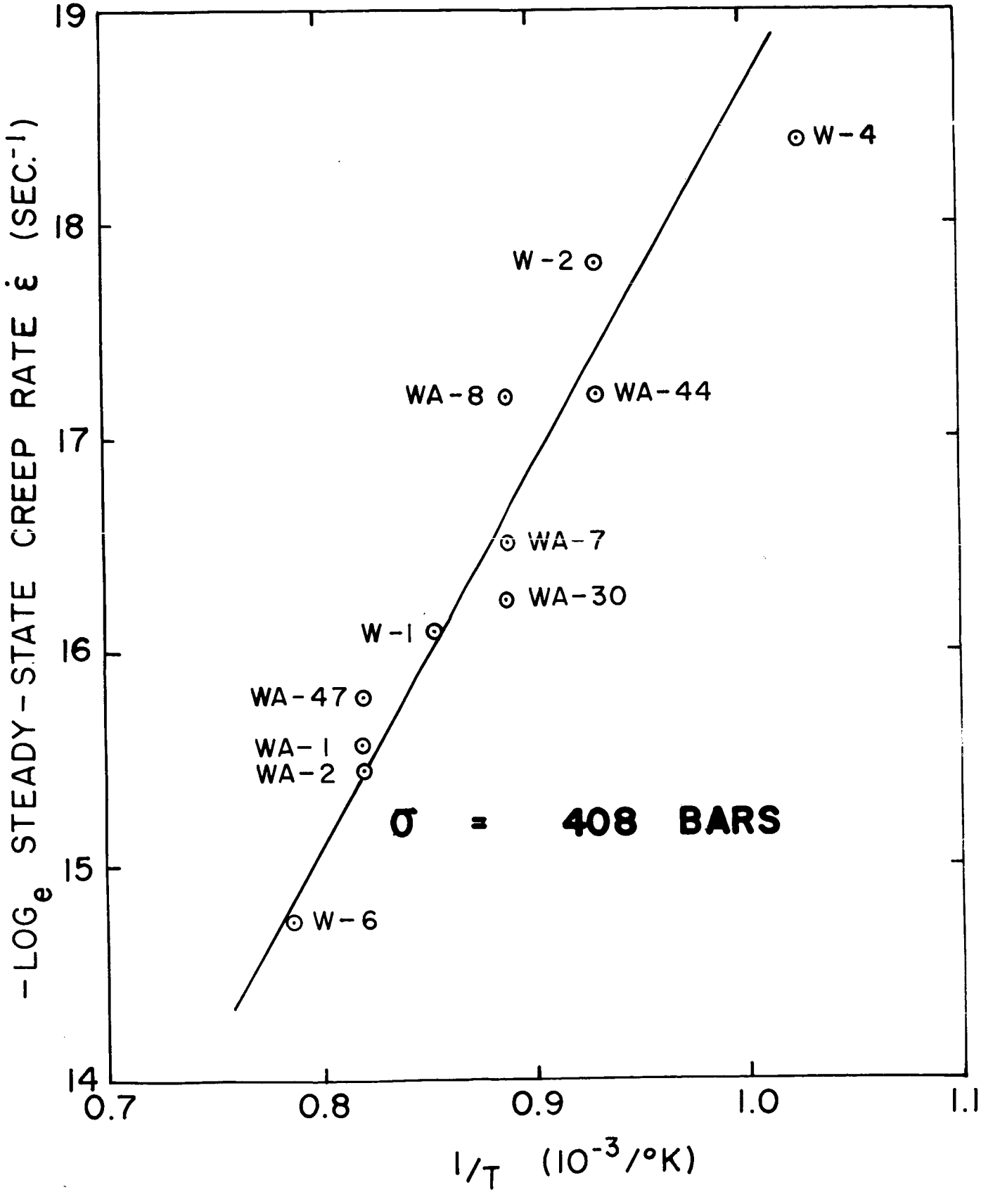

Figure 19. Natural logarithm of the steady-state creep rate as a function of inverse absolute temperature at 408 bars.

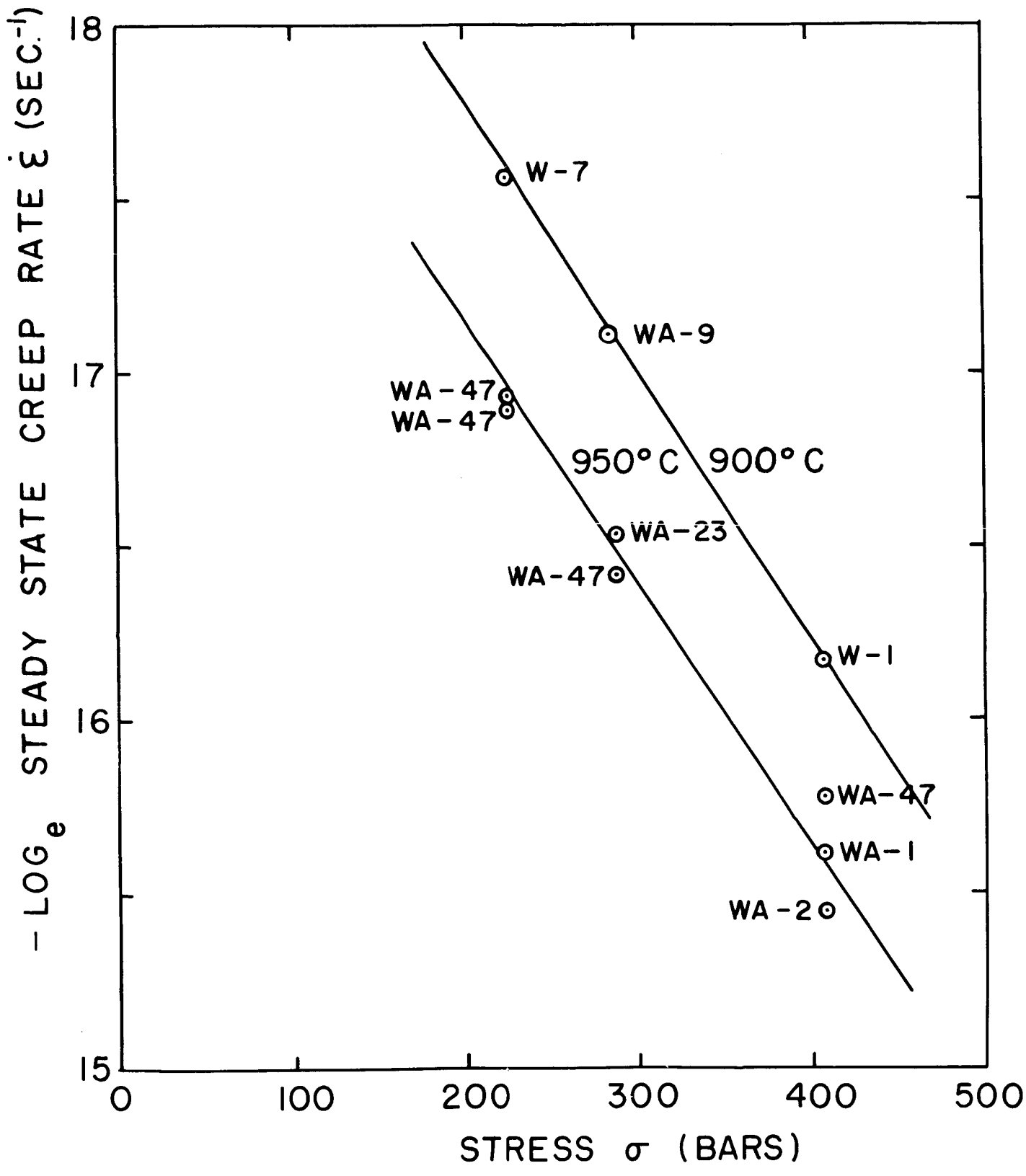

Figure 20. Natural logarithm of the steady-state creep rate as a function of axial stress at constant temperature.

$2.9 \cdot 10^{-2}$ second^{-1}. The determined values of $\dot{\epsilon}_0$, σ_0, and ΔH were then substituted into equation (3), giving an expression for the experimentally observed rate of steady-state creep as a function of temperature and axial stress of the form:

$$\dot{\epsilon} = (2.9 \cdot 10^{-2}) \sinh(\frac{\sigma}{130}) \exp(-\frac{35.1}{RT}) \quad , \qquad (9)$$

with units of $\dot{\epsilon}$ in second^{-1}, σ in bars, and T in degrees Kelvin.

Using equation (9), the steady-state creep rate was computed for each combination of temperature and axial stress employed in the experiments. The computed strain rates are compared with the corresponding values obtained experimentally in Table IV, and the results of the analysis are summarized in Figure 21. The family of curves plotted in Figure 21 show the steady-state creep rates predicted by equation (9) as a function of temperature at each of the three axial stresses applied in the tests: 226, 288, and 408 bars; the symbols plotted in Figure 21 correspond to the arithmetic mean value of the observed creep rate. The experimental data obtained at 408 bars agreed very closely with the empirical formula at all temperatures in the range from 500° to 1000°C., and the data points for both 226 and 288 bars stress at 900° and 950°C., were also in excellent accord with equation (9). The only experimental data which differed from the Ree-Eyring equation were obtained at conditions of low temperature and low axial stress. The points for 226 bars at 800° and 850°C., and for 288 bars at 800°C., showed some deviation from the predicted curves, and the creep rate observed for 288 bars at 850°C. was anomalously greater than the computed value. Despite the several discrepancies, the experimental data indicates good overall agreement with the empirical form of the Ree-Eyring formula given by equation (9).

TABLE IV

SUMMARY OF ANALYTICAL RESULTS

Temp. (°C.)	Axial Stress (bars)	Specimens Used in Mean	Steady-State Creep Rate Observed(mean) (10^{-7}sec.$^{-1}$)	Steady-State Creep Rate Calculated (10^{-7}sec.$^{-1}$)
800	226	WA-25, WA-27, WA-44	0.274	0.057
850	226	WA-11, WA-45	0.312	0.120
900	226	W-7	0.239	0.232
950	226	WA-47	0.451	0.432
1000	226	--------	-----	0.753
800	288	WA-44	0.285	0.093
850	288	WA-4, WA-45	0.747	0.197
900	288	WA-9	0.372	0.381
950	288	WA-23, WA-47	0.700	0.709
1000	288	--------	-----	1.235
500	408	W-5	~0.0	0.0001
600	408	W-3, WA-6	~0.0	0.001
700	408	W-4	0.104	0.042
800	408	W-2, WA-44	0.264	0.237
850	408	WA-7, WA-8, WA-30	0.632	0.578
900	408	W-1	0.942	0.968
950	408	WA-1, WA-2, WA-47	1.670	1.802
1000	408	W-6	4.039	3.138

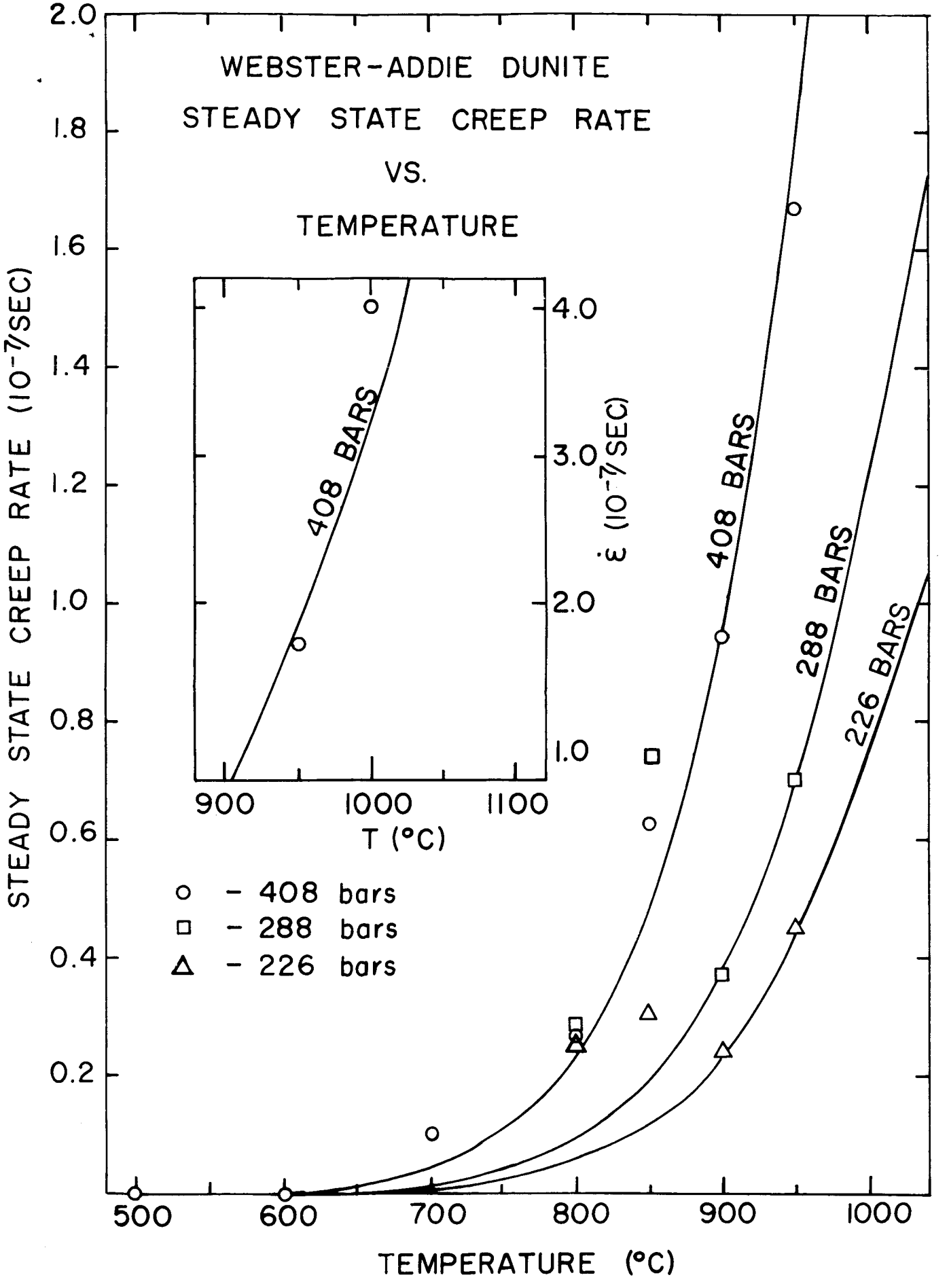

Figure 21. Comparison of the Ree-Eyring model with the mean observed steady-state creep rates.

Chapter 7

CONCLUSIONS

The twenty-two creep experiments reported here represent the first investigation of the time-dependent deformational characteristics of polycrystalline dunite subjected to conditions of deformation comparable to the high temperatures and deviations from uniform hydrostatic pressure occurring in the lower crust and top layers of the mantle. Although the specimens were unjacketed and hydrostatically confined only by atmospheric pressure, it proved possible to prevent cracking due to thermal stresses at high temperatures by means of slow rates of heating and cooling. Since there is evidence suggesting that hydrostatic pressures of the order of 10^{-4}-10^{-5} bars have only a small effect upon the creep properties of polycrystalline materials, the omission of a confining pressure should not make the experiments untenable simulations of the upper mantle. The technical advantages of being able to omit the hydrostatic confining pressures used by previous investigators of rock deformations are very large. The experiments thus established a strong presumption that the conditions under which creep deformation takes place in the upper mantle can be investigated in the laboratory with comparatively simple techniques.

The most significant result of the investigation is that temperature is the most important physical parameter affecting the time-dependent deformations of rocks at high temperatures and moderate differential stresses. The steady-state creep of dunite is affected by both stress difference and temperature, but the experimental results show that the rate of creep is effectively controlled only by temperature. Increasing the axial

stress on the specimens from 226 to 408 bars at 950°C., caused only about a four-fold increase of the strain rate in steady-state creep; while an increase in temperature at 408 bars from 700° to 950°C., increased the rate of deformation by about a factor of twenty.

The temperature and stress dependence of the steady-state creep rates measured were found to follow the equation:

$$\dot{\epsilon} = (2.9 \cdot 10^{-2}) \sinh\left(\frac{\sigma}{130}\right) \exp\left(-\frac{35.1}{RT}\right) .$$

The excellent agreement with this equation of the data obtained at temperatures of 900°C. and above, indicates that the high-temperature creep behavior of dunite under stress differences up to 400 bars is well-defined by the Ree-Eyring model of steady-state creep and, therefore, is caused primarily by a single diffusion-activated mechanism; namely, grain boundary sliding induced by dislocation slip and(or) thermal softening. The data obtained at 408 bars also agreed very closely with the above equation at all temperatures in the range from 500° to 1000°C., indicating that the Ree-Eyring mechanism dominates the steady-state creep deformation throughout this temperature range at stresses of 400 bars and above. These conclusions are supported by the fact that the estimate of the activation energy for steady-state creep in dunite obtained here of 35.1 kcal mole^{-1} is also consistent with values for the rocks of the crust and mantle obtained from theoretical considerations based on the Ree-Eyring diffusion model (Cook, 1963).

The possibility that mechanisms other than thermally-activated diffusion were active during the steady-state deformations

produced at low temperatures and stresses is suggested by the deviations from the Ree-Eyring model of the mean creep rates observed for temperatures of 800° and 850°C., at stresses of 226 and 288 bars. The mean creep rates measured at 800°C. show little variation with changes in axial stress in the range from 226 to 408 bars (Table IV), and fall close to the value predicted by the Ree-Eyring equation for 408 bars; this would appear to indicate that at temperatures near 800°C., the steady-state creep rate is completely independent of stress and is controlled only by temperature. However, it is difficult to support this argument in view of the results at higher temperatures, since it is reasonable to expect that the deformations observed at higher temperatures would exhibit even a smaller dependence on axial stress; whereas the creep rates measured at temperatures above 800°C. reflect a non-negligible and consistent variation with changes in differential stress. However, it is significant that the deviations of the data from the Ree-Eyring curves showed no consistent pattern and occurred only for the steady-state creep rates measured at low temperatures and stresses where structural defects, such as voids and micro-fractures, have the strongest influence on the effective mechanical properties of the specimens. Hence, the most reasonable interpretation of the deviations from the Ree-Eyring model of steady-state creep is that they result from small differences in the mechanical properties and slight inhomogeneities in the structure of the specimens.

APPENDIX I

Scaled Drawings of the Apparatus Details

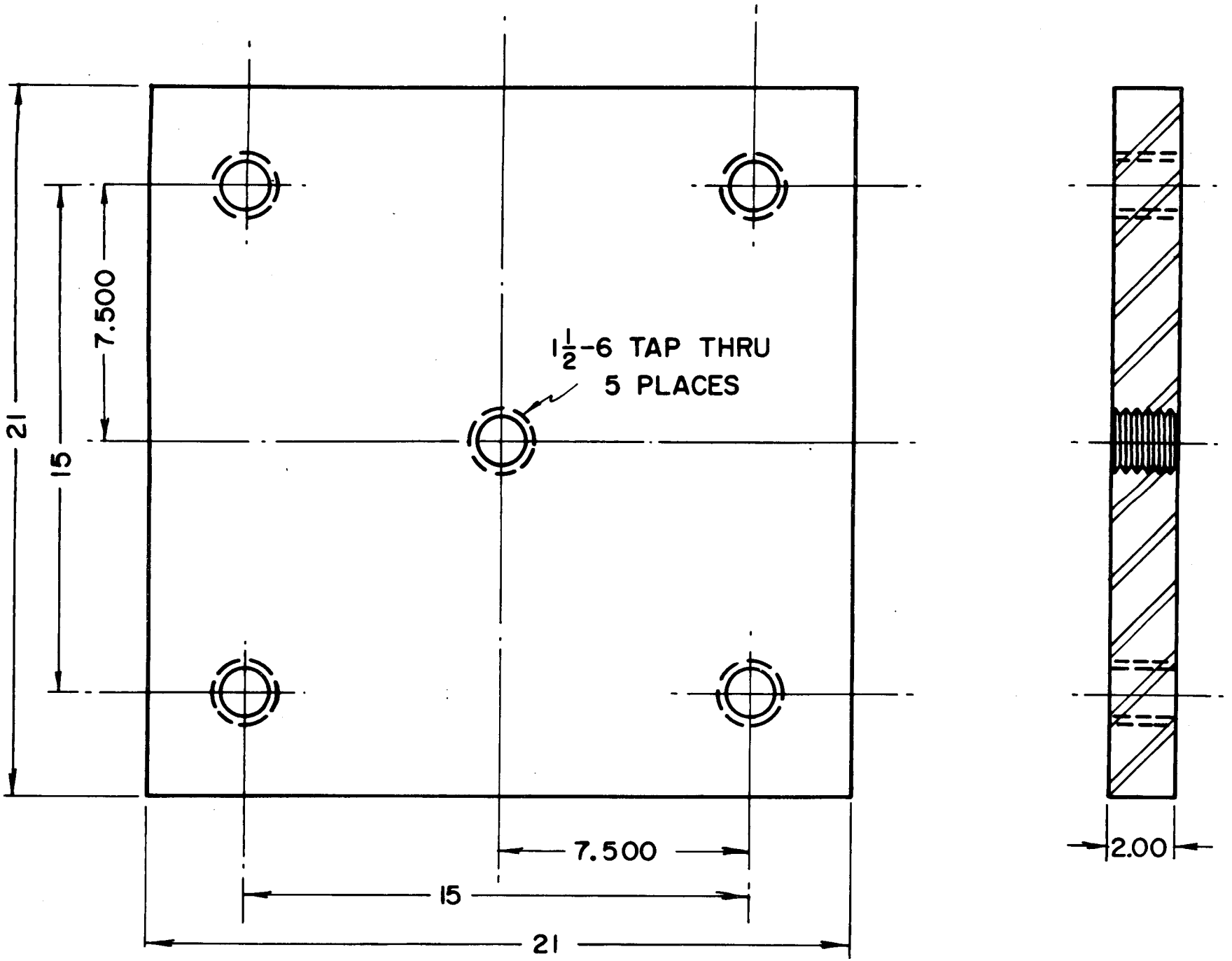

DETAIL 1 LOWER PLATE

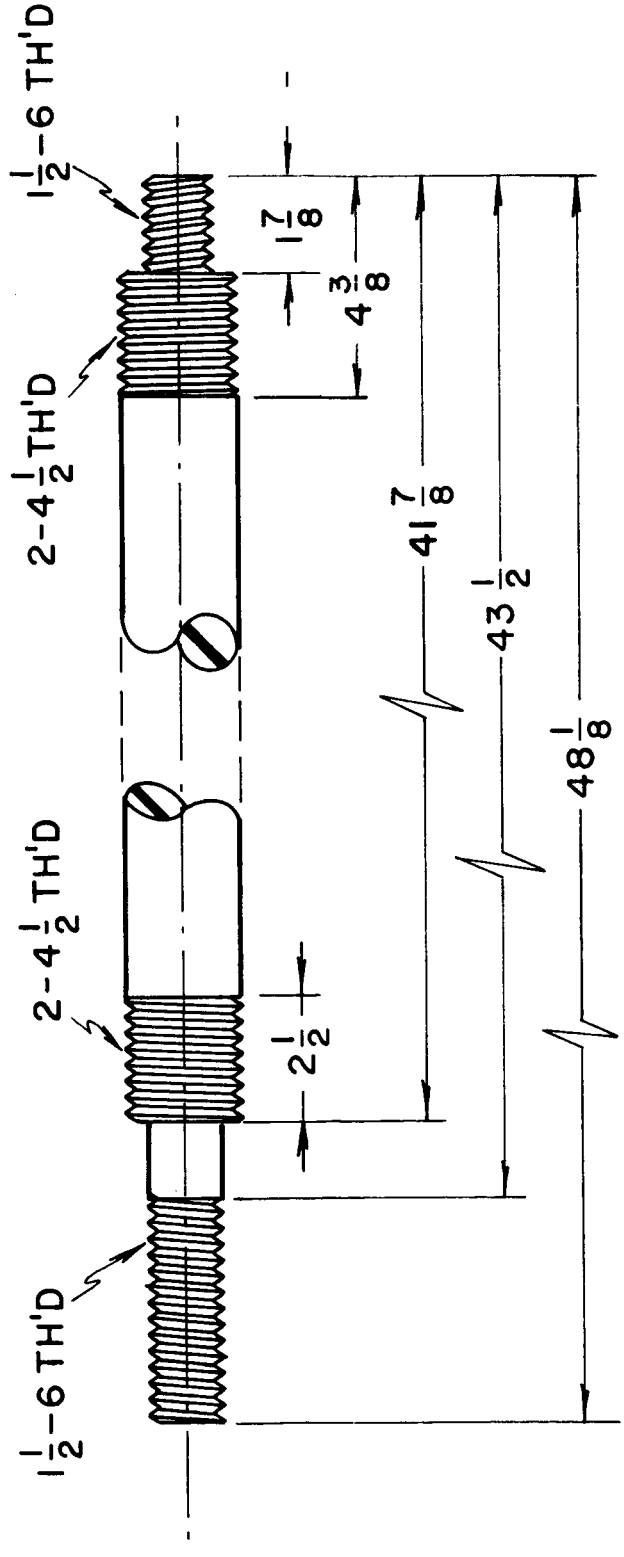

TEST STAND SUPPORT ROD
1020 STAINLESS STEEL
DETAIL 2

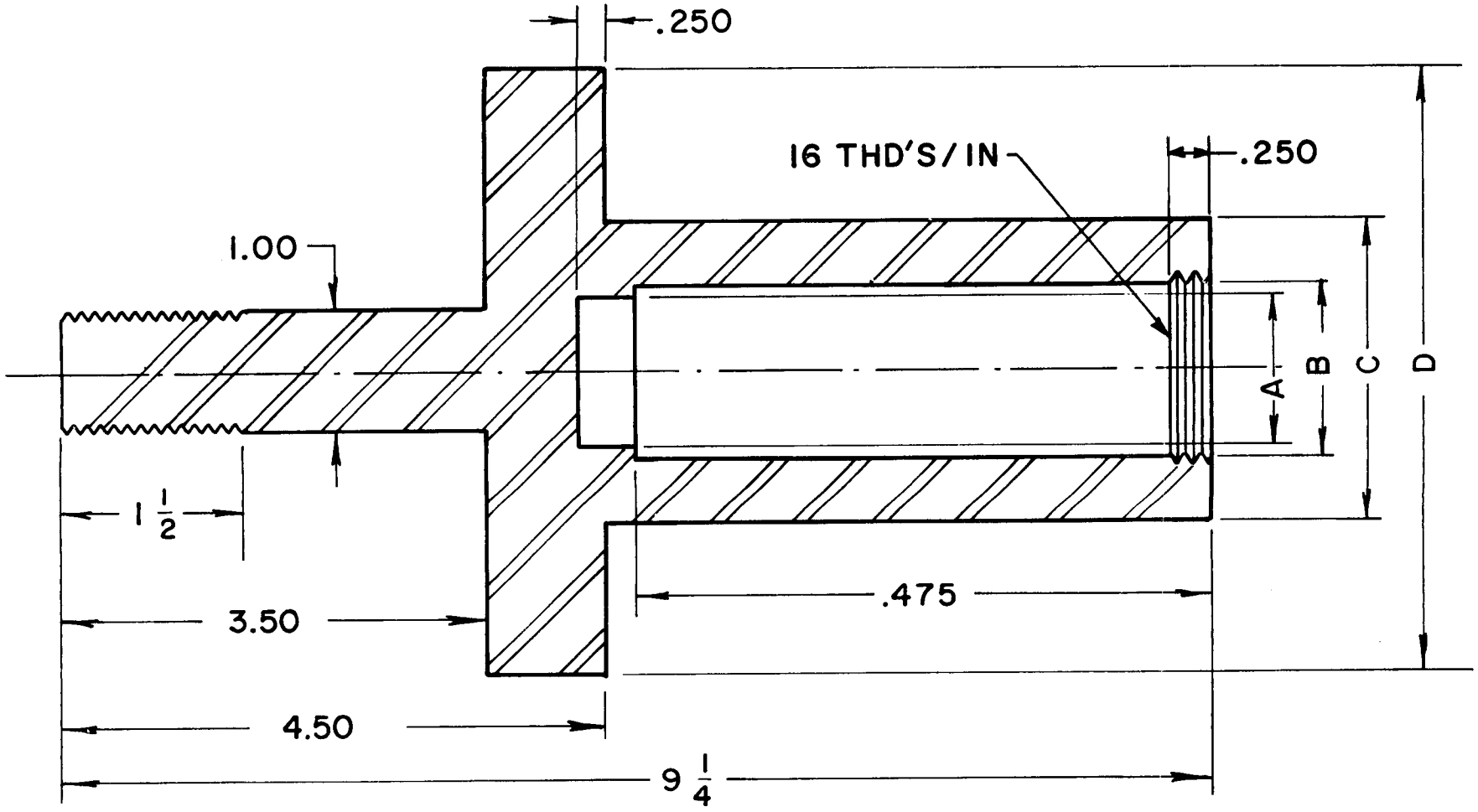

DIAMETER	DIMENSION
A	SEE BEARING
B	$1.5625 \pm^{0.0005}_{0.0000}$
C	$2.490 \pm^{0.000}_{0.005}$
D	$5.00 \pm^{0.000}_{0.050}$

LOWER RAM BEARING HOUSING
1141 STEEL
DETAIL 3

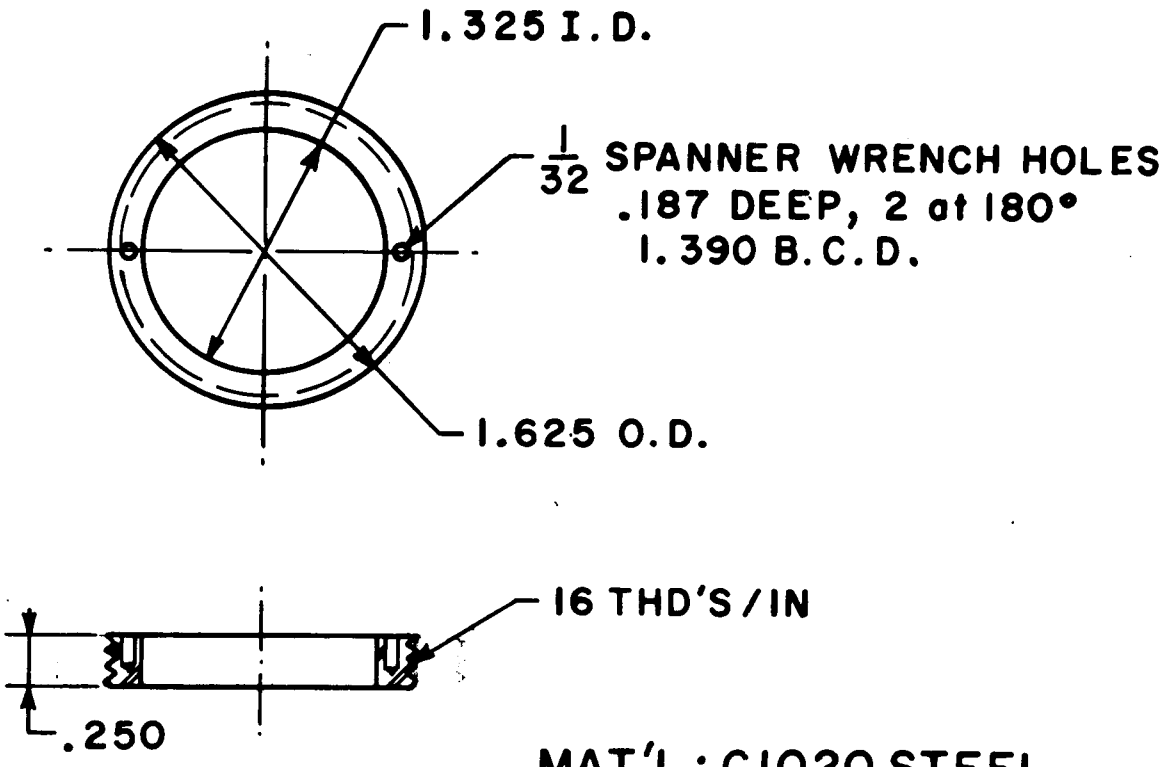

DETAIL 4
RETAINING RING-LOWER BEARING HOUSING

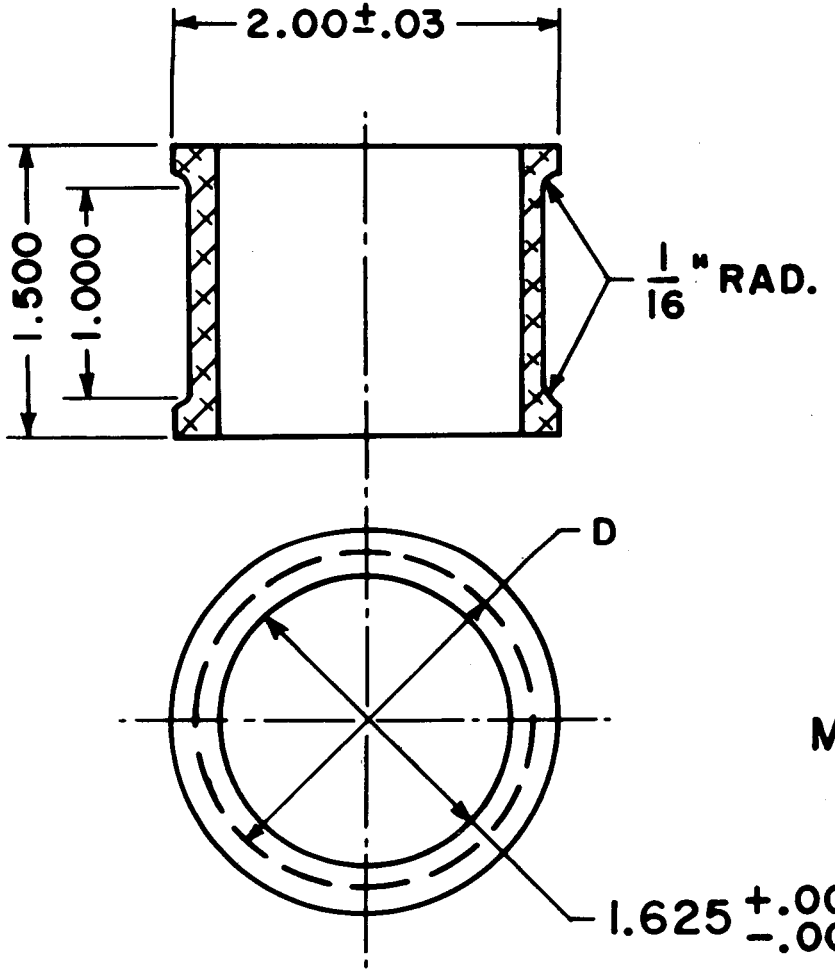

D INCHES ±0001	MAX. LOAD POUNDS
1.6288	100
1.6439	500
1.6626	1000
1.7175	2500
1.8052	5000
1.9690	10000

MAT'L: 7075-T6 ALUMINUM

LOAD CELL
DETAIL 5

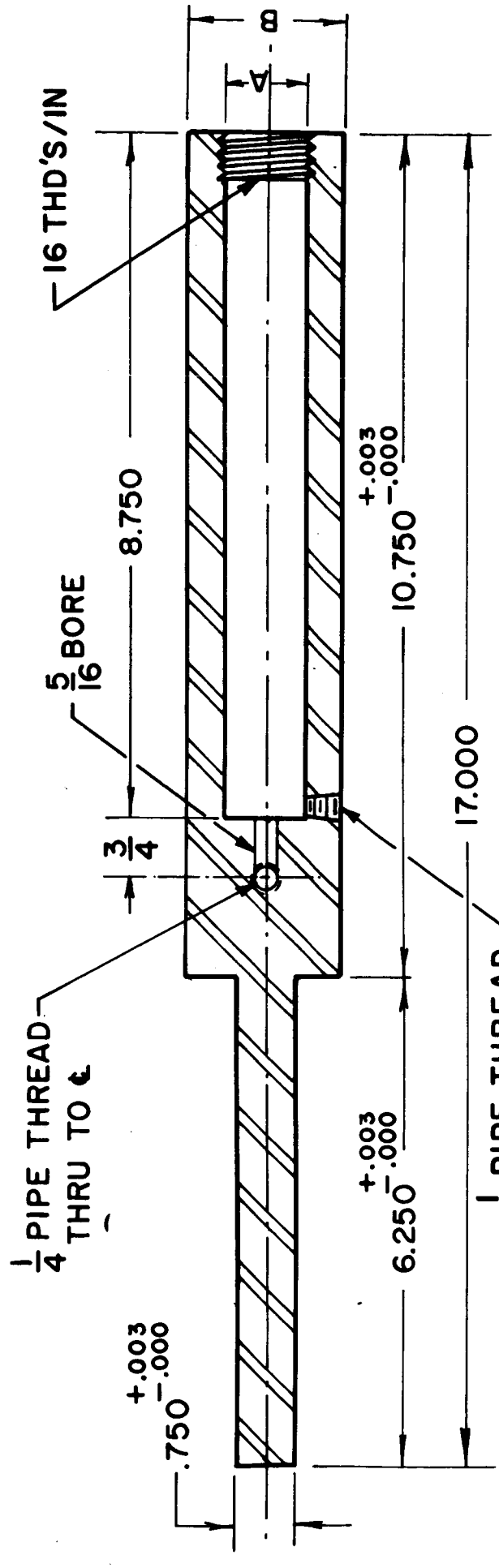

DIAMETER	DIMENSION
A	1.160 +.000 -.003
B	2.100 +.000 -.003

LOWER RAM
310 STAINLESS STEEL
DETAIL 6

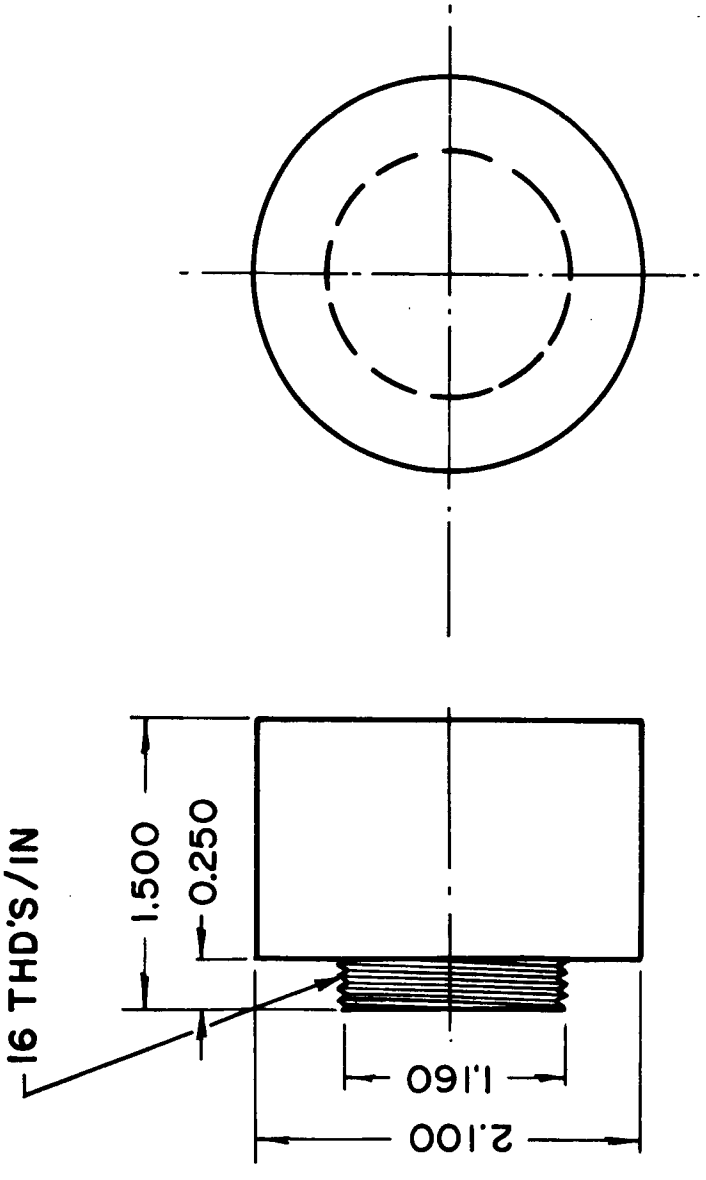

310 STAINLESS STEEL

CLOSURE PLUG FOR UPPER AND LOWER RAM

DETAIL 7

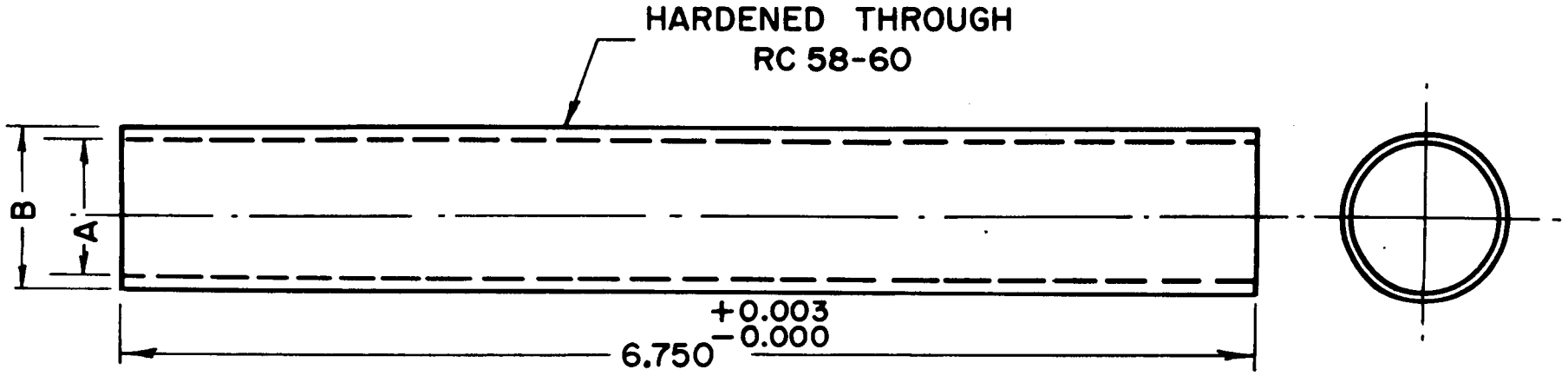

DIAMETER	DIMENSION
A	PRESS FIT ON PART 6
B	$0.9995^{+0.0000}_{-0.0005}$

1060 ST'L HARDENED & GROUND

DETAIL 8 LOWER RAM BEARING SHAFT

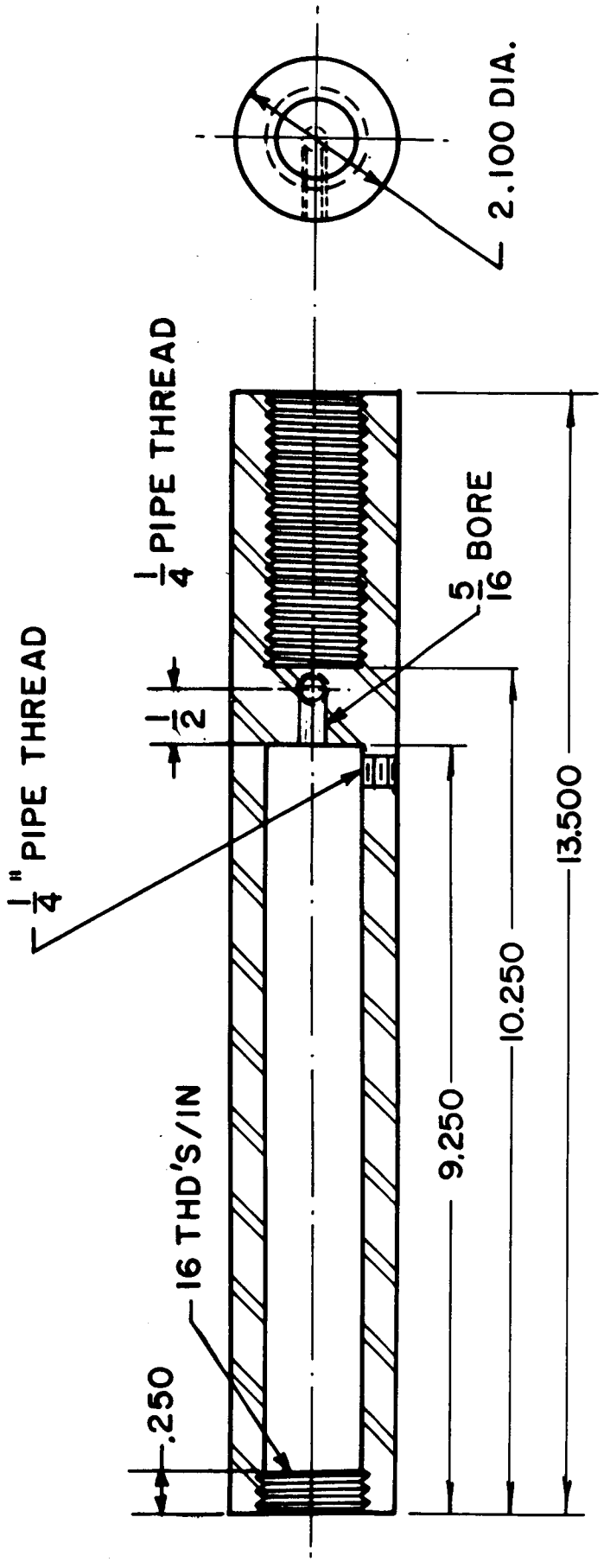

UPPER RAM "B"
DETAIL 9

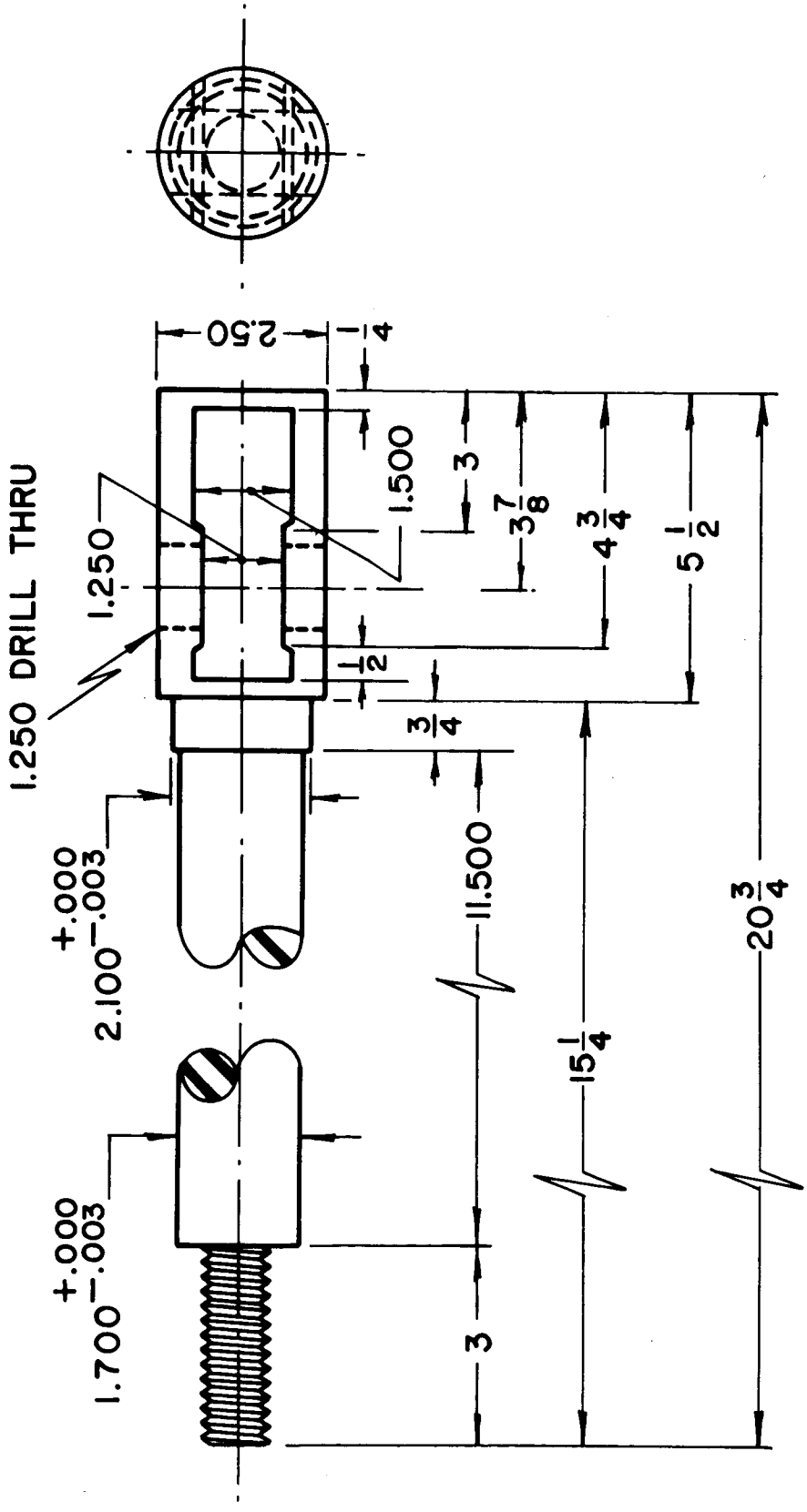

DETAIL 10 UPPER RAM "A"
310 STAINLESS STEEL

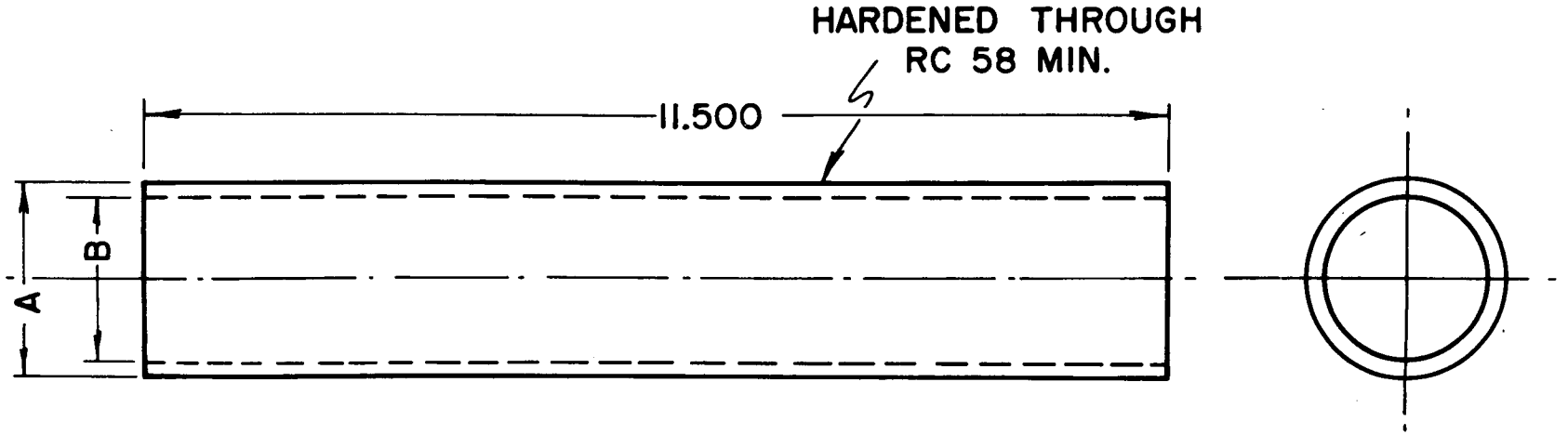

DIAMETER	DIMENSION
A	1.9990±.0002
B	TO BE PRESS FIT ON 1.700 DIA. OF PART 10.

1060 ST'L HARDENED & GROUND

DETAIL II UPPER RAM BEARING SHAFT

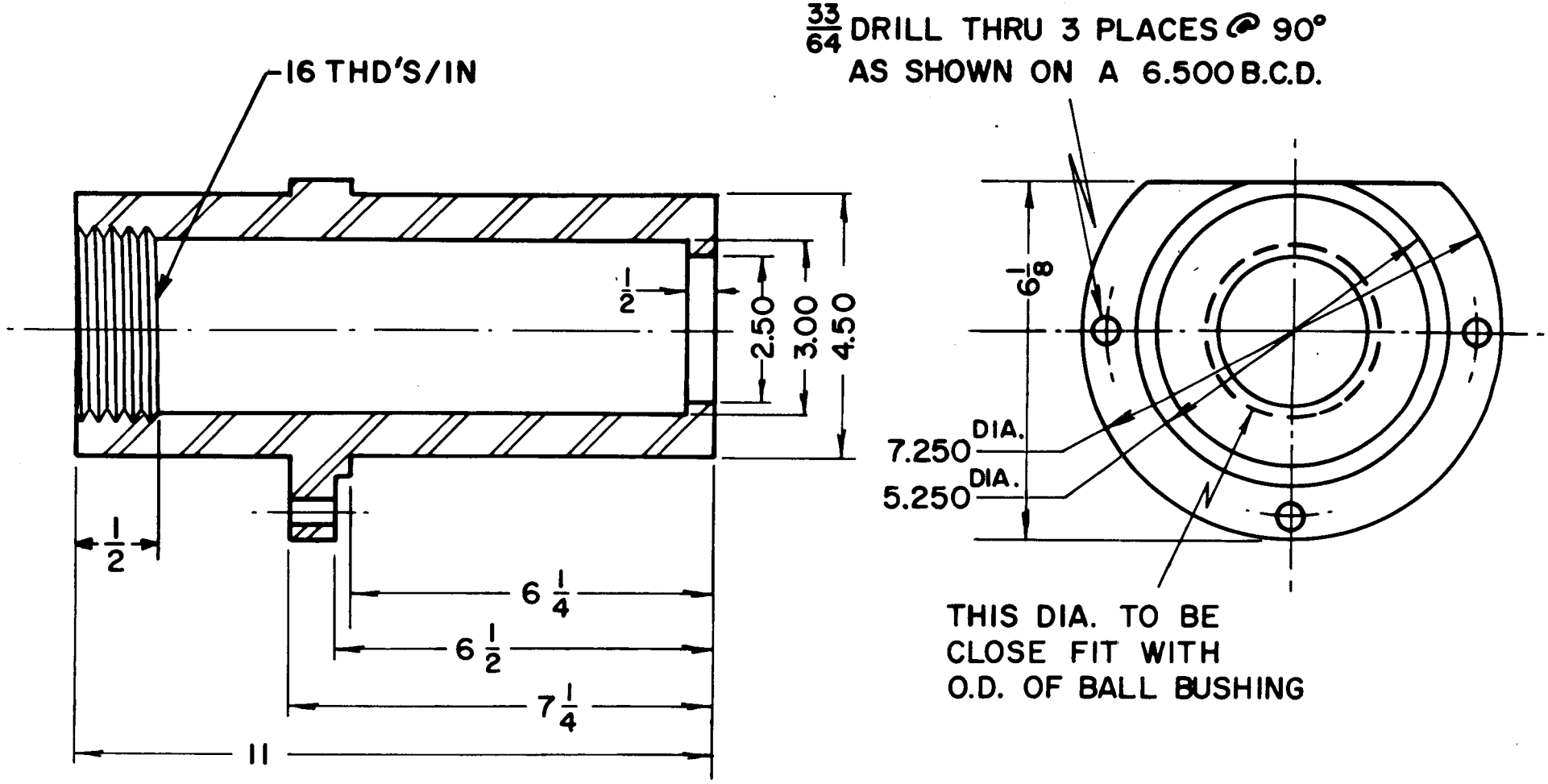

DETAIL 12 UPPER RAM BEARING HOUSING

1020 STEEL

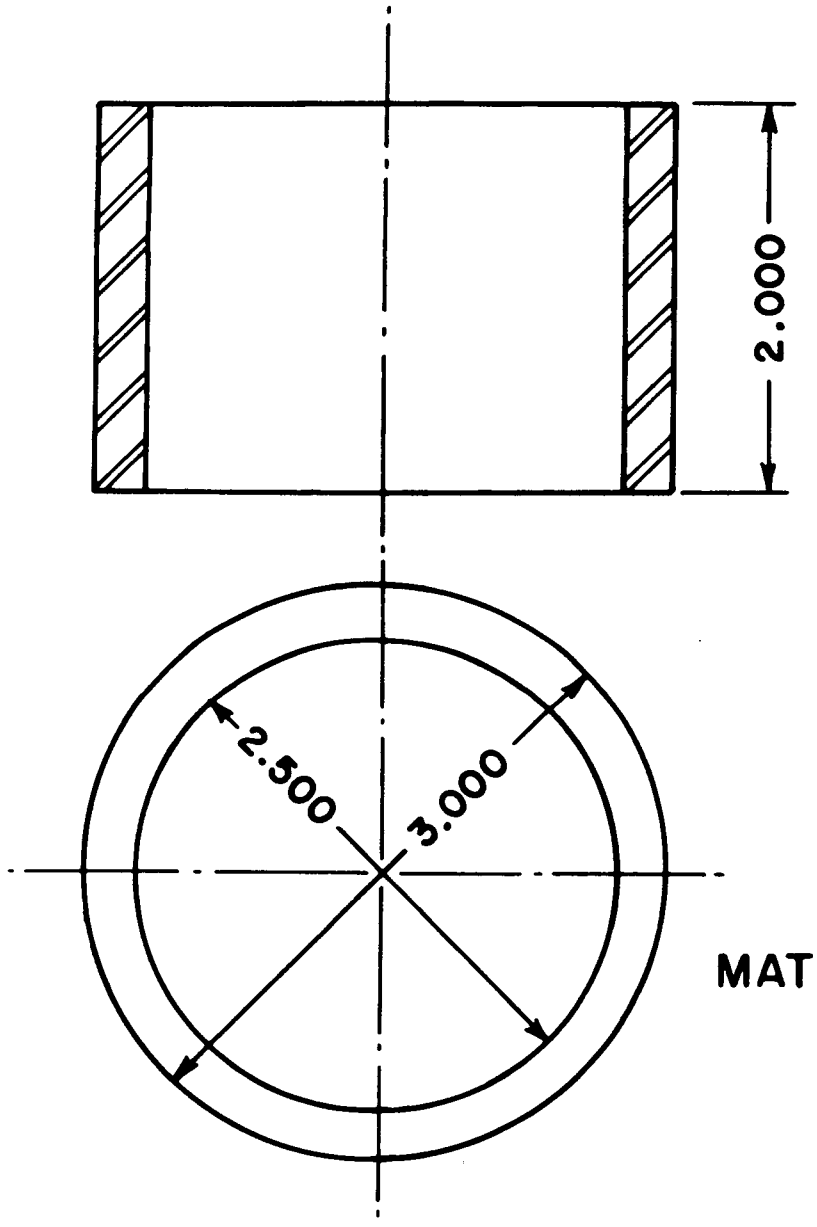

MAT'L-C1020 STEEL

SPACER—UPPER BEARING HOUSING

DETAIL 13

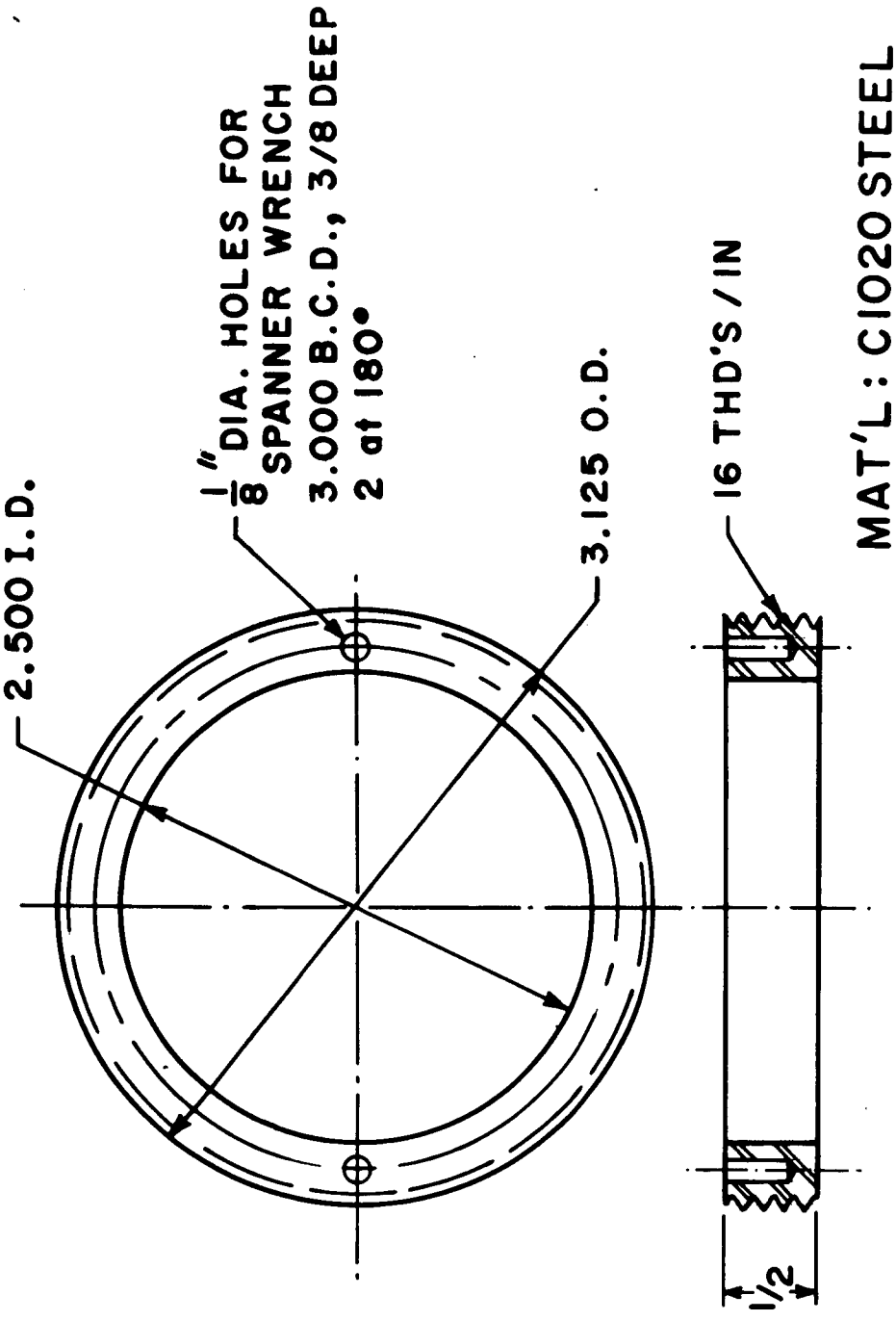

MAT'L: C1020 STEEL

DETAIL 14

RETAINING RING-UPPER BEARING HOUSING

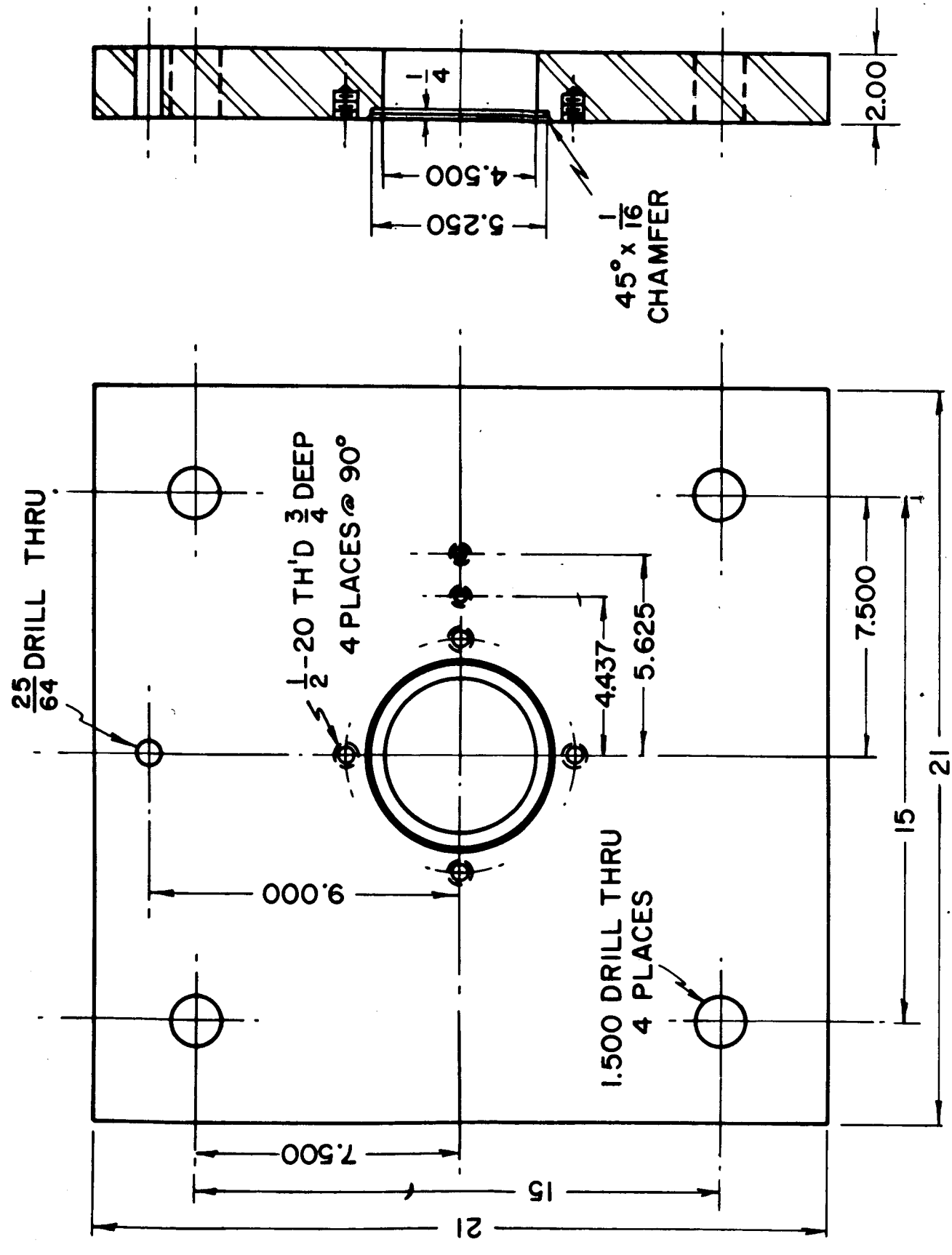

UPPER PLATE OF TEST STAND
DETAIL 15

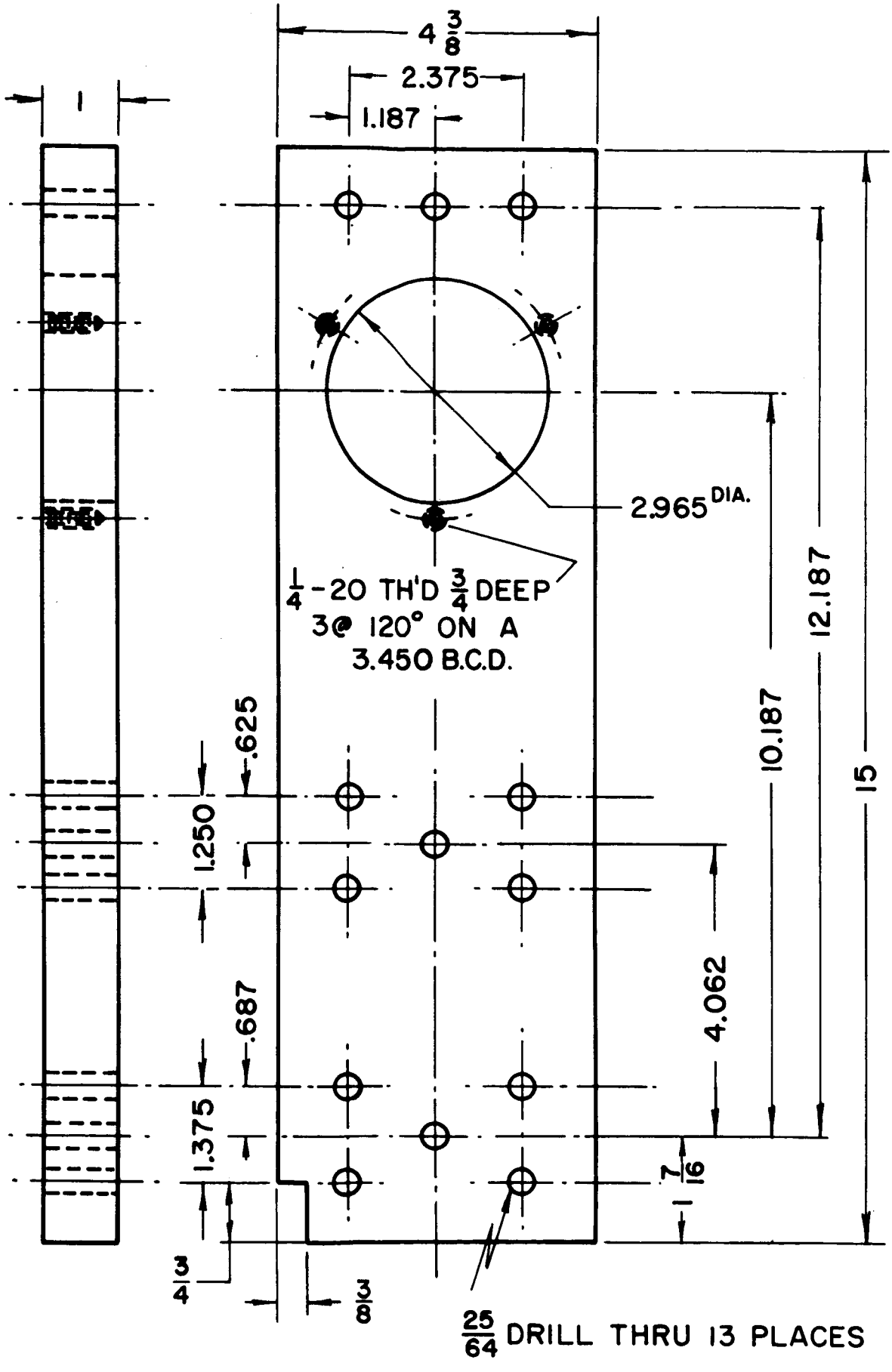

6061 T6 ALUMINUM

FULCRUM BEARING HOUSING ASSEMBLY PART A
DETAIL 16

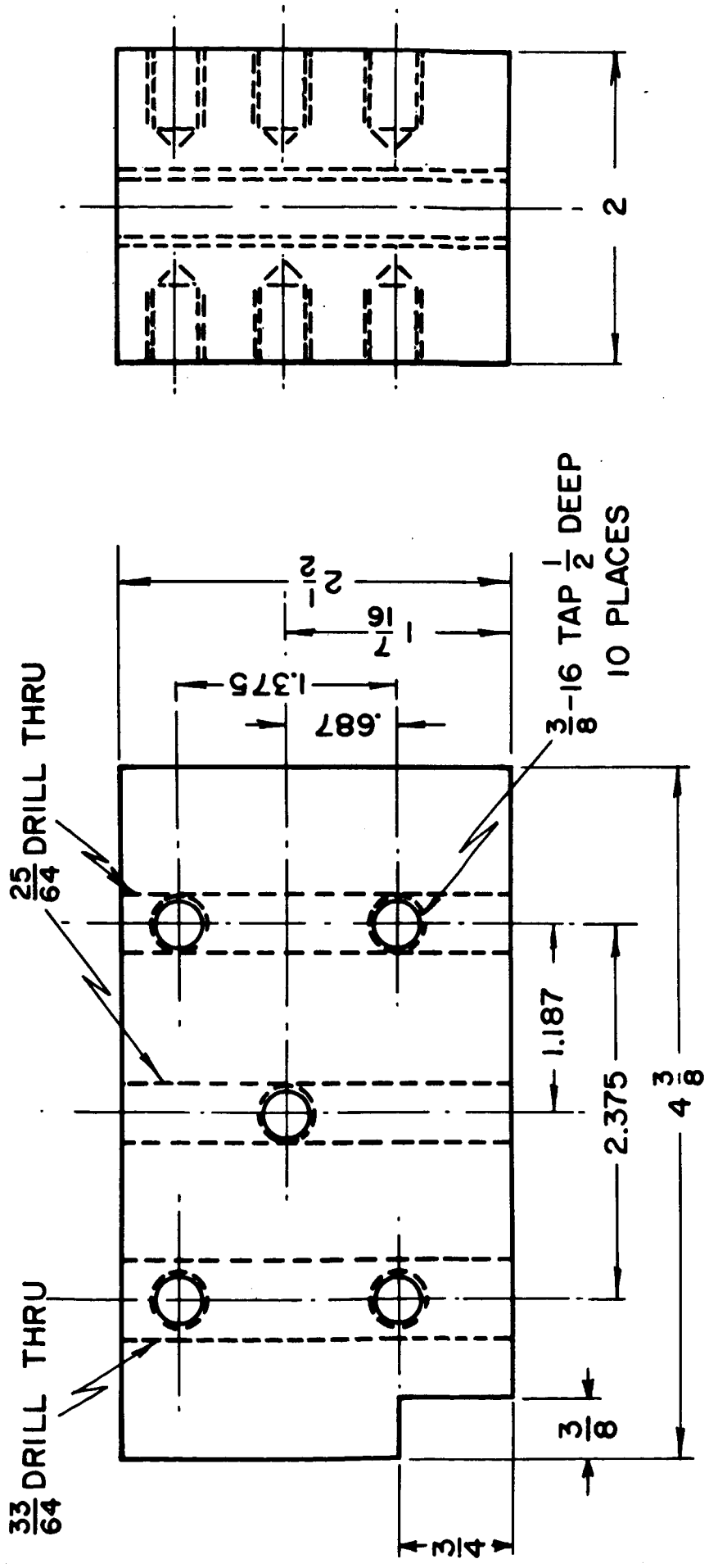

6061 T6 ALUMINUM

SPACER BLOCK "B"

DETAIL 17

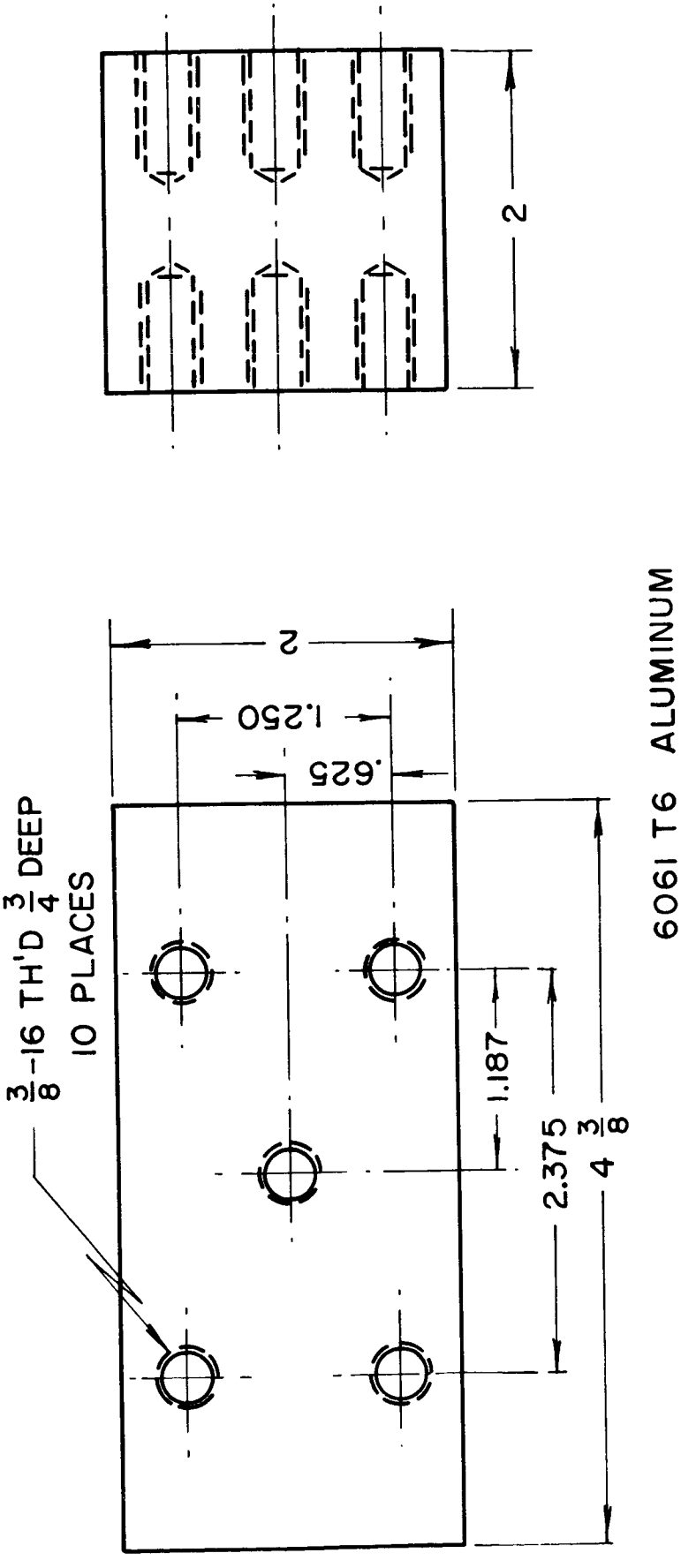

SPACER BLOCK "C"
DETAIL 18

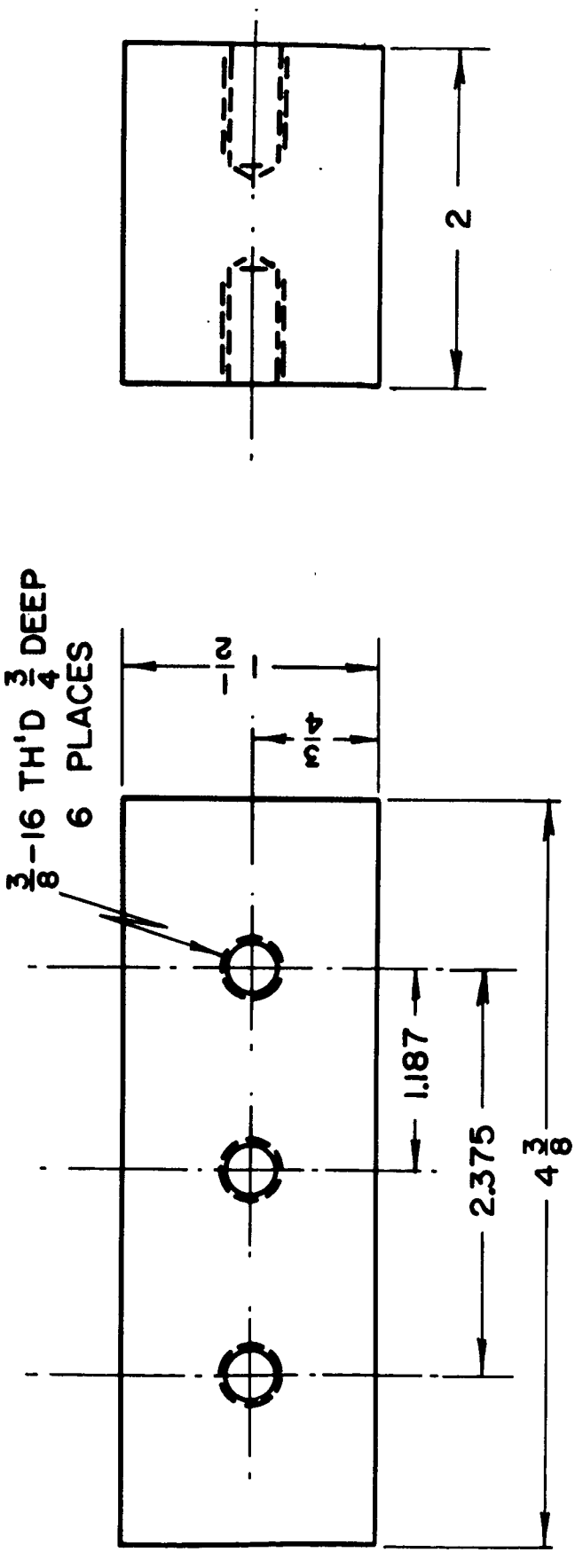

6061 T6 ALUMINUM

SPACER BLOCK "D"
DETAIL 19

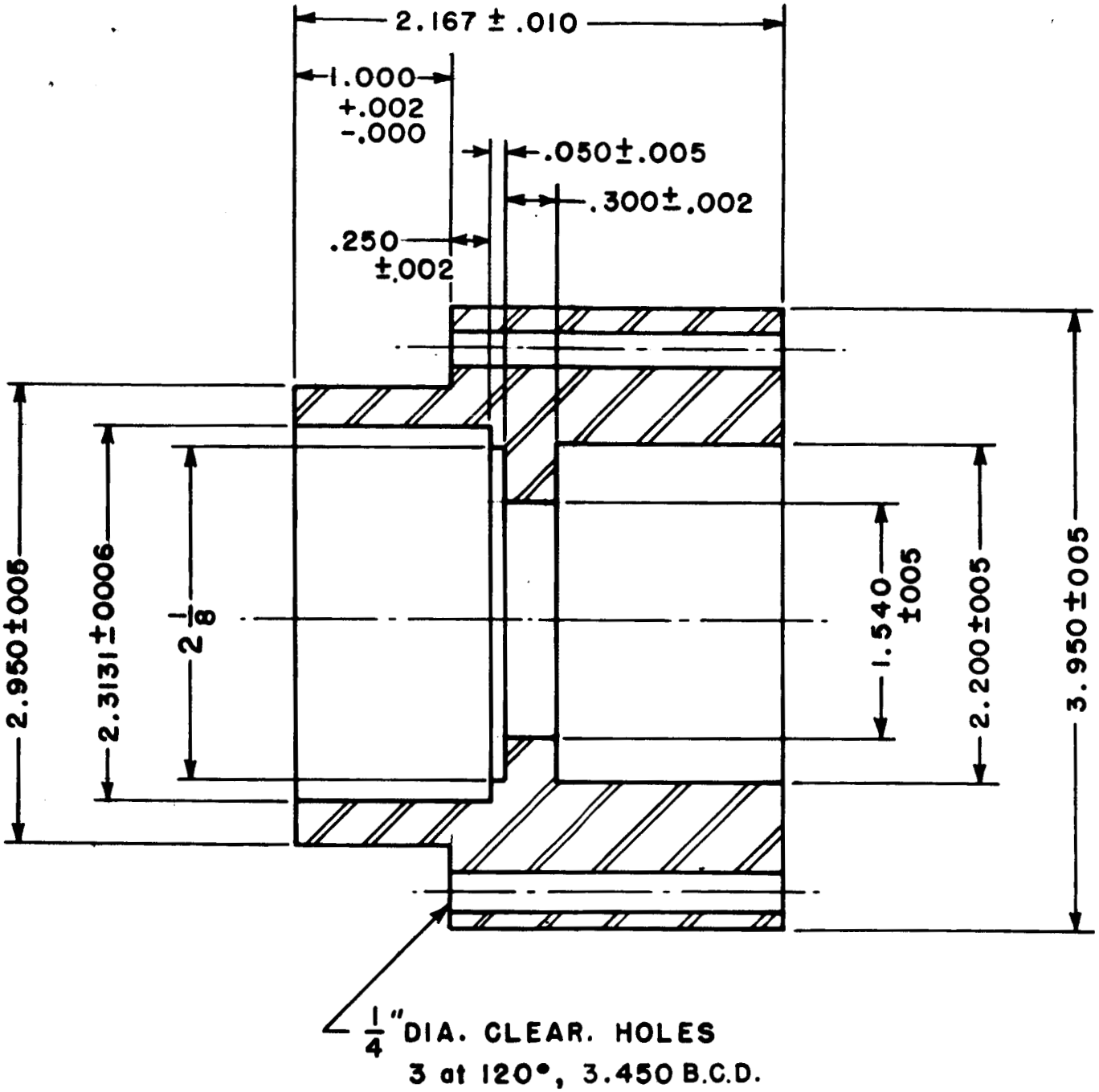

MAT'L-C1020 STEEL

DETAIL 20

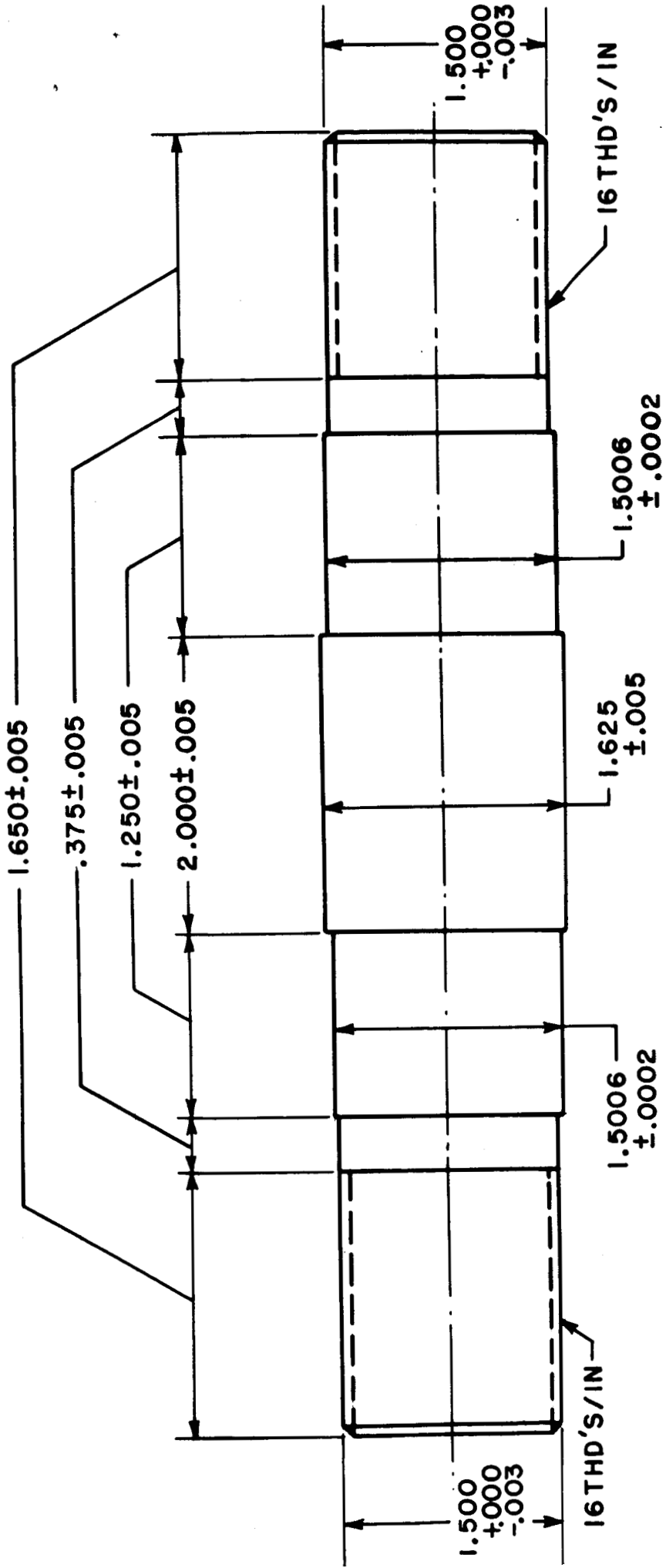

DETAIL 21
MAT'L: DRILL ROD

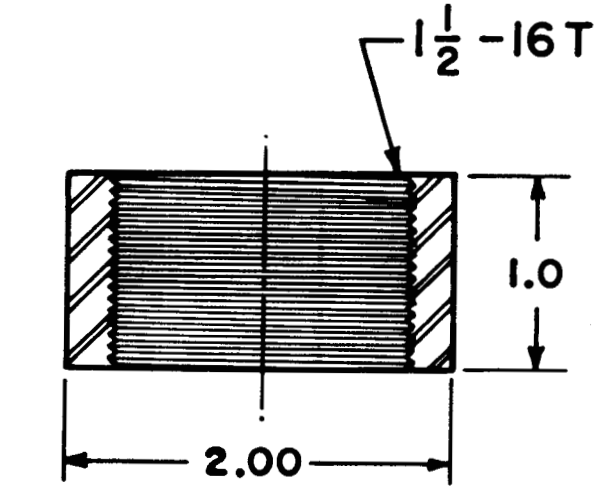

MAT'L – C1020 STEEL

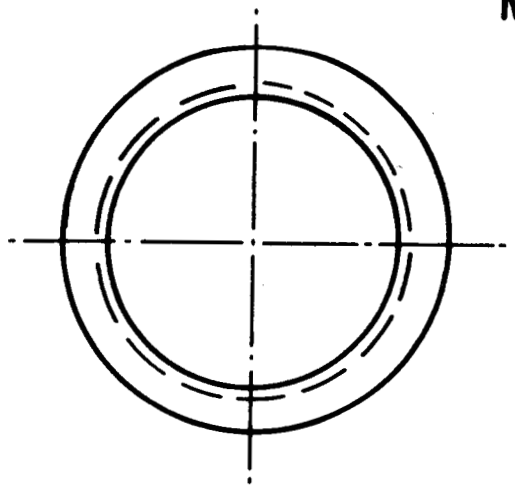

DETAIL 22

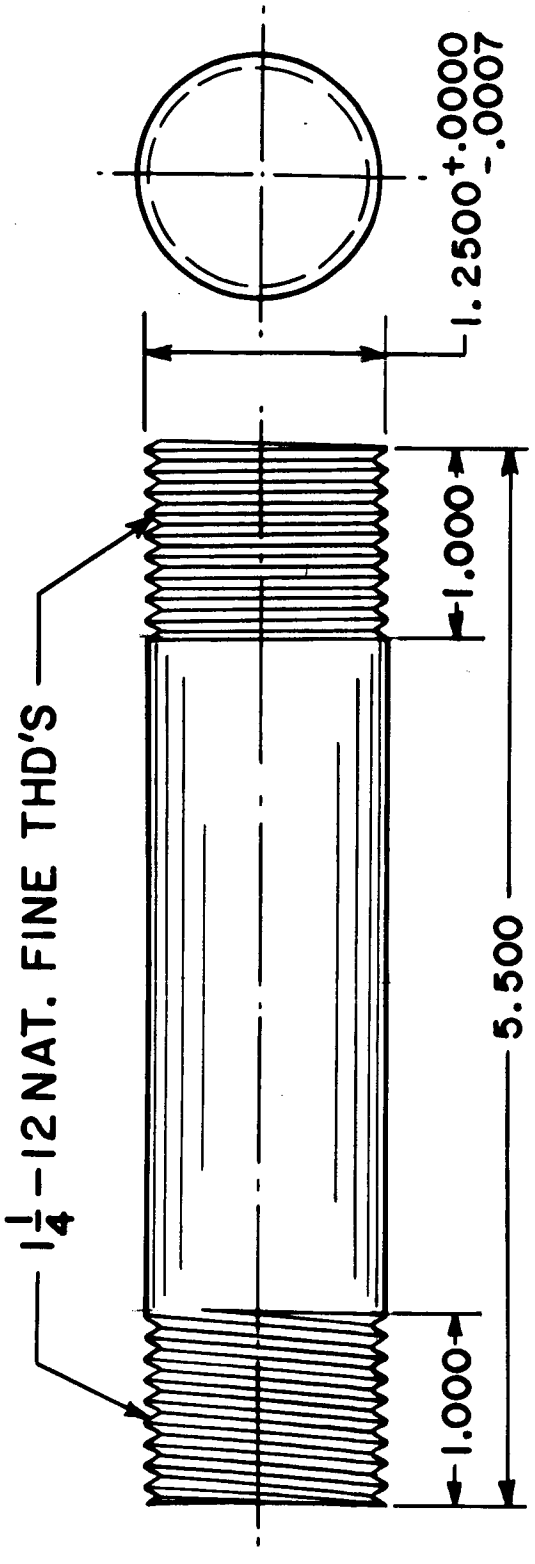

LOADING BAR
MAT'L: DRILL ROD
DETAIL 23

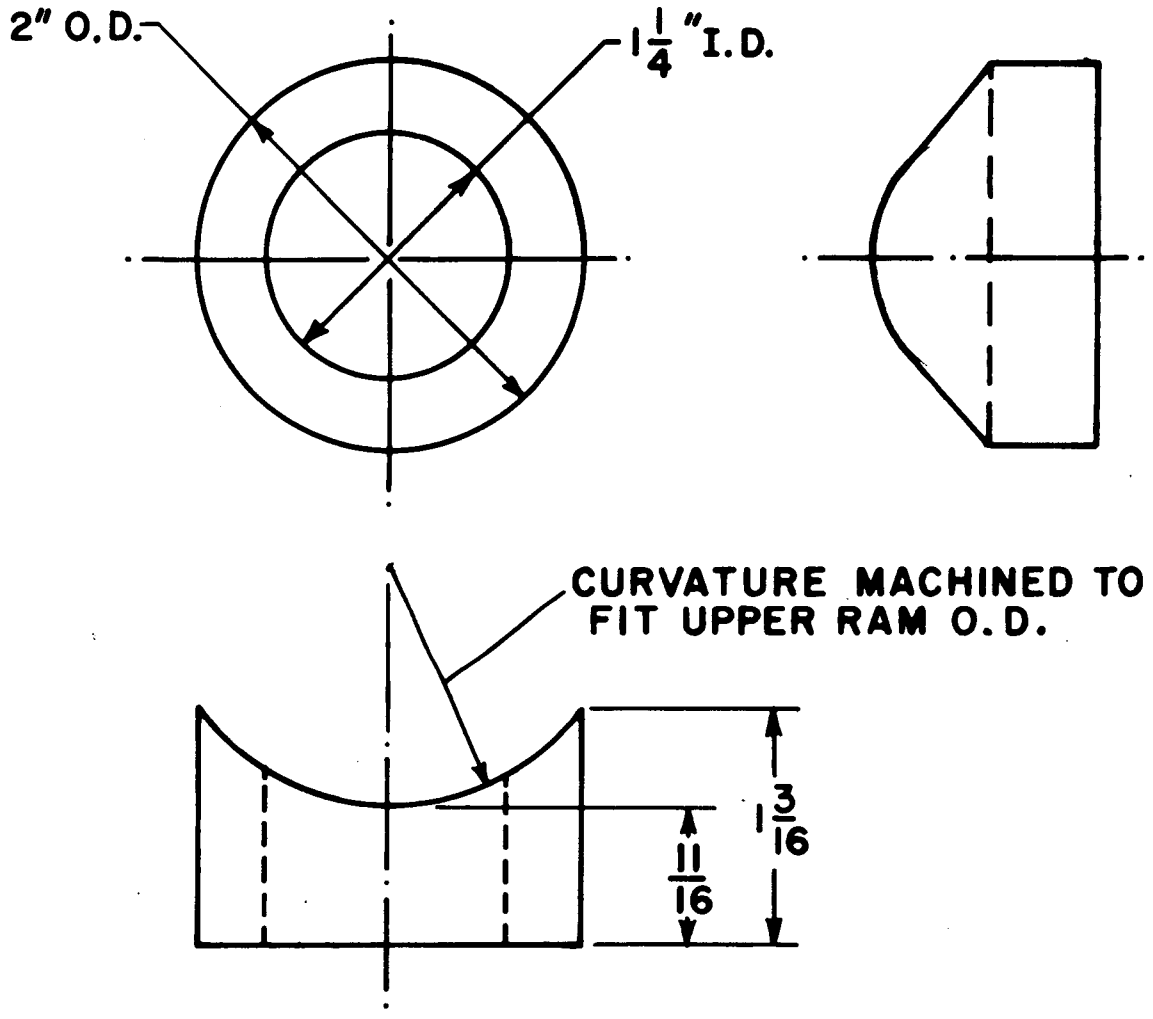

DETAIL 24

LOADING BAR CLAMPING WASHER

MAT'L: C-1020 STEEL

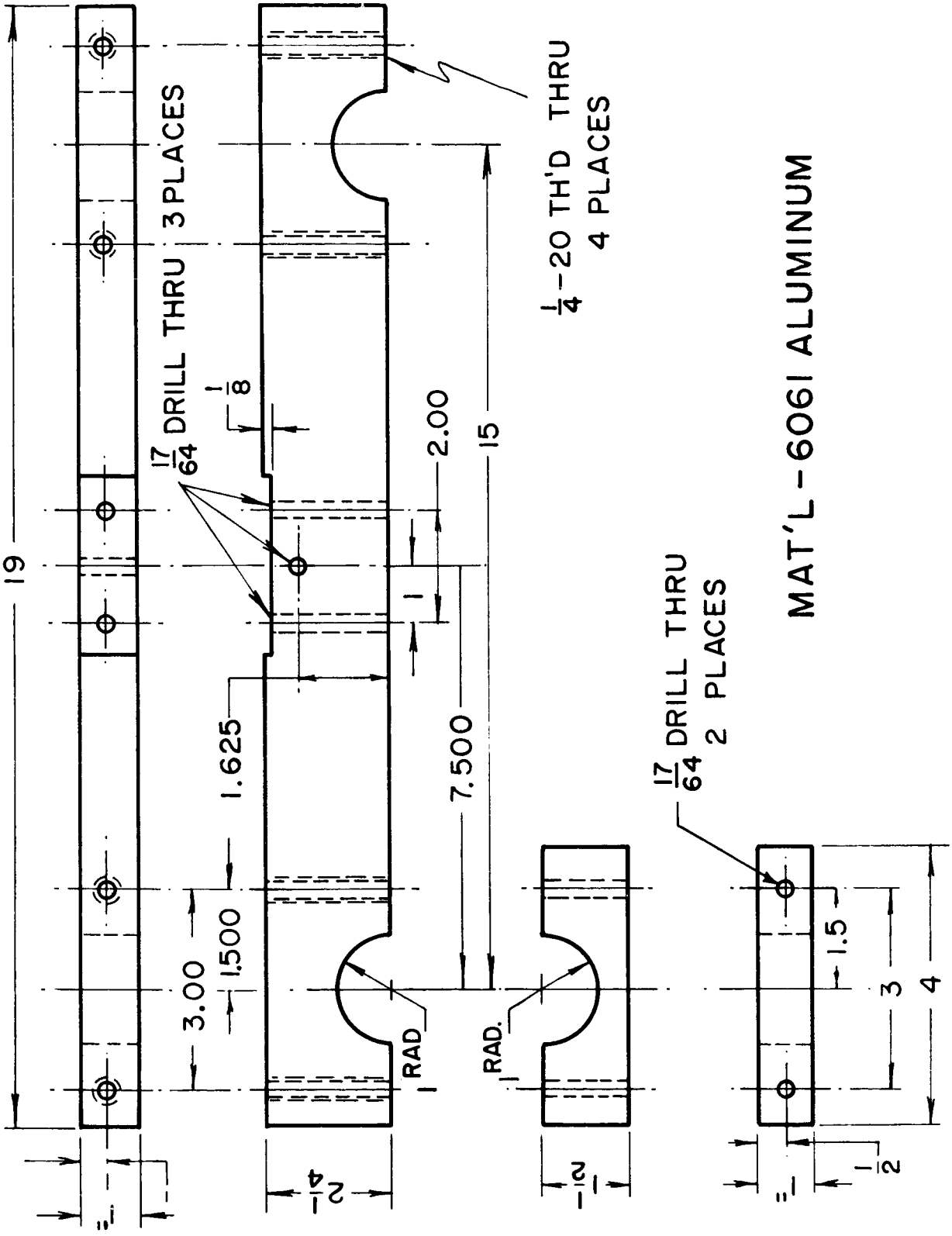

FURNACE MOUNTING BAR ASSEMBLY
DETAIL 25

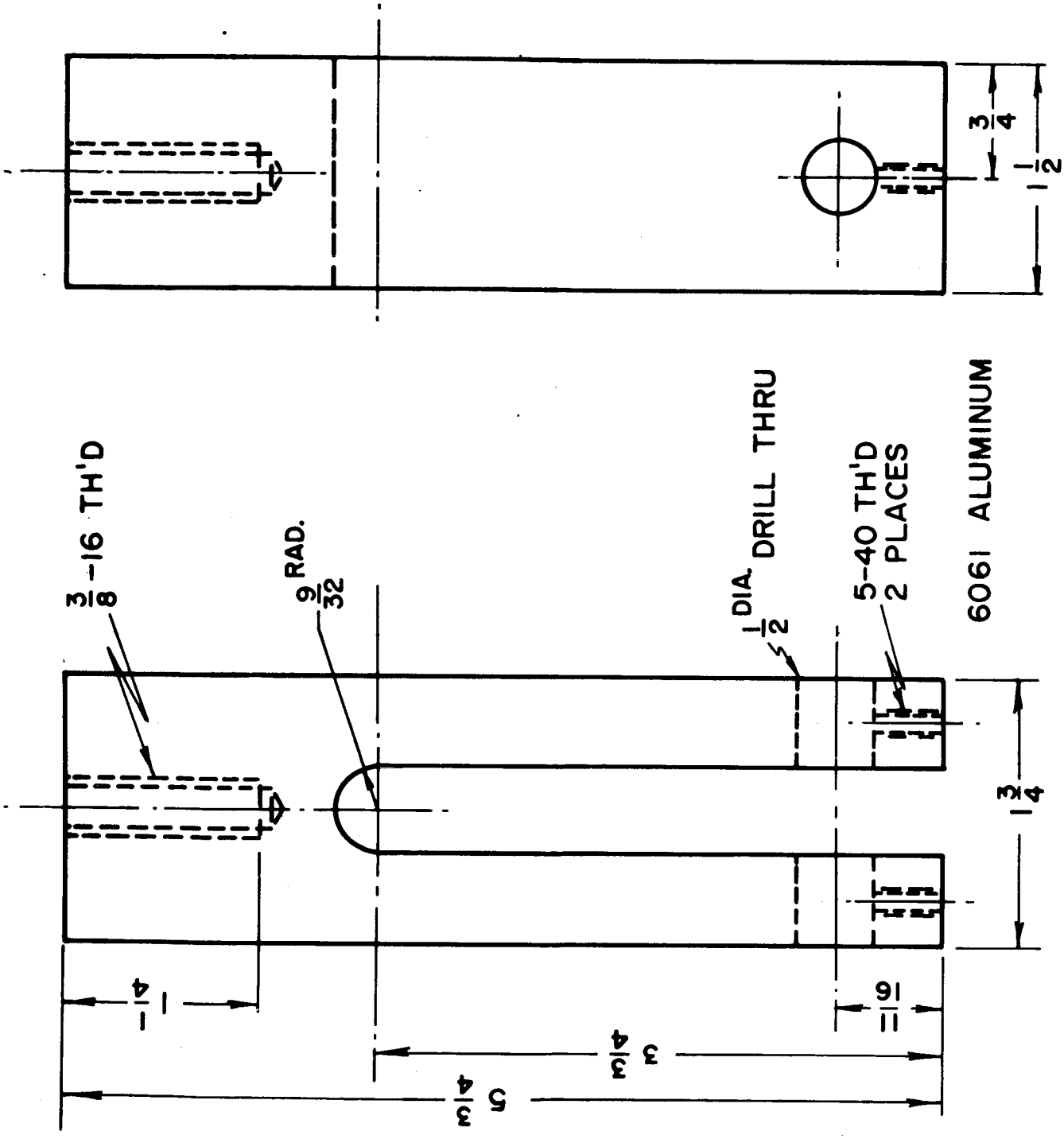

DETAIL 26 PULLEY BLOCK

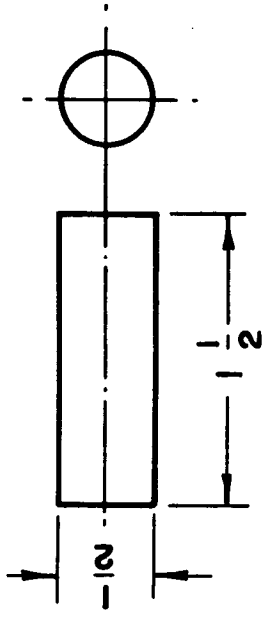

1020 STEEL

DETAIL 27 DRIVE PIN

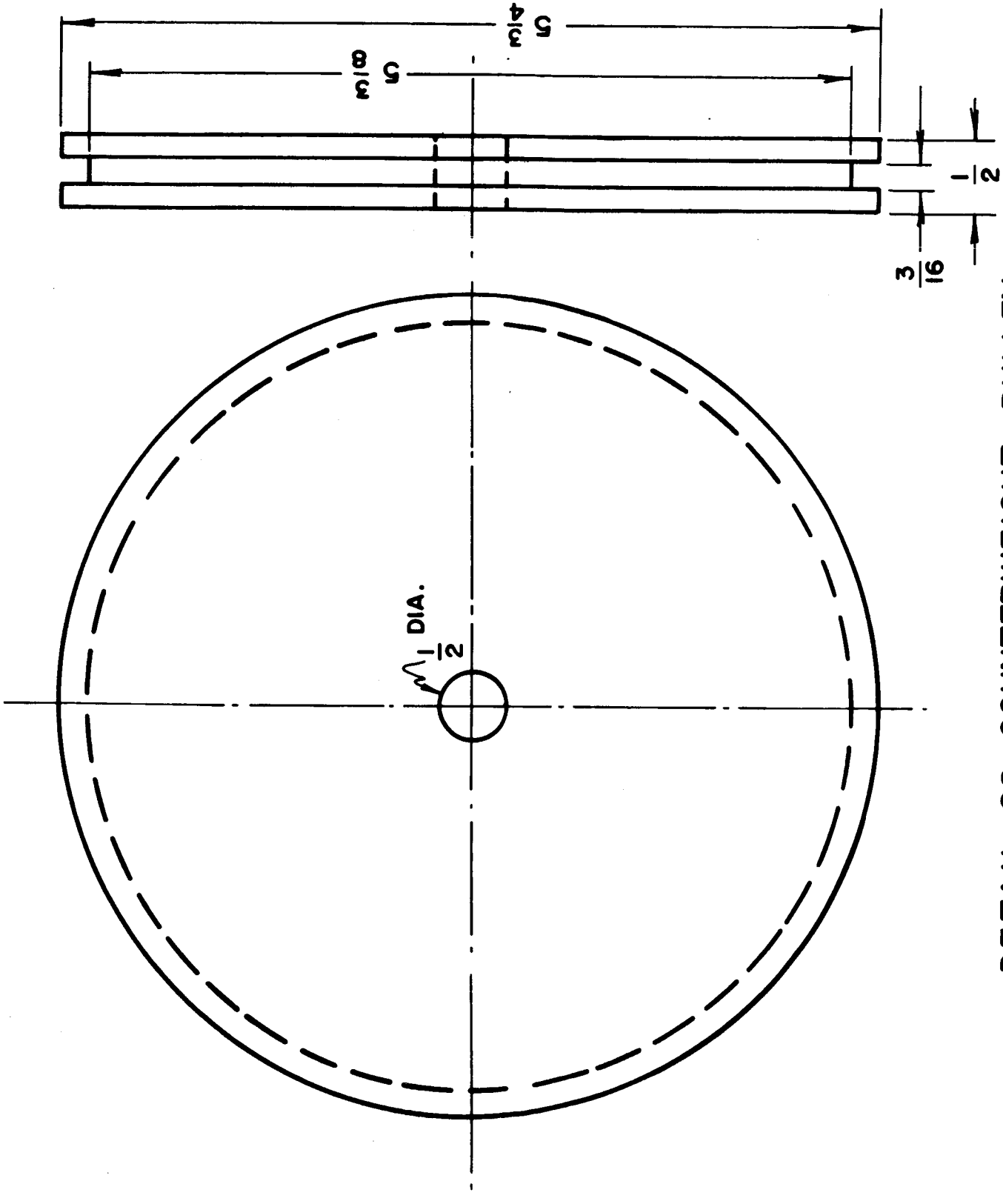

DETAIL 28 COUNTERWEIGHT PULLEY
6061 T6 ALUMINUM

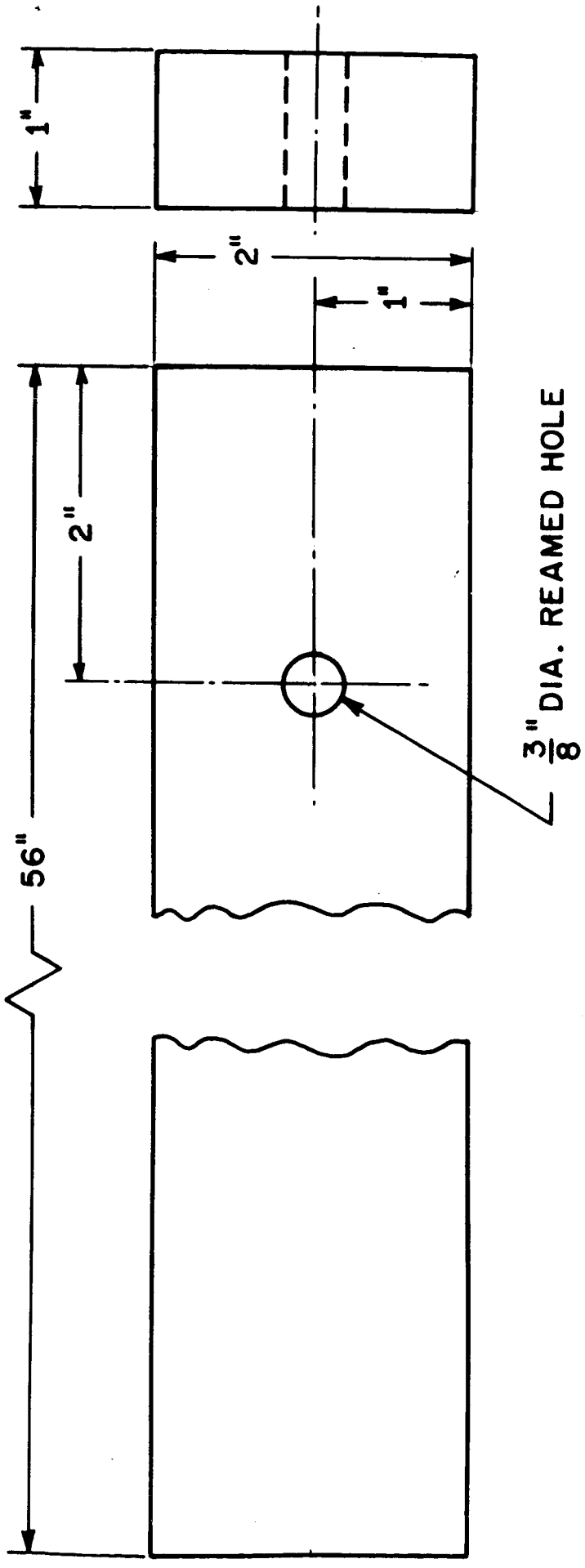

LEVER ARM
MAT'L: C4140 STEEL
DETAIL 29

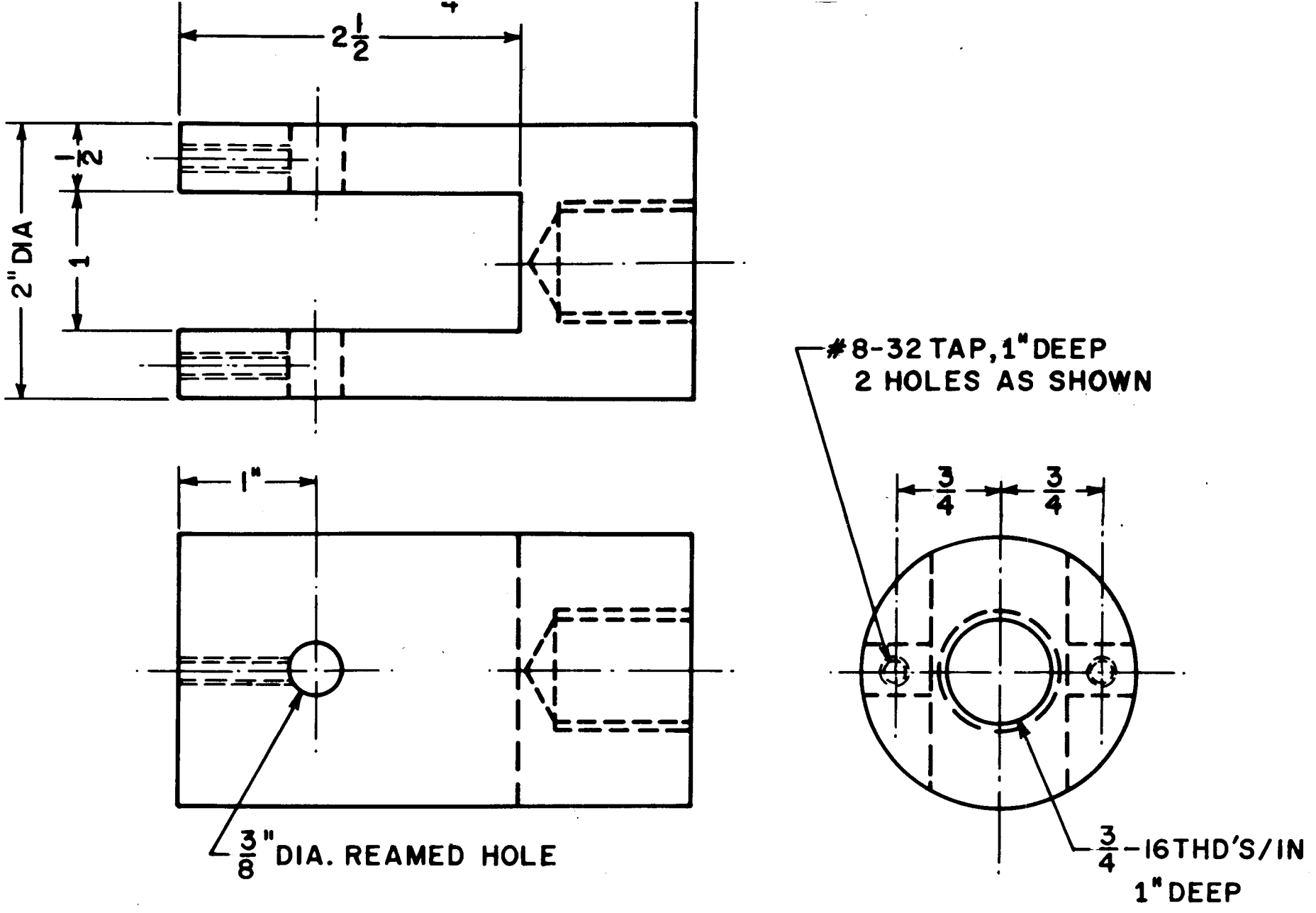

YOKE
MAT'L: 305 S.S.
DETAIL 30

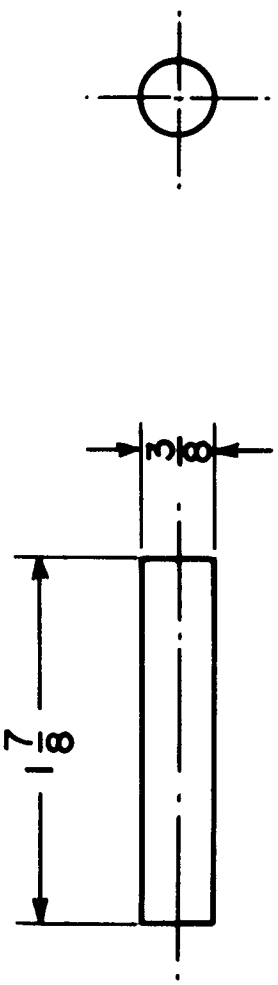

DRIVE PIN
MAT'L: 305 ST. STEEL
DETAIL 31

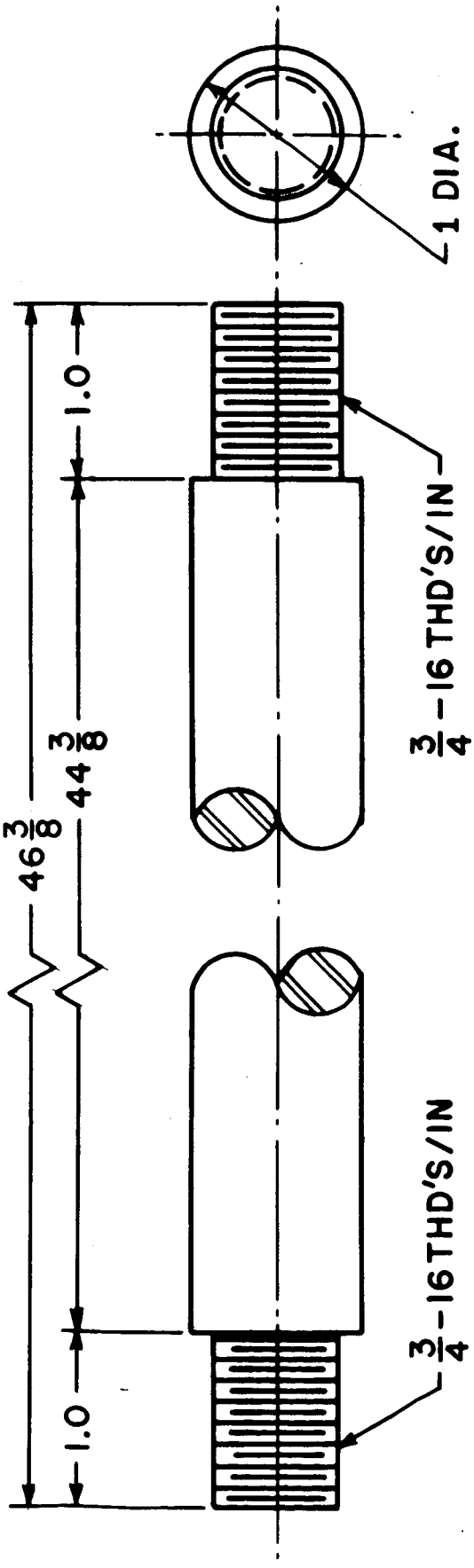

CONNECTING BAR
MAT'L: 305 ST. STEEL
DETAIL 32

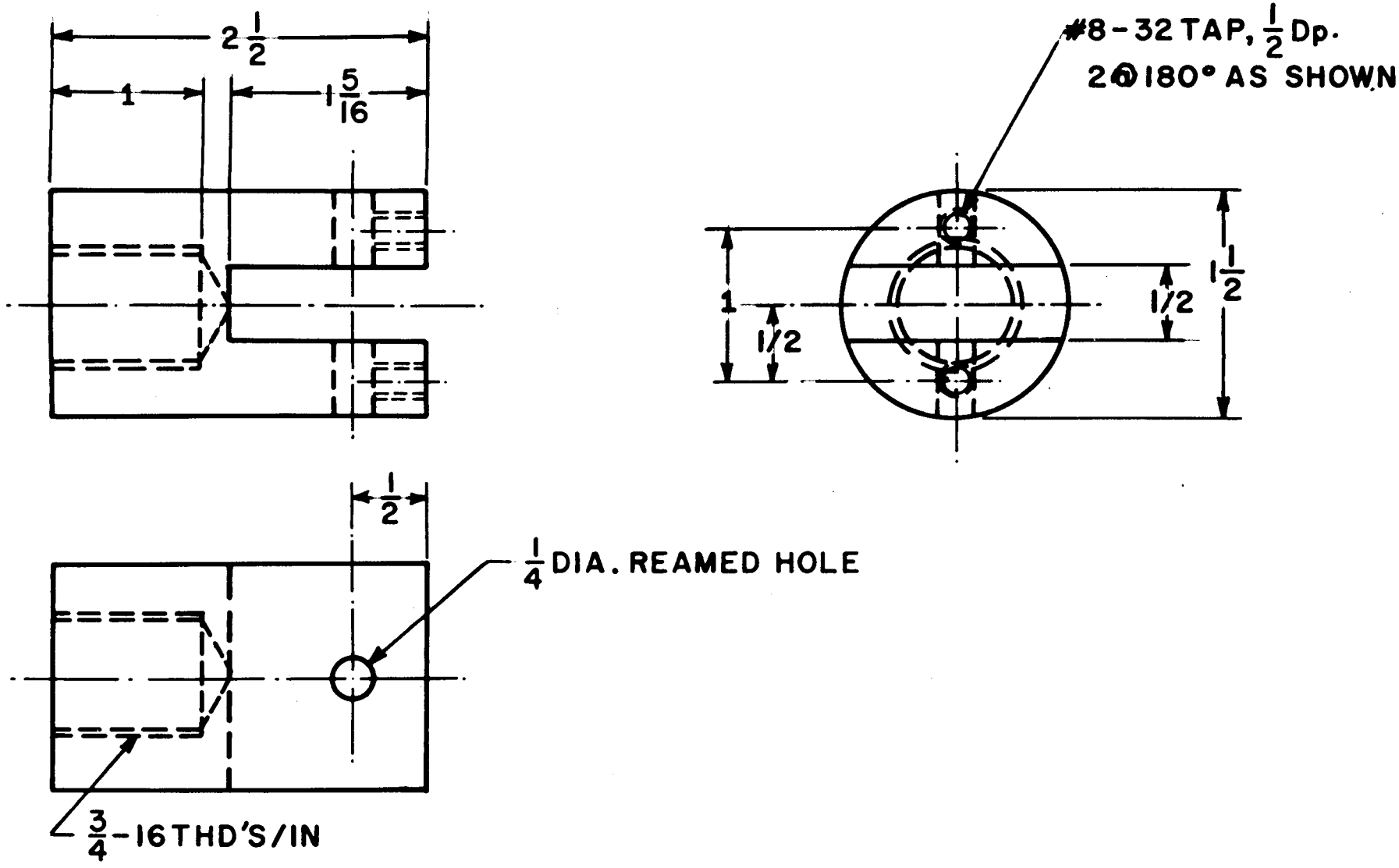

YOKE
MAT'L: 305 ST. STEEL
DETAIL 33

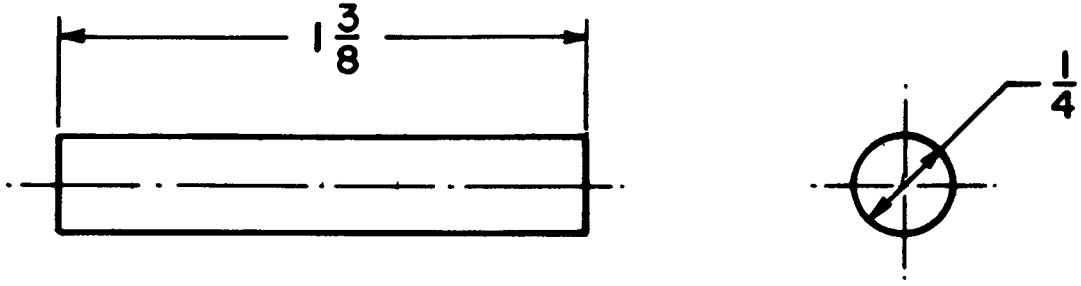

DRIVE PIN
MAT'L: 305 ST. STEEL
DETAIL 34

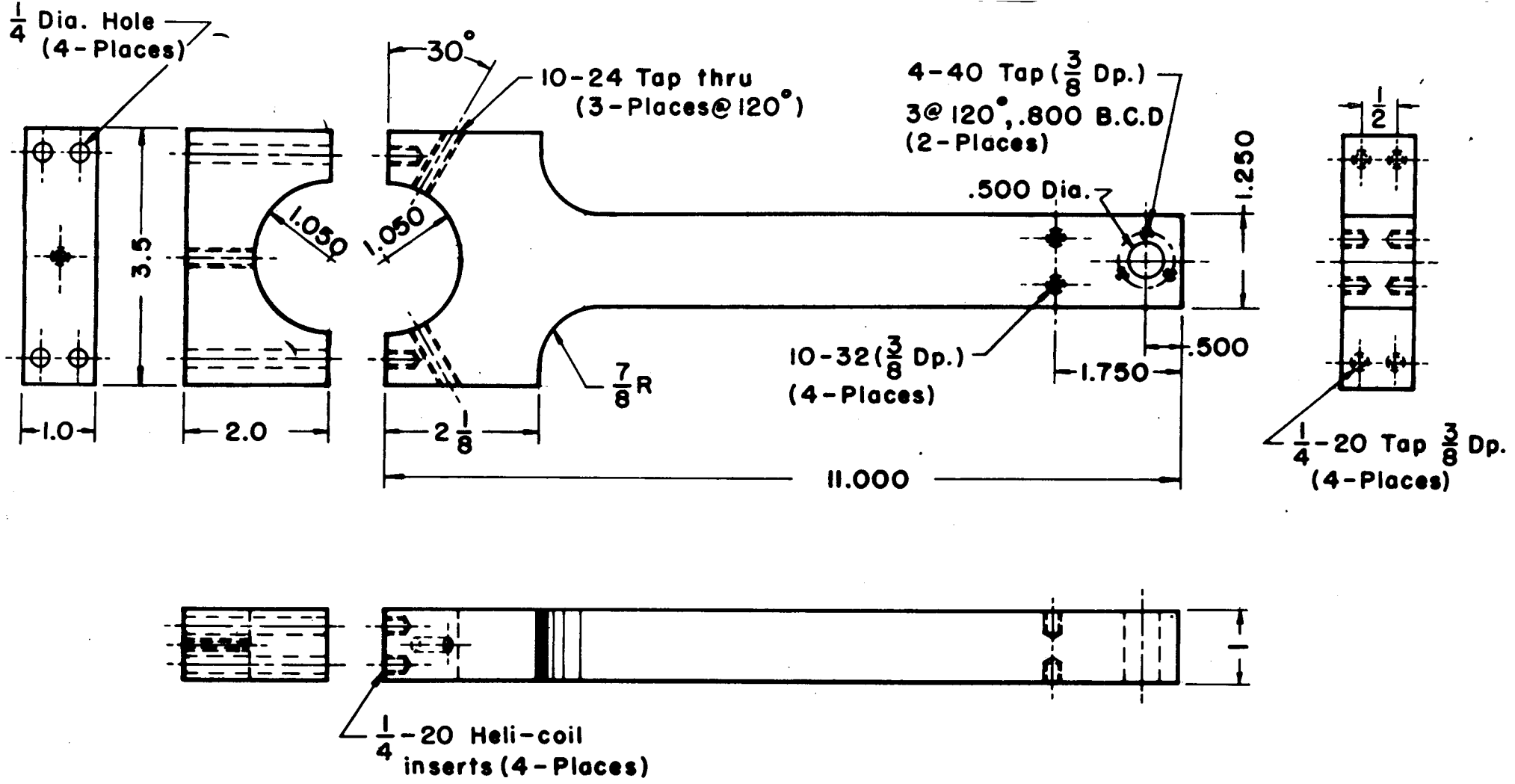

BEARING MOUNTING ARM ASSEMBLY

MAT'L: TYPE CP-130 PHENOLIC
(NEMA GRADE G-7)

DETAIL 35

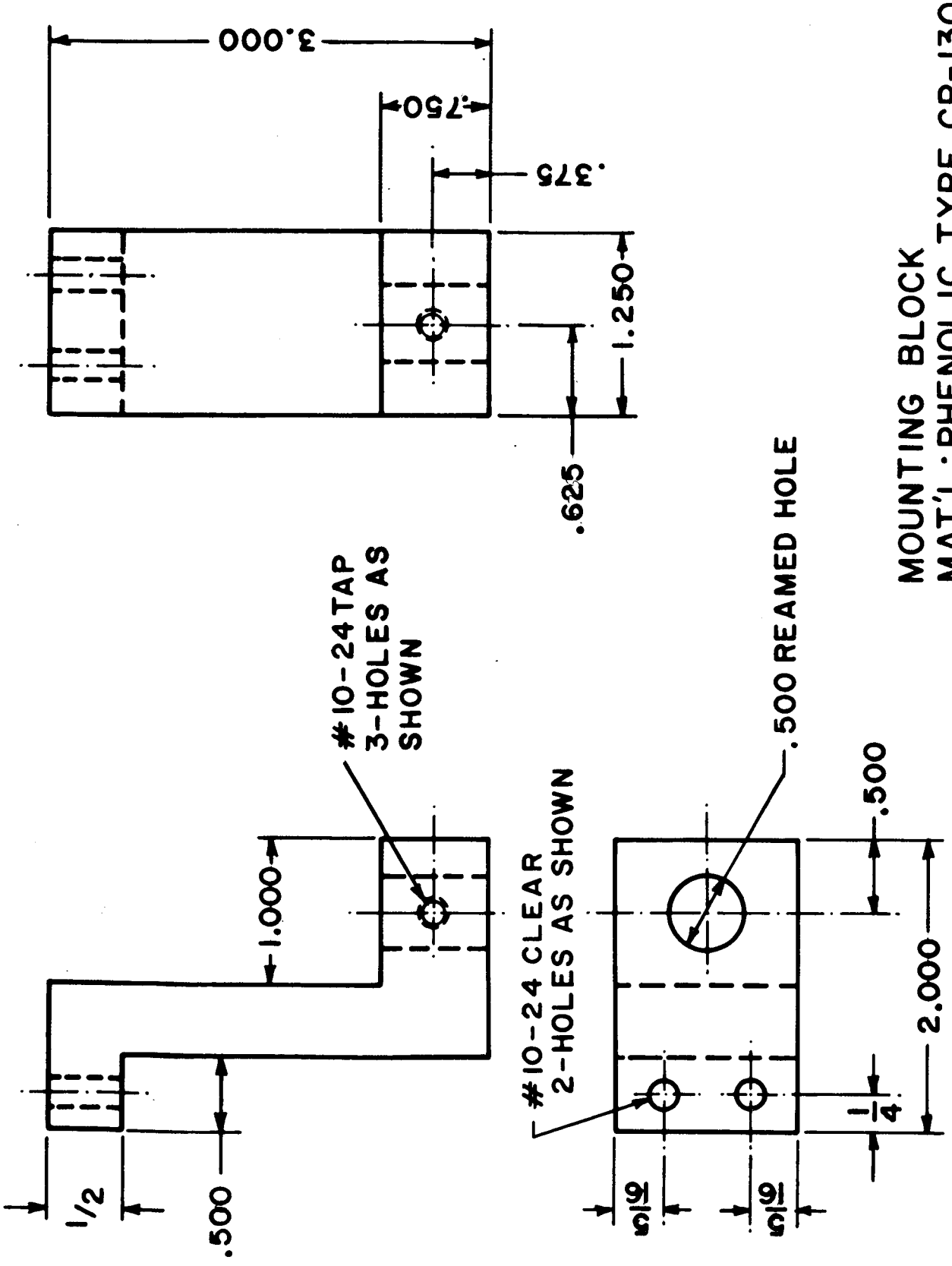

MOUNTING BLOCK
MAT'L: PHENOLIC TYPE CP-130
(NEMA GRADE G-7)

DETAIL 36

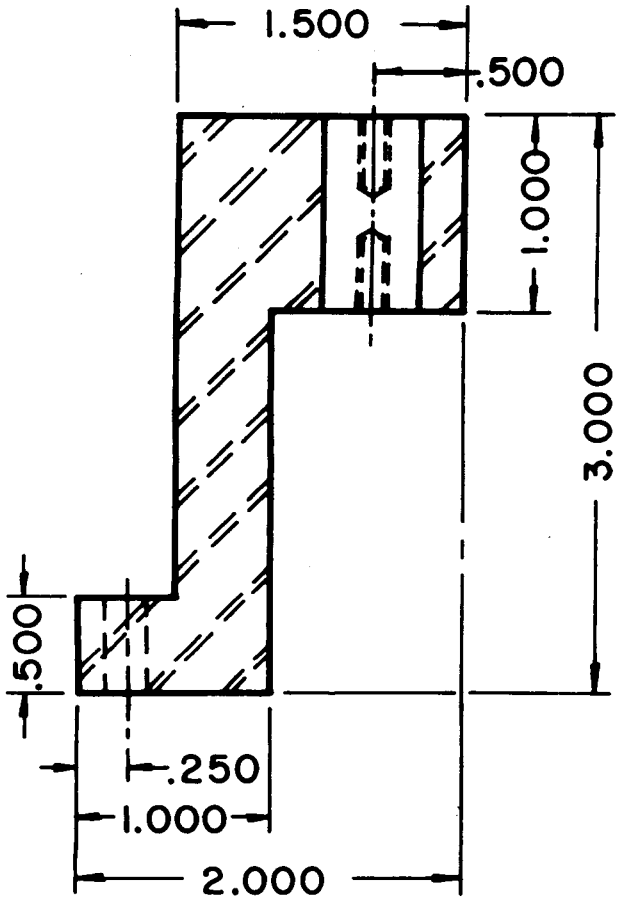

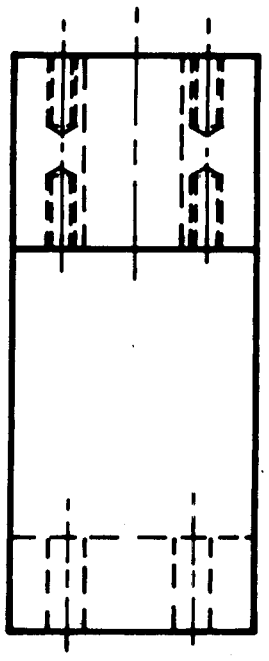

CORE ROD
BEARING MOUNTING
MAT'L: Type CP-130 PHENOLIC
(NEMA GRADE G-7)

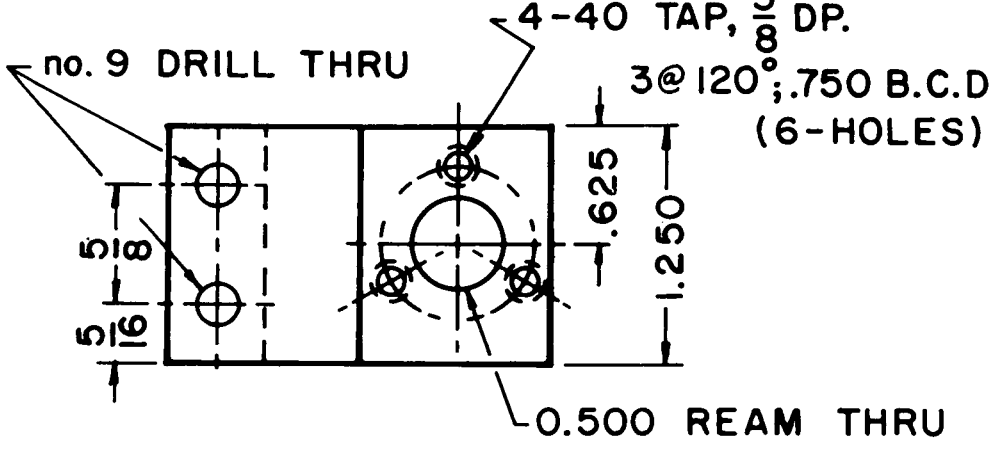

DETAIL 37

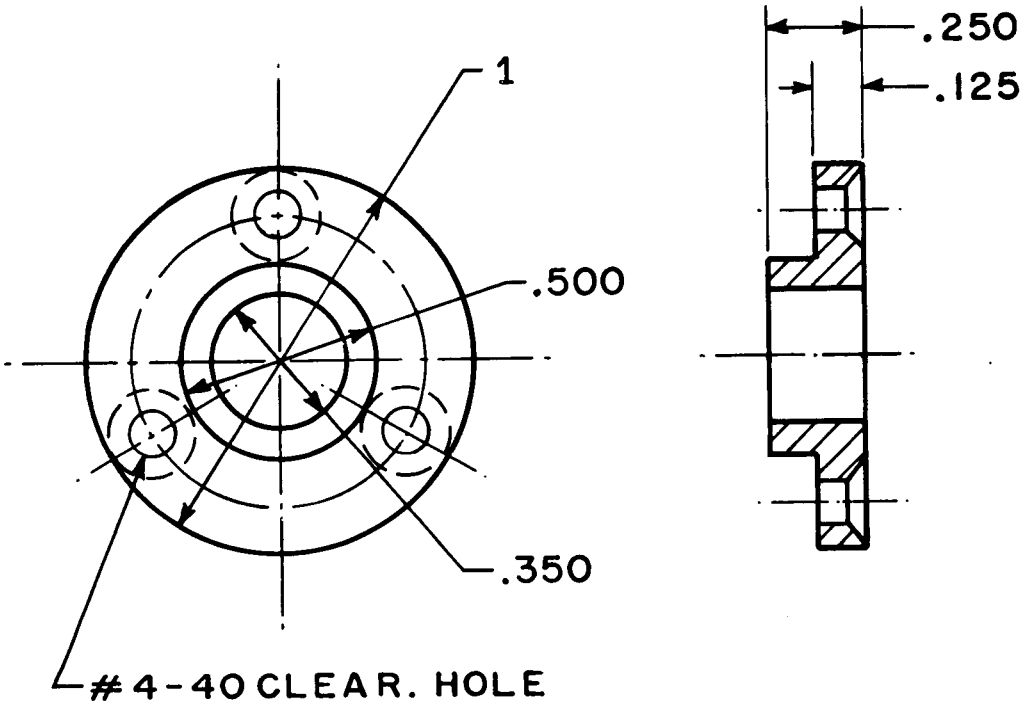

BEARING RETAINING RING
MAT'L: PHENOLIC TYPE CP-130
(NEMA GRADE G-7)

DETAIL 38

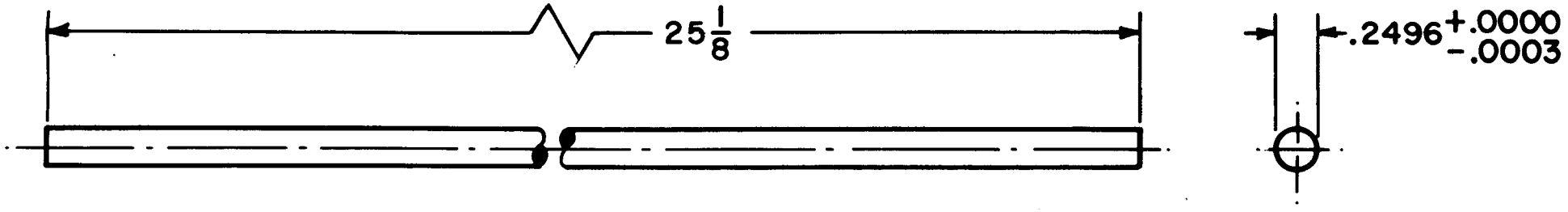

MAT'L: TYPE 440C ST. STEEL
HARDENED TO RC55C

PUSH ROD
DETAIL 39

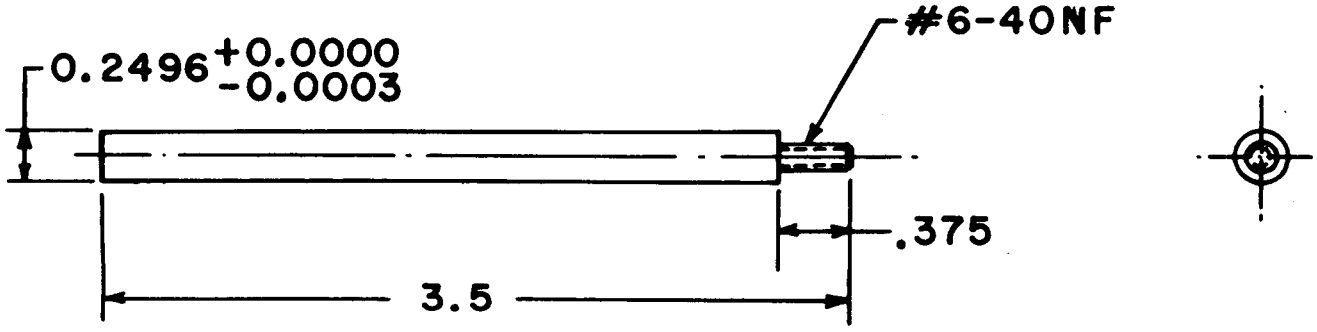

STRAIN TRANSDUCER CORE ROD
MAT'L: TYPE 305 STAIN. STEEL

DETAIL 40

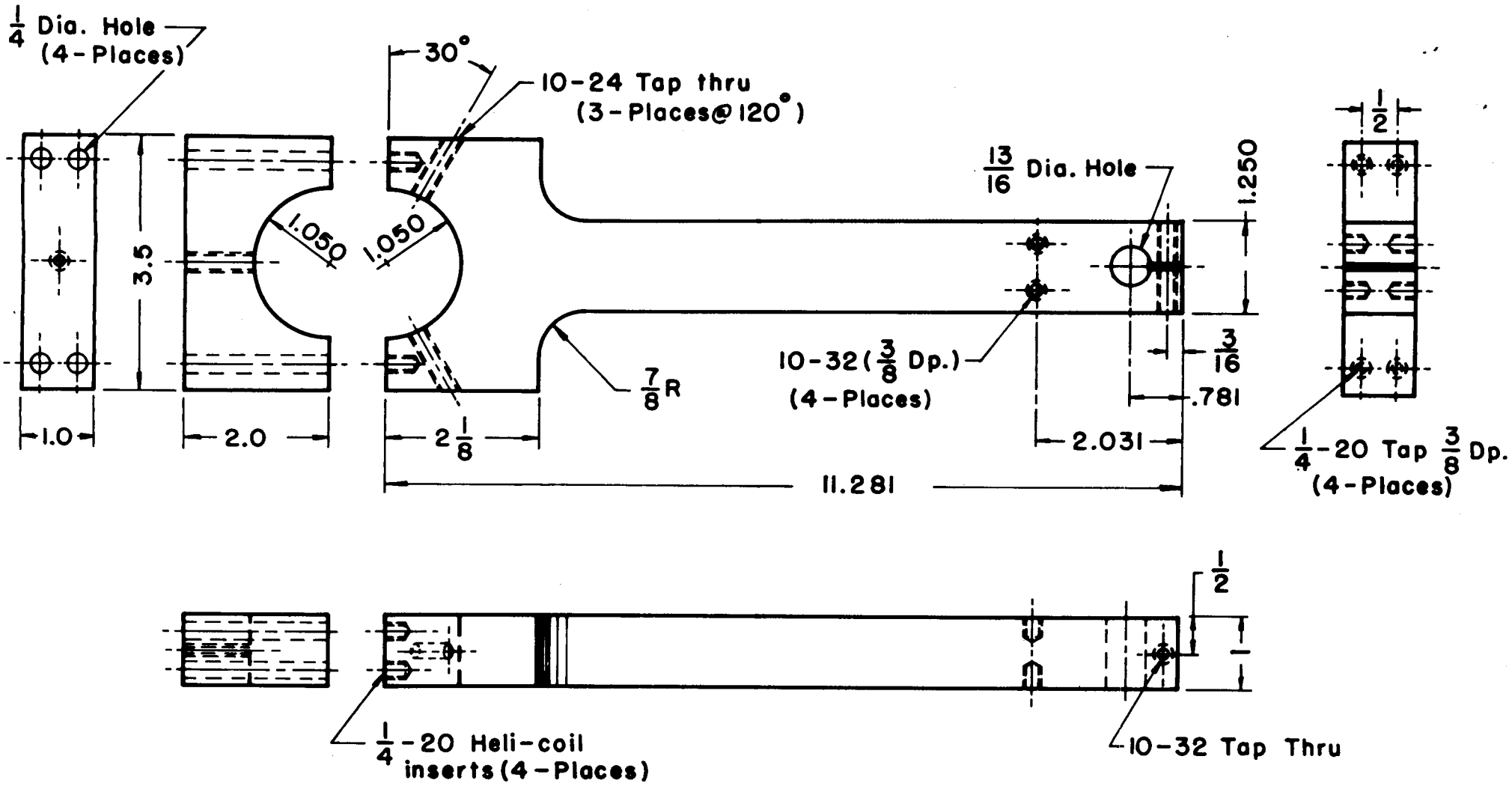

STRAIN TRANSDUCER MOUNTING ARM ASSEMBLY
MAT'L: TYPE CP-130 PHENOLIC
(NEMA GRADE G-7)

DETAIL 41

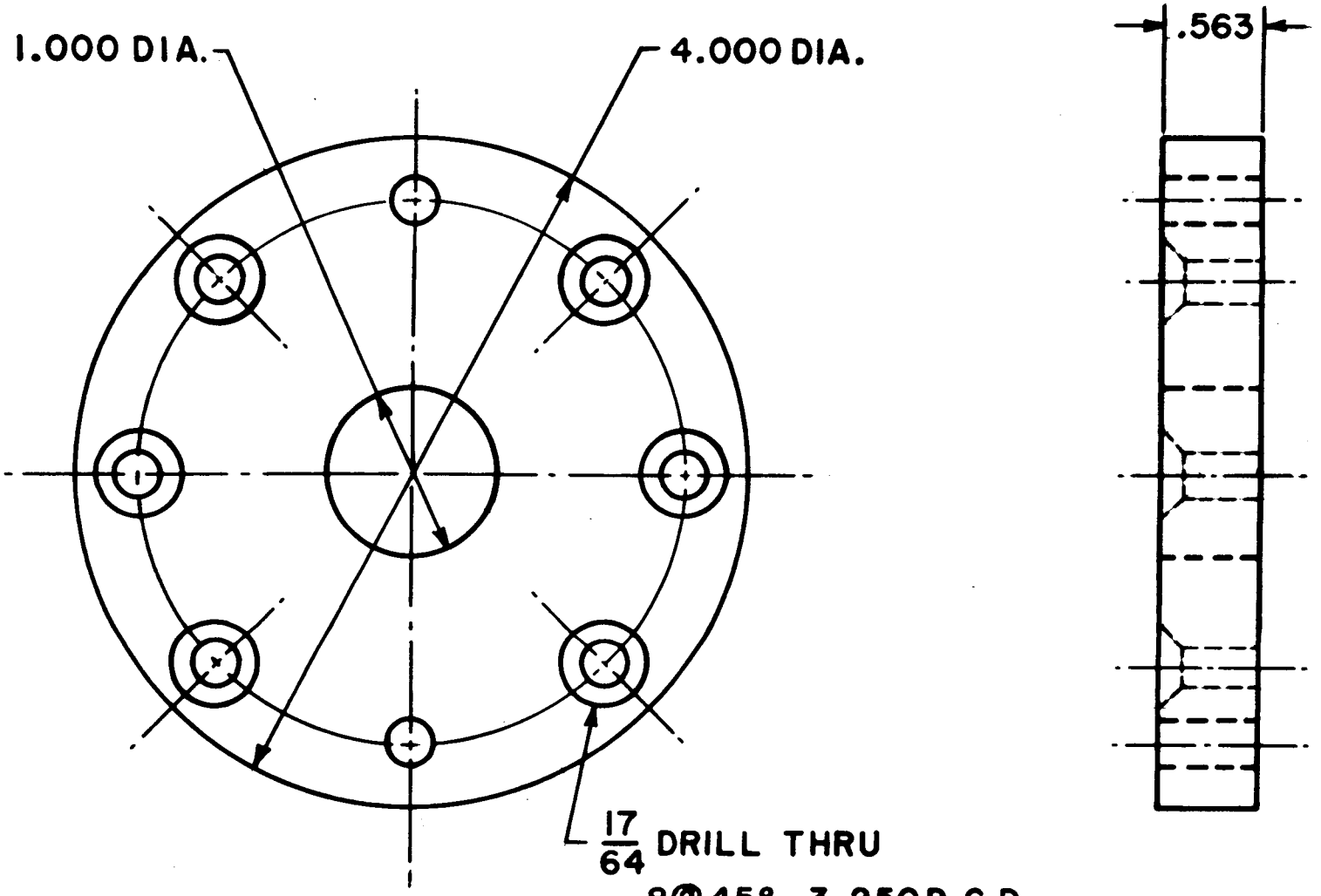

JACK MOUNTING PLATE
MAT'L:304 ST. STEEL
DETAIL 42

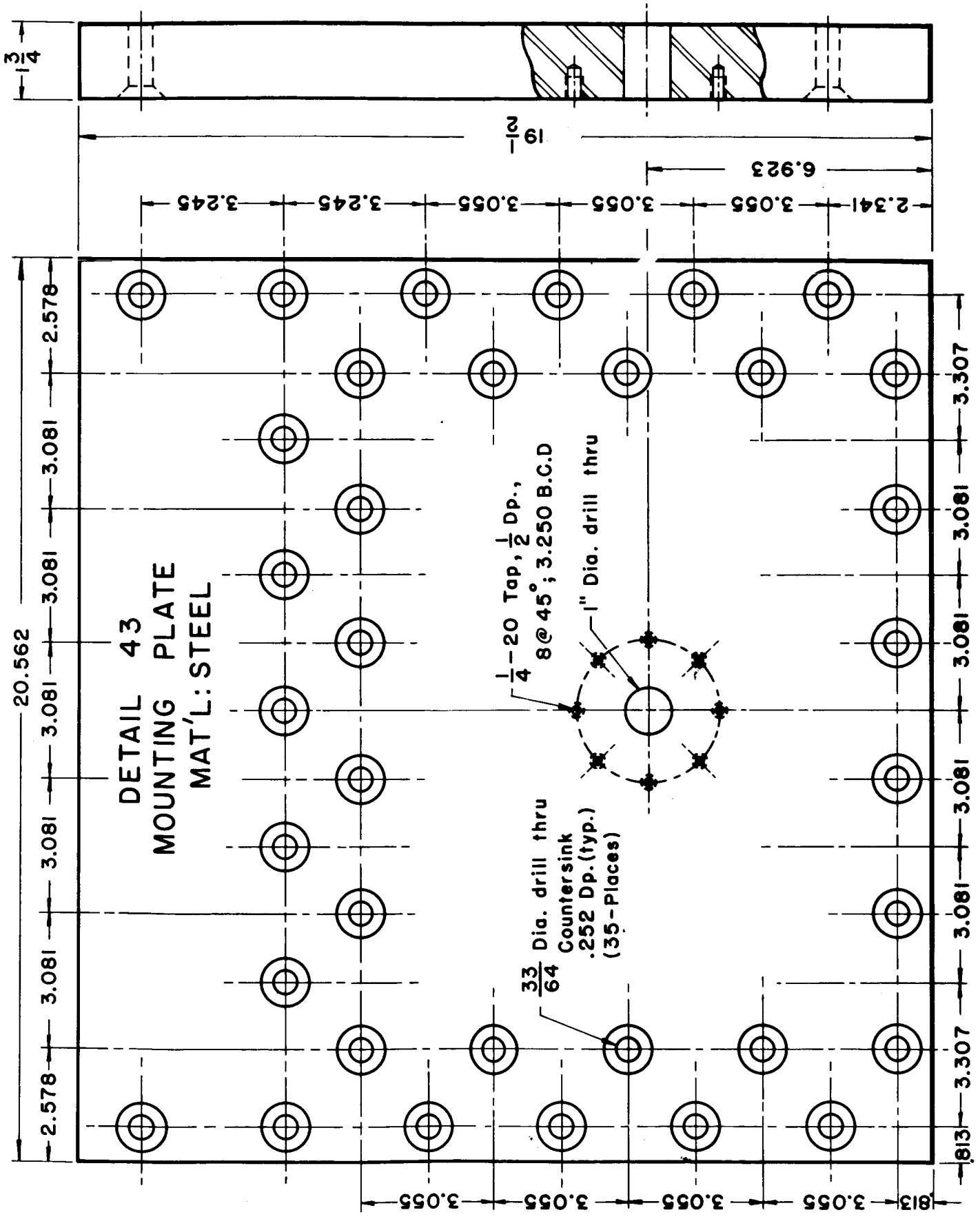
DETAIL 43
MOUNTING PLATE
MAT'L: STEEL
1/4-20 Tap, 1/2 Dp.,
8@45°; 3.250 B.C.D
1" Dia. drill thru
33/64 Dia. drill thru
Countersink
.252 Dp.(typ.)
(35-Places)
3/4
19
6.923
2.341
3.055
3.055
3.245
3.245
20.562
2.578
3.081
3.081
3.081
3.081
3.081
3.081
2.578
3.307
3.081
3.081
3.081
3.081
3.307
813
3.055
3.055
3.055
3.055
813

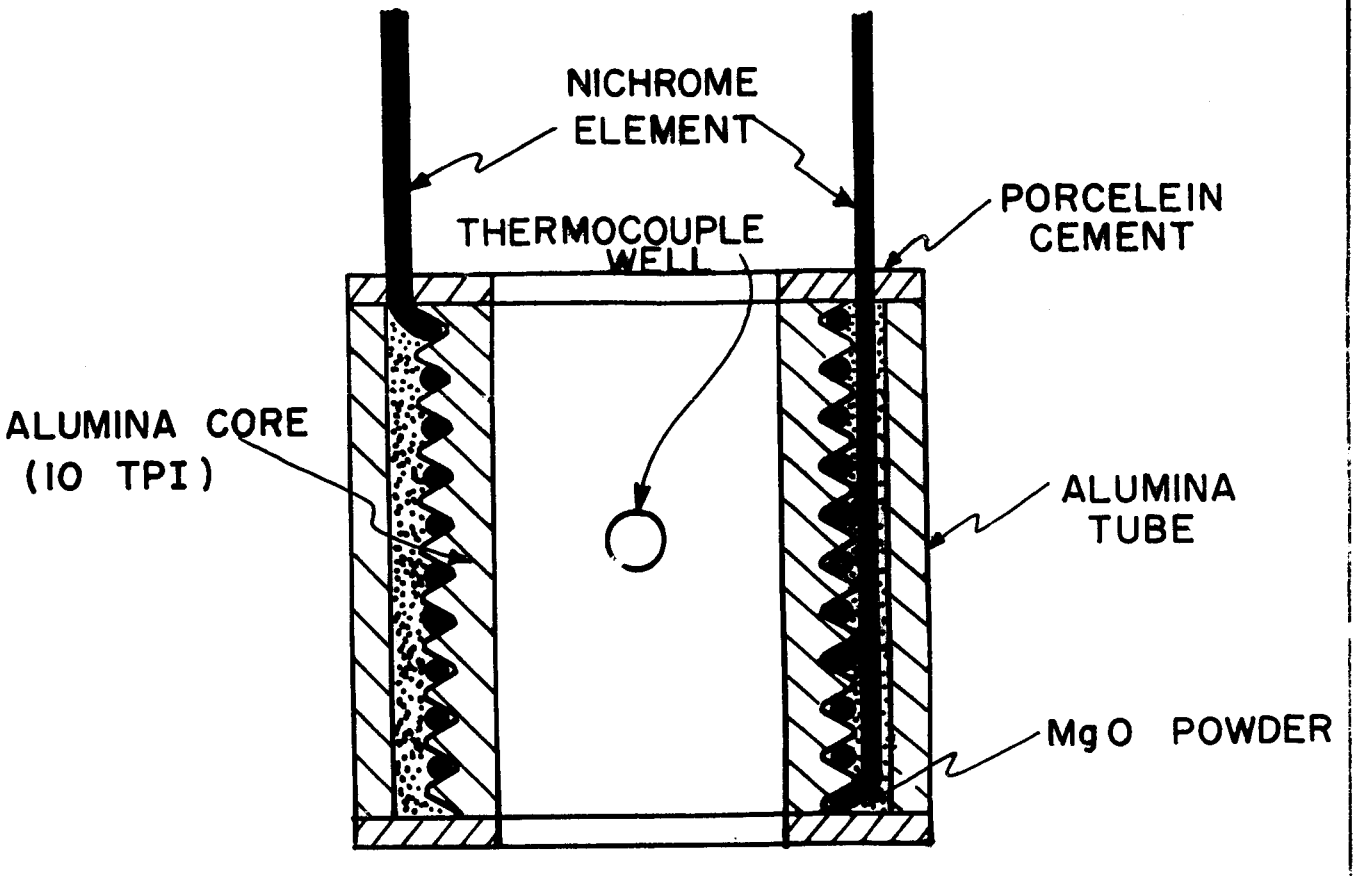

DETAIL 44

INTERNAL FURNACE

Scale: 1/2" = 3/4"

REFERENCES

Andrade, E. N. da C., On the viscous flow in metals and allied phenomena, Proc. Royal Soc., 84A, 1, 1911.

Andrade, E. N. da C., The flow in metals under large constant stresses, Proc. Royal Soc., 90A, 329, 1914.

Bowen, N. L., and O. F. Tuttle, The system MgO-SiO_2-H_2O, Geol. Soc. Amer. Bull., 60, 439, 1949.

Cook, M. A., Viscosity-depth profiles according to the Ree-Eyring viscosity relations, J. Geophys. Res., 68, 3515, 1963.

Dillon, O. W., Experimental data on aluminum as a mechanically unstable solid, J. Mech. Phys. Solids, 11, 289, 1963.

Dillon, O. W., Waves in mechanically unstable bars, Trans. ASME, 33E, 267, 1966.

Dorn, J. E., The spectrum of activation energies for creep, in Creep and Recovery (Seminar), Amer. Soc. for Metals, 255, 1957.

Glen, J. W., Experiments on the deformation of ice, J. Glaciology, 2, 111, 1952.

Glen, J. W., The creep of polycrystalline ice, Proc. Royal Soc., 228A, 519, 1955.

Glen, J. W., The mechanical properties of ice: I. The plastic properties of ice, Advan. Phys. 7, 254, 1958.

Griggs, D. T., Deformation of rocks under high confining pressures, J. Geol., 44, 541, 1936.

Griggs, D. T., Creep of rocks, J. Geol., 47, 225, 1939.

Griggs, D. T., Experimental flow of rocks under conditions favorable to recrystallization, Geol. Soc. Amer. Bull., 51, 1001, 1940.

Griggs, D. T., and N. E. Coles, Creep of single crystals of ice, U. S. Army Snow, Ice, and Permafrost Research Establishment, SIPRE Report 11, 1954.

Griggs, D. T., F. J. Turner, I. Borg, and J. Soska, Deformation of yule marble: Part IV-effects at 150°C., Geol. Soc. Amer. Bull., 62, 1385, 1951.

Griggs, D. T., F. J. Turner, I. Borg, and J. Soska, Deformation of yule marble: Part V-effects at 300°C., Geol. Soc. Amer. Bull., 64, 1327, 1953.

Handin, J., Strength and ductility, in Handbook of Physical Constants, Geol. Soc. Amer. Mem. 97, 223, 1966.

Hardy, H. R., Time-dependent deformation and failure of geologic materials, Quart. Colo. School Mines, 54, 134, 1959.

Heard, H. C., The effect of large changes in strain rate in the experimental deformation of rocks, J. Geol., 71, 162, 1963.

Iida, K., T. Wada, Y. Aida, and R. Schichi, Measurements of creep in igneous rocks, J. Earth Sci., Nagoya Univ., 8, 1, 1960.

Jellinek, H. H. G., and R. Brill, Viscoelastic properties of ice, J. Appl. Phys., 27, 1198, 1956.

LeComte, P., Creep and internal friction in rock salt, Doctoral thesis, Harvard University, 1960.

Lomnitz, C., Creep measurements in igneous rocks, J. Geol., 64, 473, 1956.

Michaelson, A. A., The laws of elastico-viscous flow. Part I., J. Geol., 25, 405, 1917.

Michaelson, A. A., The laws of elastico-viscous flow. Part II., J. Geol., 28, 18, 1920.

Miller, R., The Webster-Addie ultramafic ring, Jackson County, North Carolina, and secondary alteration of its chromite, Amer. Min., 38, 1134, 1953.

Misra, A. K., and S. A. F. Murrell, An experimental study of the effect of temperature and stress on the creep of rocks, Geophys. Jour., 9, 509, 1965.

Murrell, S. A. F., and A. K. Misra, Time-dependent strain or 'creep' in rocks and similar non-metallic materials, Trans. Instn. Min. Metall., Lond., 71, 353, 1962.

Mott, N. F., The mechanical properties of metals, Proc. Phys. Soc., 64B, 729, 1951.

Mott, N. F., A theory of work-hardening of metals; II: Flow without slip-lines, recovery, and creep, Phil. Mag., 44, 742, 1953.

Nadai, A., The influence of time upon creep, the hyperbolic sine creep law, in Stephen Timoshenko 60th Anniversary Volume, Macmillan Company, 1938.

Nadai, A., and P. G. McVetty, Hyperbolic sine chart for estimating working stresses of alloys at elevated temperatures, Proc. Amer. Soc. Testing Materials, 43, 735, 1943.

Nishihara, M., Creep of shale and sandy-shale, J. Geol. Soc. Japan, 58, 373, 1952.

Orowan, E., The creep of metals, J. West Scotland Iron and Steel Inst., 54, 45, 1947.

Orowan, E., Mechanical properties of crust and mantle, Boeing Scientific Research Lab. Doc. D1-82-0485, 1965.

Phillips, P., The slow stretch in India rubber, glass, and metal wires when subjected to a constant pull, Phil. Mag., 9, 513, 1905.

Prandtl, L., Gedanken Modell zur kinetischen Theorie der festen Koerper, Zeit. Math. Mechanik, 8, 85, 1928.

Ree, F. H., T. Ree, and H. Eyring, Relaxation theory of creep of metals, Proc. Amer. Soc. Civil Engrs., J. Engr. Mech. Div., 86, 41, 1960.

Robertson, E. C., Creep of Solenhofen limestone under moderate hydrostatic pressure, in Rock Deformation, Geol. Soc. Amer. Mem. 79, 227, 1960.

Roeser, W. F., and S. T. Louberger, Methods of testing thermocouple materials, National Bureau of Standards Circular 590, 1958.

Stavrolakis, J. A., and F. H. Norton, Measurement of the torsion properties of alumina and zirconia at elevated temperatures, J. Amer. Cer. Soc., 34, 374, 1951.

Stimson, H. F., International practical temperature scale of 1948(Text revision of 1960), J. Res. Nat. Bur. Stands., 65A, 231, 1961.

Wachtman, J. B., and L. H. Maxwell, Plastic deformation of ceramic-oxide single crystals, J. Amer. Cer. Soc., 37, 291, 1954.

Watstein, D., Effect of straining rate on the compressive strength and elastic properties of concrete, J. Amer. Concrete Inst., 24, 729, 1953.

Wygant, J. F., Elastic and flow properties of dense, pure oxide refractories, J. Amer. Cer. Soc., 34, 374, 1951.

ABSTRACT

Twenty-two creep experiments were performed on cylindrical specimens of fine-grained polycrystalline dunite from the Webster-Addie ultramafic complex in Jackson County, North Carolina. The experiments were conducted in a new, uniaxial compression apparatus at high temperatures, up to 1000°C., and differential stresses up to 400 bars at atmospheric pressure. By means of slow heating up and cooling down, it proved possible to prevent crumbing and cracking of the specimens, in the absence of either jacketing or confining pressure. Primary and secondary stages of creep were observed in most of the tests. Temperature, and not axial stress, was found to have the strongest influence on the measured deformations. Steady-state creep rates of about 10^{-7}-10^{-8} sec.$^{-1}$ were obtained which varied with temperature and axial stress according to the empirical form of the Ree-Eyring equation. An activation energy for creep of 35.1 kcal mole^{-1} was computed, and grain boundary creep was indicated as the mechanism causing the steady-state deformations. Not surprisingly, the investigation showed that the chemical and crystalline properties of rocks are widely variable parameters which are also the ones most difficult to control.

Since there is evidence which suggests that hydrostatic pressures of the order 10^4-10^5 bars, as found in the upper mantle, should have only a small effect upon the creep properties of crystalline materials, the omission of a confining pressure should not make the experiments an unrealistic simulation of the lower crust and upper mantle; concurrently, this provides significant technical advantages. The investigation thus established a strong presumption that conditions under which creep deformation takes place in the upper mantle can be investigated in the laboratory with comparatively simple techniques.